



HAL
open science

Recent progress in heteroatom doped carbon based electrocatalyst for oxygen reduction reaction in anion exchange membrane fuel cells

Rambabu Gutru, Zarina Turtayeva, Feina Xu, Gaël Maranzana, Ravikumar Thimmappa, Mohamed Mamlouk, Alexandre Desforges, Brigitte Vigolo

► To cite this version:

Rambabu Gutru, Zarina Turtayeva, Feina Xu, Gaël Maranzana, Ravikumar Thimmappa, et al.. Recent progress in heteroatom doped carbon based electrocatalyst for oxygen reduction reaction in anion exchange membrane fuel cells. *International Journal of Hydrogen Energy*, 2023, 48, pp.3593 - 3631. 10.1016/j.ijhydene.2022.10.177 . hal-03867056

HAL Id: hal-03867056

<https://hal.science/hal-03867056>

Submitted on 15 Mar 2023

HAL is a multi-disciplinary open access archive for the deposit and dissemination of scientific research documents, whether they are published or not. The documents may come from teaching and research institutions in France or abroad, or from public or private research centers.

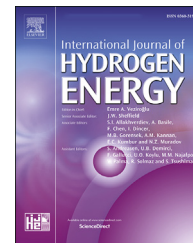
L'archive ouverte pluridisciplinaire **HAL**, est destinée au dépôt et à la diffusion de documents scientifiques de niveau recherche, publiés ou non, émanant des établissements d'enseignement et de recherche français ou étrangers, des laboratoires publics ou privés.



ELSEVIER

Available online at www.sciencedirect.com

ScienceDirect

journal homepage: www.elsevier.com/locate/he

Review Article

Recent progress in heteroatom doped carbon based electrocatalysts for oxygen reduction reaction in anion exchange membrane fuel cells



Rambabu Gutru ^{a,b,c,*}, Zarina Turtayeva ^b, Feina Xu ^b, Gaël Maranzana ^b, Ravikumar Thimmappa ^c, Mohamed Mamlouk ^c, Alexandre Desforges ^a, Brigitte Vigolo ^a

^a Université de Lorraine, CNRS, Institut Jean Lamour, F-54000, Nancy, France

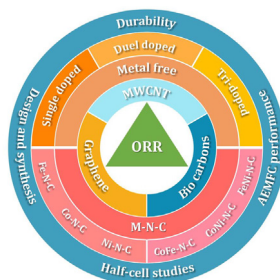
^b CNRS-Université de Lorraine UMR 7563, F-54504, Vandoeuvre-lès-Nancy, France

^c School of Engineering, Newcastle University, Newcastle Upon Tyne, NE1 7RU, UK

HIGHLIGHTS

- Overview of oxygen reduction reaction principle and mechanism.
- Design and development of heteroatom doped carbon based electrocatalysts.
- Half-cell studies of various heteroatom doped electrocatalysts.
- AEMFC performance of heteroatom doped carbon catalysts.
- Overview on the stability of heteroatom doped electrocatalysts.

GRAPHICAL ABSTRACT



ARTICLE INFO

Article history:

Received 22 August 2022

Received in revised form

6 October 2022

Accepted 19 October 2022

Available online 15 November 2022

Keywords:

Oxygen reduction reaction

AEMFC

Heteroatom doped carbon

Non-precious catalysts

ABSTRACT

Oxygen reduction reaction (ORR) is a key step in many electrochemical devices such as fuel cells and metal-air batteries. However, the reaction proceeds at a significant overpotential requiring Pt-based catalysts. The scarcity and economical challenges associated with Pt is one of the major limitations for the commercialization of the devices. In this context, the electrochemical research community is constantly exploring other low-cost and earth-abundant materials as ORR catalysts. Carbon nanomaterials are identified as promising electrocatalysts due to their superb electronic conductivity together with high specific surface area. However, the low reactivity of carbon is the major limiting factor in the fabrication of ORR catalysts. Recent studies have proved that chemical modification of the carbon network (substitution of foreign atoms, Ex: N, S, B, F, P) could alter the reactivity of carbon nanomaterials for ORR. Many doping strategies have been proposed including single atom doping, co-doping and multi-atom doping. The heteroatom doped carbons

* Corresponding author. School of Engineering, Newcastle University, Newcastle Upon Tyne, NE1 7RU, UK.

E-mail address: rambabu.gutru@newcastle.ac.uk (R. Gutru).

<https://doi.org/10.1016/j.ijhydene.2022.10.177>

0360-3199/© 2022 The Author(s). Published by Elsevier Ltd on behalf of Hydrogen Energy Publications LLC. This is an open access article under the CC BY license (<http://creativecommons.org/licenses/by/4.0/>).

MWCNTs
Graphene and bio-waste derived
carbon

have delivered promising results towards ORR in alkaline media. This review presents a rational approach of doping methods and the electrochemical properties of heteroatom doped carbons, and we believe that this review could be a guiding material to design advanced non-noble catalysts for ORR in the coming future.

© 2022 The Author(s). Published by Elsevier Ltd on behalf of Hydrogen Energy Publications LLC. This is an open access article under the CC BY license (<http://creativecommons.org/licenses/by/4.0/>).

Contents

Introduction	3594
Oxygen reduction reaction in alkaline media	3594
General principle and mechanism of ORR in alkaline media	3595
Electrocatalysts for ORR in anion exchange membrane fuel cells	3598
Carbon nanotubes	3598
Graphene	3599
Bio-mass derived carbon	3599
Heteroatom doped carbon design and synthesis	3599
Nitrogen-doped CNTs	3601
Boron-doped CNTs	3605
Phosphorous-doped CNTs	3607
Co-doped CNTs	3607
Metal-nitrogen-doped CNTs	3610
Nitrogen-doped graphene	3611
Sulfur-doped graphene	3611
Phosphorus-doped graphene	3612
Co-doped/multi heteroatom doped graphene	3612
Metal, heteroatom co-doped graphene	3615
Bio-inspired ORR catalysts	3617
AEMFC performance and stability	3620
Conclusions and future prospective	3621
Declaration of competing interest	3623
Acknowledgements	3623
References	3623

Introduction

Oxygen reduction reaction (ORR) and oxygen evolution reactions (OER) play a critical role on the performance of electrochemical devices such as fuel cells, electrolyzers, and metal-air batteries [1]. In particular, for ORR which occurs at the cathode of fuel cells and the cathode of metal air-batteries during the discharge. On the other hand, OER occurs at the anode of the electrolyser during water splitting and the cathode of metal air batteries during the charging process. Fig. 1 shows the applications of oxygen electrocatalysis in various electrochemical devices. Considering, the importance of oxygen electrode reaction in afor esaid devices, there is an urgent requirement to fabricate high performance durable oxygen electrocatalysts. Currently, Pt-based catalysts are preferred for ORR [2], while IrO₂/RuO₂ are the state-of-art catalysts for OER [3,4]. However, these materials are scarce and expensive, limiting their widespread usage [5]. Alternatively, transition metal-based electrocatalysts are explored for ORR [6] and metal oxides/hydroxides are explored for OER [7–9].

Oxygen reduction reaction in alkaline media

As mentioned above, fuel cells are one of the most widely used electrochemical systems where the ORR catalysts have an important contribution in the overall performance. Although, a wide range of fuel cells exists; alkaline fuel cells have seen remarkable growth over the past decade due to the rapid development in anion exchange membrane (AEM) research [10–13]. The use of solid electrolyte minimizes the problem of electrolyte leakage and carbonate corrosion, also making the design of the system simple and compact [14,15]. The anion exchange membrane fuel cell (AEMFC) research is further geared up due to its intrinsic advantages namely improved reaction kinetics, wider choice of materials due to its high pH atmosphere [16,17]. In addition, fuel crossover is minimum in AEMFC configuration as the electro-osmotic drag is from cathode to anode [17,18]. Despite these inherent advantages of AEMFC, there are still some challenges in current AEMFC technology. Poor hydroxide conductivity, weak durability of AEMs, scarcity of robust

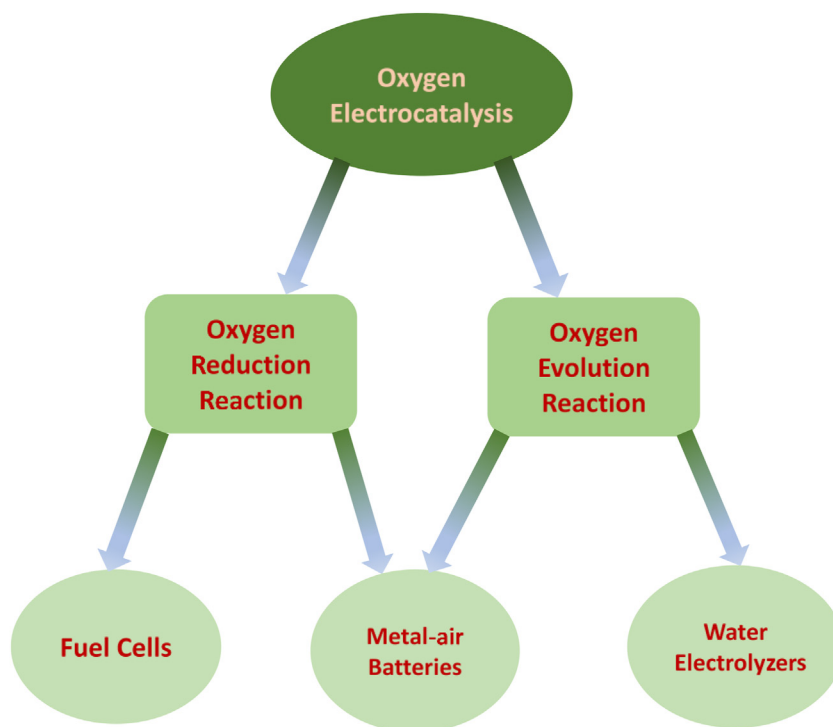


Fig. 1 – Classification of oxygen electrocatalysis and their applications in electrochemical devices.

electrocatalysts, lack of knowledge on operating conditions such as water management are some of them to name [19–21]. Potential application of AEMFC in the near future urgently requires to overcome these issues and to address open questions by the researchers. Electrocatalysis research particularly requires a great attention as the performance of membrane electrode assembly (MEA) is majorly influenced by the activity of the anode and cathode [22]. In other words, the hydrogen oxidation reaction (HOR) that occurs at the anode and the oxygen reduction reaction (ORR) at cathode side of MEA play a vital role towards the deliverable power output of any AEMFC system. Fig. 2 shows the AEMFC designed with anodic and cathodic reactions.

As deduced from many theoretical and experimental studies, among HOR and ORR in fuel cells, the later one is more sluggish as it is difficult to break the O–O bonds due to their high binding energy, 498 kJ mol^{-1} [23,24]. ORR is complicated involving multiple steps and intermediate reactions. On the other hand, HOR is relatively faster and straightforward. It is well established that the sluggish kinetics of ORR results in significant over potential and is the major contributor to the performance loss during the operation of the cell. Further, the sluggish kinetics of ORR demands higher amount of noble metal catalysts such as Pt, enhancing therefore the cost of the overall system [25,26]. The ORR can proceed either $2e^-$ or $4e^-$ path way and the later one is preferred due to the maximum energy output. In the $2e^-$ pathway, peroxide is produced as an intermediate product, leading not only to reducing the efficiency of the cell but also to accelerating the degradation of AEM and other cell components [27].

General principle and mechanism of ORR in alkaline media

As described above ORR is irreversible involving many absorption and desorption steps with multiple intermediates such as O, OH, HO^- , H_2O_2 . The absorption/desorption kinetics may vary with the nature of the electrolyte and catalyst used [28]. ORR starts with diffusion and adsorption of O_2 molecules on the surface of the electrocatalyst followed by electron

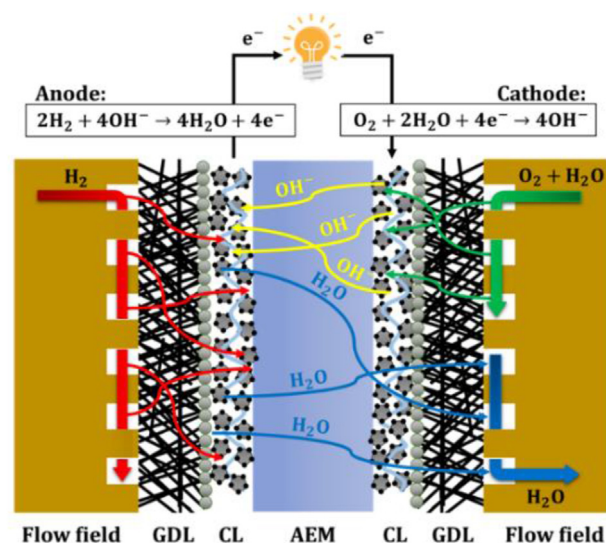


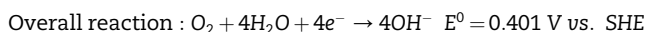
Fig. 2 – Schematic representation of AEMFC with its components.

transport from the electrode to the adsorbed O_2 and then breaking of the O–O bonds and removing the formed hydroxide ions to the solutions [29].

In alkaline media, ORR can proceed either by an associative mechanism in which there is competition between a $4e^-$ and a $2e^-$ process,

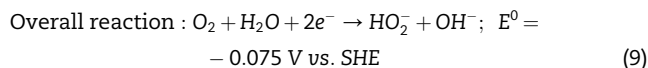
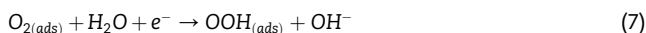


*Represents the surface active sites.



In this process, oxygen is reduced by $4e^-$ and consequently $4 OH^-$ are produced.

On the other hand, ORR can also follow a $2e^-$ pathway producing peroxide ions.



Owing to the low solubility of O_2 in aqueous solutions, a robust technique such as rotating disk electrode (RDE) which involves the forced transport of reactants is commonly employed to measure the ORR activity of a given catalyst. RDE consists of a disk electrode of a certain diameter which acts as a support to the catalyst and is connected to a shaft that controls the rotating speed (Fig. 3(a)). Generally, the catalyst is coated on the disc (Ex: glassy carbon) to form a thin film. This thin film is tested using linear sweep voltammetry (LSV) to confer various experimental indicators (Onset potential (E_{onset}), half-wave potential ($E_{1/2}$), and limiting current density (j_L) for the ORR activity of the catalyst as shown in Fig. 3(b). E_{onset} is defined as the potential where the ORR current starts to increase sharply. Limiting current density is defined as the maximum ORR current where the saturation is reached, $E_{1/2}$ is the potential measured at half of the limiting current.

These RDE measurements are performed in a standard three-electrode system containing a reference and counter electrode controlled (RDE being the third electrode in the system) by an electrochemical workstation. Koutecky Levich (K–L) equation is used to correlate the measured electrochemical and hydrodynamic properties [30]:

$$\frac{1}{j} = \frac{1}{j_L} + \frac{1}{j_K} = \frac{1}{0.62nFC_0(D_0)^{2/3}v^{-1/6}\omega^{1/2}} \quad (10)$$

where j_L , j_K are diffusion and kinetic limiting current density, respectively, ω is the angular velocity (rad./s), n electron

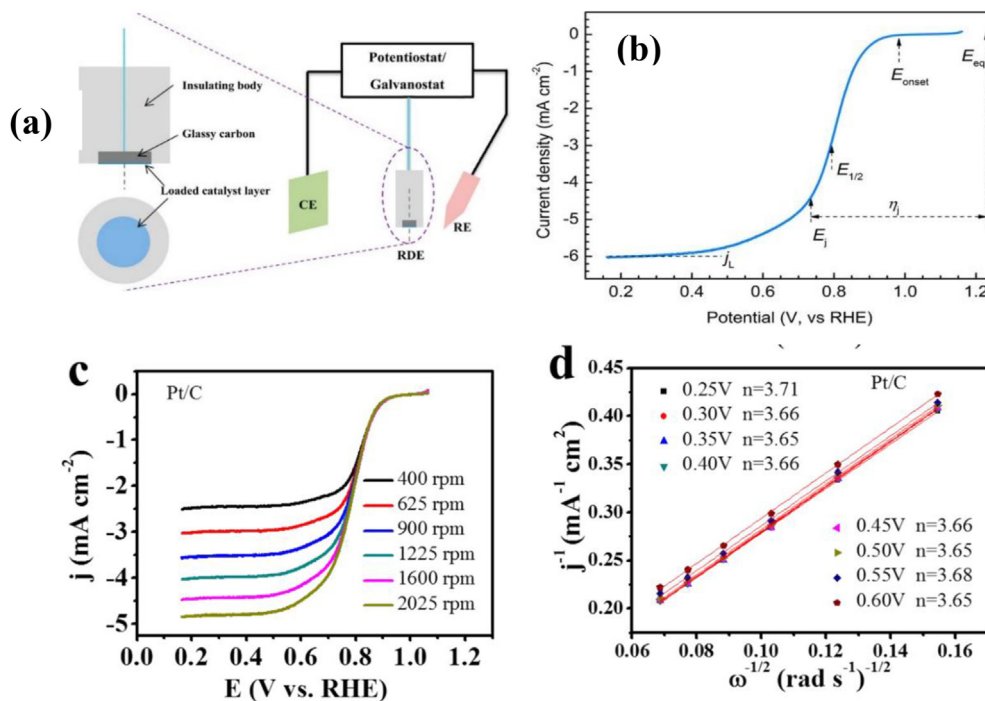


Fig. 3 – Schematic view of RDE testing setup in a three-electrode configuration (b) typical LSV curve recorded from RDE at rotating speed of 2000 rpm, (c) LSV curves recorded with RDE from 400 to 2500 rpm in O₂ saturated 0.1 M KOH for Pt/C catalyst and (d) corresponding K-L plots and electron transfer number, reproduced with permission from Refs. [31,32].

transfer number, C_0 and D_0 are the bulk concentration and diffusion coefficient of O_2 in the electrolyte, ν is the kinematic viscosity of the electrolyte and k is the electron-transfer rate constant. K-L plots are derived by measuring current density at different potentials with respect to rotation rates typically (400–2400 rpm) (Fig. 3(c)) and then plotting the inverse of current density (j^{-1}) against the inverse square root of angular velocity $\omega^{-1/2}$ as shown in Fig. 3(d) and the slope of the K-L plots are used to calculate the electron transfer number.

Another advanced technique named rotating ring disk electrode (RRDE) (Fig. 4(a)) is used to estimate the reaction intermediates and the ORR kinetics simultaneously. RRDE has a coaxial ring electrode in addition to disk electrode to detect the formation of these intermediates. The Pt ring of RRDE is set at a particular potential of 1.3–1.5 V vs. RHE in an alkaline electrolyte. Fig. 4(b) shows the typical RRDE curve obtained for 40% Pt/C on glassy carbon (GC) based disc and Pt ring. Extent of intermediates such as hydrogen peroxide yield and electron transfer number can be calculated from RRDE results directly, which is an added advantage compared to RDE measurements.

$$\text{Peroxide yield : } \% (H_2O_2) = 200 \times \frac{I_{R/N}}{I_D + I_{R/N}} \quad (11)$$

$$\text{Electron transfer number : } n = 4 \times \frac{I_D}{I_D + I_{R/N}} \quad (12)$$

Butler-Volmer equation is used to explain the η - j characteristics at equilibrium as represented below [33,34].

$$j = j_0 \left[\exp\left(\frac{a_a n F \eta}{RT}\right) \right] - \left(\frac{a_c n F \eta}{RT}\right) \quad (13)$$

As the oxygen electrode reactions are highly irreversible, it would be more appropriate to describe the oxygen reaction currents at higher over-potentials as below.

$$j_a = j_0 \exp\left(\frac{a_a n F \eta_a}{RT}\right) \quad (14)$$

$$j_c = -j_0 \exp\left(\frac{a_c n F \eta_c}{RT}\right) \quad (15)$$

Where the subscripts a,c represents anodic and cathodic, respectively.

Tafel slope b which is obtained by the Tafel equations is a reaction mechanism indicator, Tafel equations are semi logarithmic form of the above equations j_a and j_c .

$$\eta_a = \frac{RT}{nF a_a} \ln j - \frac{RT}{nF a_a} \ln j_0 = b \ln j - a \quad (16)$$

$$\eta_c = \frac{RT}{nF a_c} \ln j_0 - \frac{RT}{nF a_c} \ln j = a - b \ln j \quad (17)$$

Tafel plots are obtained by the applied potential and logarithmic of kinetic current density as represented below.

Generally, the slope of -60 mV/dec represents a pseudo two electron reaction as the rate determine step, whereas for the first electron reduction rate determining step the b value is observed as -120 mV/dec [37].

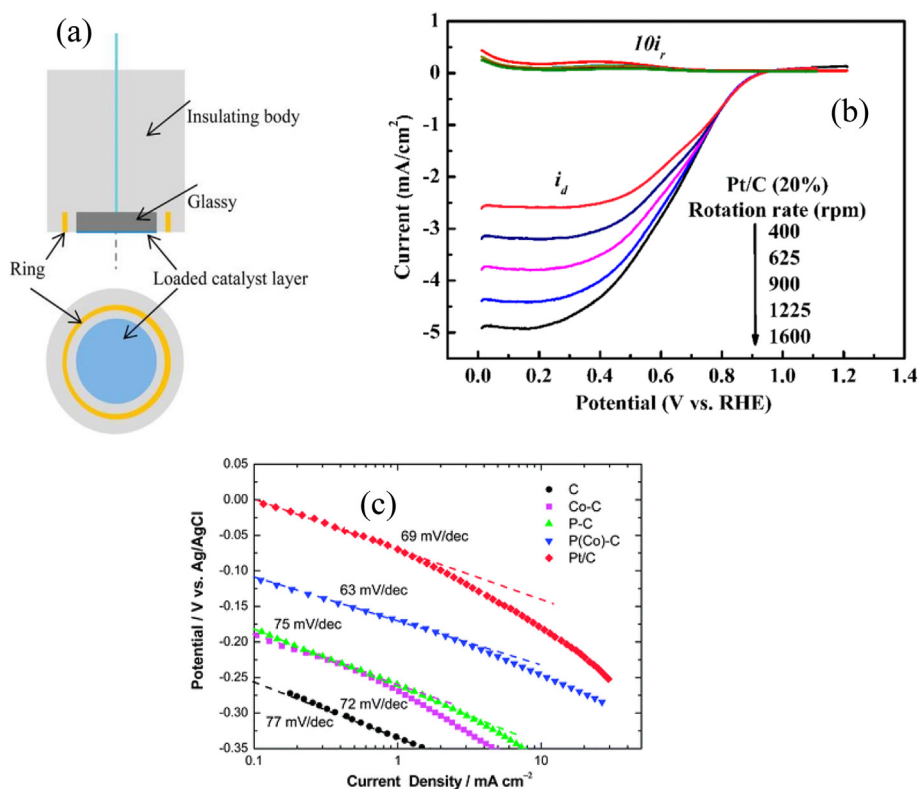


Fig. 4 – (a) Schematic view of RRDE and (b) ORR polarization curves measured using RRDE system at different rotation rates in 0.1 M KOH electrolyte saturated with O_2 , (c) Tafel plots various carbon based catalysts and Pt/C in O_2 saturated 0.1 M KOH at a rotating speed 1600 rpm. Reproduced with permission from Refs. [31,35,36].

Electrocatalysts for ORR in anion exchange membrane fuel cells

Realizing the importance of non-noble sustainable catalysts that can catalyze ORR through $4e^-$ transfer is the need of the hour and has huge potential opportunities as the ORR catalysts and play an important role in stabilizing the AEMFC performance. Many varieties of electrocatalysts have been already developed such as transition metal oxides [38], including perovskites [39], metal sulfides [40], metal organic framework (MOF) based catalysts [25]. Although the first row 3d elements such as Co and Fe and their derivatives show promising ORR activity competing with that of Pt. Their poor electronic conductivity and weak stability hinder their capabilities as best ORR catalysts. Nanocarbon based electrocatalysts are gaining significant interest in recent times due to their high electronic conductivity, diverse structures and their high surface area and porosity that can host large number of reactants. Nanocarbons have been derived from various earth abundant sources including bio-waste which is a unique opportunity, unlikely to be with other class of electrocatalysts. Moreover, the electronic conductivity is much better than transition metal-based electrocatalysts.

Among various carbon nanostructures carbon nanotubes (CNTs), graphene, bio-waste derived carbons are the major candidates widely used not only as electrocatalytic materials but also in various components of fuel cells such as additive in membranes [41–43], gas diffusion layers and bi-polar plates, thanks to their good electronic conductivity and robust mechanical stability [14,15]. As far as electrocatalysis is concerned, these materials have brought significant possibilities and revealed exciting opportunities to fabricate non-precious metal catalysts for various electrochemical reactions namely ORR and oxygen evolution reaction (OER). However, they were largely explored as ORR candidates as the OER involves significantly higher potentials above 1.4 V vs. RHE where these materials are likely to be unstable due to corrosion issues. Pristine nanocarbons however often suffer from low active sites and predominantly catalyze the ORR via $2e^-$ transfer which is not the purpose of their development. Hence several modification strategies have been proposed such as doping by heteroatoms in the carbon framework and coupling with various inorganic and organic nanomaterials. These modified nanocarbons with unique electronic structure have shown an accelerated electron transfer and mass transfer during ORR [16]. Regarding ORR, heteroatom doping of nanocarbons is largely considered and the resultant compounds with controlled physicochemical properties are beneficial to catalyze the ORR through $4e^-$ transfer [17].

In this review, we made an attempt to rationalize the various doping and co-doping strategies developed for CNTs, graphene and bio-waste derived carbon and their electrochemical properties towards ORR in alkaline medium.

Among the various types of carbon, CNTs, graphene and bio-waste derived carbon are widely explored for heteroatom doping and studied for ORR activity in alkaline media. Fig. 5 represents the number of articles published on these carbon based ORR catalysts during the last decade. A timely and dedicated review on these materials in terms of their ORR

application is interesting to not only for the fuel cell research community but also for the metal air battery (MAB) field. This review provides the concise and collective information about the challenges in ORR, material perspectives and methodologies. In addition, a brief description about ORR and experimental protocols to measure ORR activity are also discussed.

Although there are some reviews on the ORR catalysts, an updated and a dedicated review on CNTs, graphene and bio-sourced carbons is not found in the literature yet. Such review furnishes hence the opportunity to boost the challenging research activities of great importance for the technologies of the future.

Carbon nanotubes

CNTs are unique 1D structures formed with cylindrically rolled graphene sheets, both single-walled carbon nanotubes (SWCNTs) and multiwall carbon nanotubes (MWCNTs) represented in Fig. 6 have been widely explored as catalyst materials due to their high specific surface area, chemical stability along with excellent electronic conductivity. SWCNTs are single rolled graphene sheets having a diameter range of 0.5–12 nm with different tube lengths starting from a few micrometers depending on manufacturing and treatment techniques. MWCNTs consist of multi rolled layers of graphene inserted one into the others and the number of graphene walls may reach more than 25 walls with an interspacing of 0.34 nm. The outside diameter of MWCNTs ranges from 1 nm to 50 nm while the inside diameter is several nanometers. From a modification perspective, MWCNTs are convenient to modify and cheaper to produce in large quantities [44]. Despite these attractive properties, the electrochemical properties of CNTs were found to be disappointed due to surface inertness caused by delocalized π electrons. The electrochemical stability depends on the degree of graphitization. Heteroatom doping was particularly beneficial

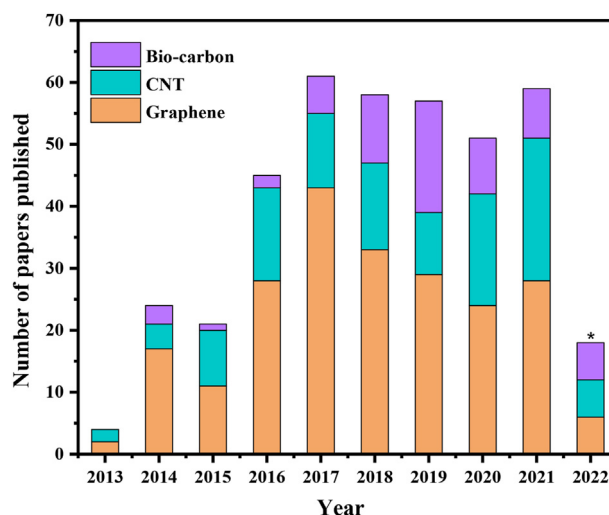


Fig. 5 – Number of articles published on heteroatom doped CNTs, graphene and bio carbons for ORR in alkaline medium. (*articles published until July 2022). (Source web of science using the key words: CNT, graphene, bio carbon, ORR, alkaline medium).

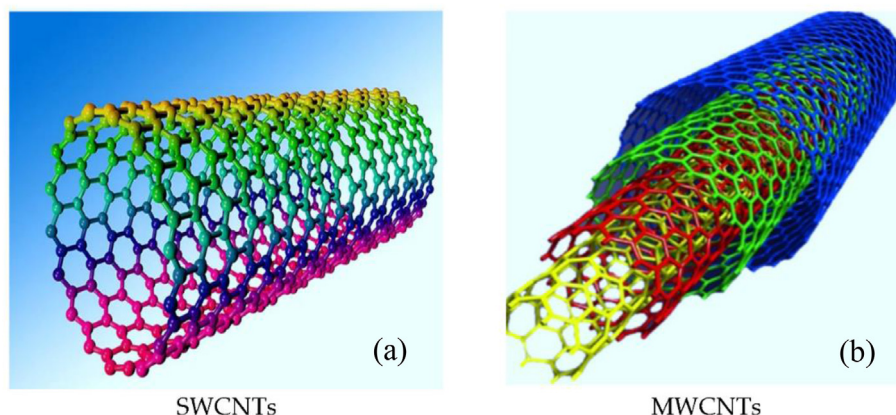


Fig. 6 – Structure of (a) a single wall carbon nanotube (SWCNT) and (b) a multi-wall carbon nanotube (MWCNT). Reproduced with permission from [45].

to change the electrical nature of carbon and numerous attempts have been made to prepare doped CNTs which alters the electronic structure of CNTs and makes them active for ORR. Table 1 summarizes the various hetero atom doped CNTs that are recently reported for ORR in alkaline media and their corresponding electrochemical properties.

Graphene

Since the discovery of graphene, the material research has taken a new outlook with fascinating properties of graphene such as electronic, surface, and mechanical properties. Electrocatalysis research is widely benefited from graphene and its derivatives. Graphene typically represents a single layer sp^2 carbon atoms arranged in a regular hexagonal pattern. Nevertheless, the term graphene is commonly used in the literature for its derivatives as well often multiple stacked layers [46]. In the beginning days of its discovery, it has been proposed as a good support for Pt based catalyst due to its good electrochemical stability and ability to distribute the nanoparticle uniformly to provide higher active area. Later, when the ORR research is turned towards Pt free catalyst, graphene and its derivatives have been considered as good candidates to replace Pt especially in alkaline media [47]. The high surface area together with its graphitic nature and its chemical tunability made it possible to derive several graphene-based electrocatalysts for ORR such as heteroatom doped graphene, metal-heteroatom doped graphene [48] which will be discussed in the following sections.

Graphene can be derived from many methods including exfoliation of graphite, CVD and pyrolysis as represented in Fig. 7(a) [49]. However, the modified Hummers' method was largely reported to synthesize graphene (Fig. 7(b)).

As far as metal free ORR catalysts are concerned, graphene has been identified as a standalone electrocatalyst. However, similar to other high surface area carbon nanomaterials, pristine graphene exhibited limited ORR activity showing selectivity of $2e^-$ ORR over $4e^-$ pathway which is undesirable. As in the case of MWCNTs, heteroatom doping was proposed to increase the ORR activity of graphene while benefitting from its other advantageous properties. In fact, graphene is

more suitable for heteroatom doping owing to its chemical reactivity and ease of tunability. Table 2 highlights the recent reports on hetero atom doped graphene for ORR in alkaline media.

Bio-mass derived carbon

Besides CNTs and graphene, electrocatalysts that derived from bio-waste have been another promising approach to fabricate a sustainable novel cathode for AEMFC as these materials are readily available and could be processed using thermal treatment [50]. Million tons of bio-waste from various sources such as animal waste, agricultural waste and human activities are produced worldwide every year. Thus converting biomass into electrocatalysts is a sustainable solution to develop large scale electrode materials also beneficial towards waste management [51,52]. Bio-waste majorly contains carbohydrates as building blocks so it can be a rich source of carbon. Depending upon the source and pyrolysis temperature, diverse morphologies can be obtained. In addition, various heteroatoms belong to intrinsic composition of the biomaterials hence upon the pyrolysis they transform into heteroatom-doped carbon matrix. Table 3 shows the various heteroatom doped carbons derived from bio-mass and their ORR properties in alkaline media.

Heteroatom doped carbon design and synthesis

In the beginning days, various types of carbon atoms have been used as support for the precious metals like Pt and Pd due to their high electronic conductivity, high surface and mechanical stability. Nanocarbons, especially, have been shown to increase the catalyst utilization through wide distribution of active centers and thus reduce the catalysts loading [53,54]. However, pristine nanocarbons are inferior to ORR activity due to the lack of electrocatalytic active centers. Later on, intensive efforts have been made to increase the ORR activity of these nanocarbons by structural and chemical modifications to modify their electronic structure. Among them, heteroatom doping with N, S, B, and P has been shown to be a

Table 1 – Varies heteroatom doped CNTs reported in the literature for ORR in alkaline media.

Catalyst	Doping method	Doped element (s) %	ORR onset potential (V)/	Half wave potential	Electron transfer number	Ref.
N-CNT	In-situ, alumina template	N-8 at%	−0.05 vs Ag/AgCl	NR	3.8	[65]
N-CNT	ball milling process	N – 3.1 at%	−0.159 V vs Ag/AgCl	NR	3.3	[67]
PN-ACNT	injection-assisted CVD method of TPP	P - 0.8 at% N - 2.9 at%	−0.09 V Vs Pt–C/GC electrode	NR	3.67	[77]
N-CNT	floating catalyst CVD method using ferrocene, pyridine or acetylene and argon	N - 3–6%	−0.22 V VS nonaligned CNT	NR	3	[94]
N-UCNT	pyrolysis of oxidized unzipped carbon nanotubes	N – 6.65 at%	−0.08 V vs N-CNT	NR	3.38	[95]
SN-CNT	by the pyrolysis of 65 N-doped CNTs with sulfur precursor.	S – 0.18 at% N – 3.02 at%	0.56 V vs Ag/AgCl	NR	3.4	[80]
B-MWCNTs	thermal annealing in boric acid	B – 1.51–2.37 at%	NR	NR	3.3	[71]
B - CNT	–	2.24 at%			2.5	[96]
BN-CNTs	direct synthesis or post-treatment methods	N – 1.39–1.57 at% B – 0.35–1.68 at%	NR	NR	NR	[97]
Co–N/MWCNT	wet impregnation and heat treatments	Co – 0.8 at% N – 6.7 at%	+0.55 V vs RHE	NR	NR	[98]
M/N-CNTs, M = Fe, Co, Ni	solid-state thermal reaction		Co/N-CNT 0.94 V Fe/N-CNT 0.96 V Ni/N-CNT 0.91 V	Co/N-CNT 0.84 V Fe/N-CNT 0.81 V Ni/N-CNT 0.73 V	Co/N-CNT 3.9 Fe/N-CNT 3.85 Ni/N-CNT 3.76	[99]
Fe-NCNT	pyrolysis of multi-walled carbon nanotubes in	N – 3.3 at% Fe – 1.6 at%	−0.12 V vs SCE		NR	[88]
Co-NCNT	pyrolysis of melamine formaldehyde	N – 8.04 at% Co – 0.58 at%	0.874 V vs RHE	0.041 V vs RHE	3.7	[100]
CNT@Fe-N-PC	one-step pyrolysis.	N – 5.5 at% F – 0.3 at%	+0.06 V vs RHE	0.82 V vs RHE	4	[101]
Co–N-CNT/Fe–N-CNT	synthesized by pyrolysis of MWCNT	Co–N-CNT: N – 2.2 at% Co – 0.3 at% Fe–N-CNT: N – 2.7 at% Fe – 0.2 at%	Co–N-CNT: 0.09 V vs Ag/AgCl Fe–N-CNT: 0.04 V vs Ag/AgCl	Co–N-CNT: −0.22 V vs Ag/AgCl Fe–N-CNT: −0.43 V vs Ag/AgCl	Co–N-CNT: 3.4 Fe–N-CNT: 3.6	[102]
Fe _x N-MWCNT	carboxylic functionalization	N – 4.39 at% Fe – 0.24 at%	1.0 V vs RHE	0.91 V vs RHE	4	[103]
CN _x /CB _x -GNR	thermal annealing in ammonia and boron oxide	N – 11.1 at% B – 11.3 at%	−0.08 V vs Pt/C	NR	3.91	[104]
N–F/GNFs	synthesized using melamine and ammonium fluoride as	N – 13 at% F – 1.1 at%	−0.018 V vs Pt/C	+0.08 V vs N/GNF +0.05 V vs F/GNF −0.14 V vs Pt/C	4	[105]
B _x CNT-NH ₃	CVD using TPB, benzene, and ferrocene, then thermal treated in NH ₃	B 0.84–1.93 at% N 0.58–2.19 at%	−0.31 V	NR	2.5	[82]
NCNTs	scalable floating catalyst method	N – 4.1%	0.96 V vs RHE	0.78 V vs RHE	3.92	[106]
PCNT	direct hydrothermal treatment of a CNT-H ₃ PO ₄ mixture at	P – 1.66 at%	−0.2 V vs Hg/Hg ₂ Cl ₂	NR	2.6	[76]

FeMn/N-CNT	Ex-situ Pyrolysis of MOF-74	N-6.43 at % Fe-0.24 at % Mn-0.47 at % Zn - 5%	0.96 vs RHE	0.865 V vs RHE	3.95	[92]
Co5-N-C	direct carbonization of bimetal-organic framework CoxZn100-x(adennate) 4(biphenyl)dicarboxylate)6		0.99 V vs RHE	0.86 V vs RHE	NR	[107]
SNW-Fe/N/C	carbonization at high temperature	C - 89.3% N - 3% O - 6.1% Fe - 1.6%	1.10 V vs RHE	0.944 V vs RHE	NR	[108]

B - CNT (Boron doped CNTs), N-CNT (Nitrogen doped CNTs), PN-ACNT (Phosphorus and Nitrogen doped Vertically Aligned Carbon Nanotube Arrays), SN-CNT (Sulfur and Nitrogen co-doped Carbon Nanotubes), B-MWCNTs (boron doped CNTs), BN-CNTs (B and N doped Carbon Nanotube), Co-N/MWCNT (Cobalt and Nitrogen doped CNT), N-UCNT (nitrogen-doped unzipped carbon nanotubes), N-CNT (N-doped carbon nanotubes), M/N-CNTs, M = Fe, Co, Ni (transitional metal nanoparticles encapsulated in nitrogen-doped carbon nanotubes) Fe-NCNT (iron-containing nitrogen-doped carbon nanotubes), Co-NCNT (cobalt-incorporated nitrogen-doped CNTs), NMWCNT & OMWCNTs and (oxygen- and nitrogen-functionalized multi-walled carbon nanotubes), CNT@Fe-N-PC (N-doped CNT with high concentration iron atoms), Co-N-CNT/Fe-N-CNT, Fe,N-MWCNT (Fe and N codoped multi-walled carbon nanotubes), CNx/CBx-GNR (nitrogen/boron co-doped graphene nanoribbons), N-F/GNFs (Nitrogen and fluorine co-doped graphite nanofibers), BxCNT-NH3 boron and nitrogen co-doped carbon nanotubes, NCNTs (Nitrogen-doped carbon nanotubes), PCNT (porous phosphorus-doped carbon nanotubes), FeMn/N-CNT, Co5-N-C (Cobalt N-doped porous carbon) SNW-Fe/N/C (N-doped carbon materials with transition metals).

successful strategy to change the electron distribution of dopant and adjacent carbons due to the difference between the size and the electronegativity of carbon and those of the heteroatoms. Constructing defects in carbon framework are also shown to influence the physicochemical properties substantially.

Several methods have been explored for the fabrication of heteroatom doped carbons (Fig. 8), and these methods are mainly classified into two: (i) *in-situ* doping during or (ii) post-synthesis doping. For the *in-situ* approach, the precursor or source of the chosen heteroatom is added into the synthesis process of carbon, where the formation of the graphitic lattice is observed with the direct bonding between the heteroatom and carbon. CVD, hydrothermal, sol-gel, templating, high temperature pyrolysis are commonly employed methods to prepare *in-situ* doped carbon materials. However this method has some bottle necks such as the density of the formed catalysts which is not high enough and the synthesis procedure is not easily controlled and further requires sophisticated equipment. In the *ex-situ* method, the heteroatom precursors are mixed with pre synthesized carbon (MWCNT/graphene/bio-carbon) and annealed at high temperatures. For example, melamine, boric acid are the commonly used precursors for N doping and B doping, respectively. In the *ex-situ* approach, most of the heteroatoms are on the surface and few of them enter into the carbon framework. This is the reason why the resultant catalysts exhibit low heteroatom content, in addition the other bottle neck is their ponderous procedures.

Nitrogen-doped CNTs

Owing to the similar atomic size of nitrogen and carbon which prevents lattice distortion of the carbon nanomaterials, N doping in the sp^2 carbon network is the most explored approach among all other heteroatom doping methods [59]. The N doping in carbon framework induces a positive charge on neighboring carbons due to the large difference in their respective electronegativity values (3.07 for N and 2.55 for C). The positively charged carbons could easily act as an electron donors to the oxygen molecule (O_2) to improve its dissociative adsorption. After the pioneering work by Kuanping Gong et al. in 2009 [60] that revealed excellent ORR properties of vertically aligned N doped CNTs prepared from the pyrolysis of iron(II) phthalocyanine, numerous studies have reported the use of NCNTs as metal-free catalyst for ORR in alkaline electrolyte. Subsequently, various nitrogen sources such as ethylenediamine (EDA), pyridine (Py), poly aniline have been explored for *in-situ* N doping during the growth of CNTs. In addition, melamine, urea and NH_3 vapors were used as post synthesis precursors, depending upon the nature of source, concentration of doping is affected and thus ORR activity. Zhu Chen et al. synthesized NCNTs using EDA and pyridine (Py) as the nitrogen sources in presence of ferrocene using CVD technique [61]. The concentration of nitrogen in NCNTs was 5.58, 3.41 at.% when used EDA and pyridine as N source, respectively. Coming to ORR activity, EDA treated NCNTs were found to be more active which shows a limiting current 3 times than the Py-NCNTs and better half wave potential and onset potentials along with better electron transfer and these results are directly correlated to nitrogen content. It is established

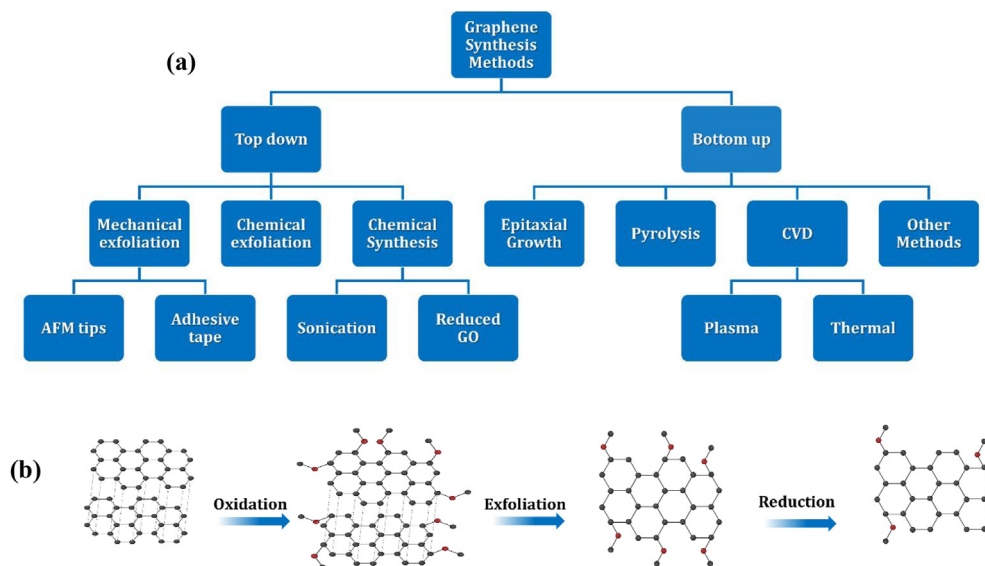


Fig. 7 – (a) Classification of graphene synthesis methods (b) Chemical synthesis method for graphene from graphite. Reproduced with permission from Ref. [49].

that the ORR activity of NCNTs are directly related to the nitrogen content, efforts have been made to increase the nitrogen doping level by exploring the variety of methods/precursors. Using floating catalyst CVD method, NCNTs were obtained with 8.6 at.% of N from the mixture of ethylene and melamine [62]. The ORR activity of this NCNT is very much similar to that measured with Pt/C in alkaline media. Although, it is believed that the total nitrogen content is responsible for the ORR activity on NCNTs, but later the researchers tried to establish the relationship between the different configurations of nitrogen and ORR activity. N doping of carbon sp^2 network results in different type of nitrogen-containing groups: namely pyridinic, pyrrolic, quaternary (or graphitic) and pyridinic-N-oxide. Fig. 9 shows these nitrogen-containing functional groups and their binding energy deduced from XPS investigations.

It is highly debatable point that which of these four configurations is actually responsible for ORR activity on N-doped carbons. The recent literature reports suggests that pyrrolic N and N-oxide are least responsible for ORR activity, contrary, graphitic N and pyridine N are active for ORR due to their favorable electronic structure for the splitting of O–O bond [64]. Various studies have reported the synthesis of NCNTs with different pyrrolic, pyridinic and graphitic N content by changing the pyrolysis temperature (Fig. 10a–d). For example, NCNTs synthesized from poly(2-methyl-1-vinylimidazole) by alumina template method [65], has 4.6 at.% of pyridinic N, 0.2 at.% of pyrrolic N and 3.3 at.% of graphitic N. RDE studies revealed that these NCNTs had comparable ORR activity in alkaline electrolyte with $4e^-$ transfer. The ORR activity of NCNTs was attributed to multiple factors such as improved electrical conductivity due to conjugation effect and improved work function. Based on these observations, it was proposed that increasing graphitic N, pyridinic N and decreasing pyrrolic N is the best strategy to get maximum ORR activity as shown in Fig. 10 (e) and further this was also proved by DFT

calculations [66]. In addition to the *in-situ* doping, it was well established that, the N doping can also be achieved using post synthesis doping. Thermal annealing of CNTs with nitrogen rich precursors (melamine, urea, ammonia, dicyandiamide etc.) at temperatures 100–600 °C could potentially result in NCNTs. As mentioned above, the overall nitrogen content and its configurations changes with the precursor. It was reported that melamine is a potential nitrogen precursor compared to urea to get maximum pyridinic/graphitic N. Under similar conditions, melamine treated CNTs showed 43% higher pyridinic/graphitic N compared to urea treated CNTs [67]. Consequently, NCNTs derived from melamine showed lower ORR over-potential (393 mV) compared to the NCNTs derived from urea (424 mV). Similarly, it was reported that 60% of higher N content was found in NCNTs derived from cyanamide compared to the NCNTs derived from dicyandiamide [68]. In the total N content, pyridinic-N constitutes 59 at.%, quaternary-N 16 at.% and pyrrolic-N 25 at.% in case of DCDA sourced NCNTs while for cyanamide sourced NCNTs it was pyridinic-N 54 at.%, quaternary-N 13 at.% and pyrrolic-N 33 at.%. And among these two prepared NCNTs, the former showed higher ORR activity despite lower N content than the later highlighting the strong dependence of ORR activity on the nitrogen configuration rather than the total nitrogen content. These results further confirmed that the choice of N precursor plays a key role in delivering outstanding ORR properties of NCNTs. The presence of these configuration on the sample depends on pyrolysis temperature. Thermal annealing of polyaniline and CNTs at 600 °C resulted high amount of pyrrolic N while annealing at 700 °C resulted high pyridinic and graphitic N [64]. However better ORR activity was found for the NCNTs obtained at 700 °C. It was explained by the maximum concentration of pyridinic/graphitic N concentration which are reported to be ORR active species while the pyrrolic N was reported to be ORR inactive which was predominant in NCNTs obtained at 600 °C as shown in

Table 2 – Varies heteroatom doped graphene based catalysts reported for ORR in alkaline media.

Catalyst	Doping method	Doped element (s)	ORR onset potential (V)/	Half wave potential	Electron transfer number	Ref.
N-RGO	facile, catalyst-free thermal annealing approach in	N-10.6 at.%	−0.25 V vs commercial Pt/C electrode	NR	3.7	[156]
N-Gr	thermal exfoliation method	NR	−0.12 V vs Ag/AgCl	0.032 V vs SCE	3.2	[110]
N-Gr	Synthesizing of graphene oxide (GO)/melamine gel mixture	N – 2.48 at.%	−0.07 V vs Pt/C	NR	NR	[157]
N-RGO	hydrothermally synthesizing of graphite oxide (GtO) and melamine	N – 4.7%	−0.155 V vs Ag/AgCl	NR	3.28	[158]
N-rGO	one-step doping procedure	N – 12.9 at.%	0.88 V vs RHE	0.76 V vs RHE	3.66	[117]
N-Gr	Pyrolysis of FeCl ₃ and cyanamide	N – 4.0% N – 12.0%	0.47 V vs Ag/AgCl	NR	3.82	[140]
N-Gr	mild tip-ultrasonic method	N – 2.38%	0.73 V vs. RHE	NR	3.2	[159]
N-rGO	electrochemical doping method	N – 6.8 at.%	−0.19 V vs Ag/AgCl	NR	3.4	[111]
NGS	carbonization of chitosan film deposited on g-C3N4 nanosheets	N – 4.12%	0.98 V vs RHE	NR	3.5	[160]
N-pGF	heat treatment	N – 6.63 at.%	−0.19 V vs Ag/AgCl	−0.064 V vs Ag/AgCl	3.9	[119]
N-MG	hydrothermal treatment	N – 2.8 at.%	0.93 V vs RHE	NR	NR	[161]
Fe3O4/N-GAs	hydrothermal self-assembly and thermal treatment	Fe ₃ O ₄ – 46.2 wt% N - 3.5 wt%	−0.19 V		3.72	[162]
S-graphene	directly annealing graphene oxide (GO) and benzyl disulfide (BDS) in argon	S-1.35 wt% -	−0.8 V vs Pt/C catalyst	NR	3.82	[127]
N/S-G	synthesized and sequential thermal annealing	N – 1.02 at.%, S – 1.32 at.%	+0.09 V vs other N/S - G	−0.093 V vs other N/S - G	3.47	[131]
NSG	synthesized by a simple two-step method	N – 9.05 at.%, S – 1.65 at.%	0.06 V vs Ag/AgCl	NR	4	[163]
3D S-GNs	heat treatment	S – 12.8 wt%	1.0.1 V vs 3D GNs	NR	3.51	[128]
Fe–N-graphene	simple and scalable synthesis	N – 0.86–6.8 at.%, Fe – 1.05–2.57 at.%	0.07 V vs N-graphene 0.08 V vs Pt/C	NR	3.99	[164]
Co/NrGO	thermal treatment	N – 3.68 wt%, Co – 10 wt%	−0.06 V vs Pt/C	NR	≈4	[146]
Fe/N/graphene	thermal treatments	N – 3.5 wt%, Fe – 1.4 wt%	0.98 V	0.83 V	3.9	[148]
FePc/ERGO	electrochemical reduction	N – 4.0 at.%	+0.045 V vs Pt/C	NR	3.94	[165]
EA-SFeNG	synthesized via facile ball milling and followed by pyrolysis process.	NR	1 V vs RHE	0.848 V vs RHE	3.81	[166]
Co/N–C -graphene hybrid	one-step pyrolysis of cobalt nitrate, sucrose and urea	Co – 0.47 at.%	−0.069 V vs SCE	−0.02 V vs Pt/C	3.3	[139]

(continued on next page)

Table 2 – (continued)

Catalyst	Doping method	Doped element (s)	ORR onset potential (V)/	Half wave potential	Electron transfer number	Ref.
Co ₃ O ₄ /NSGF	hydrothermal method	S – 3 at.% N – 0.6 at.% Co – 4.1 at.%	0.46 V vs SCE	0.034 V vs. SCE	4	[167]
Co–N–GA	hydrothermal method	RH	0.88 V vs RHE	0.73 V vs RHE	3.75	[168]
LaNiO ₃ /N,S-Gr	synthetization	N – 4.4 at.% S – 3.5 at.%	–0.05 V vs Ag/AgCl	–0.18 V vs Ag/AgCl	3.7	[169]
Gr-FePc	Modified Hummers' method	FePc – 50 wt%	NR	+0.05 V vs Pt/C catalyst	3.96	[170]
CoO–rGO(N)	incorporating CoO onto nitrogen-doped reduced graphene oxide	Co – 6.88 at.% C – 72.85 at.% N – 4.03 at.% O – 16.24 at.%	+0.95 V vs Co ₃ O ₄ /(N-rmGO) and MnCo ₂ O ₄ /N-rmGO	0.83 V vs Co ₃ O ₄ /(N-rmGO) and MnCo ₂ O ₄ /N-rmGO	3.75	[171]
PGF-Fe-NBP	hard- templating method	P – 0.43 at.% Fe – 0.3 at.% B – 17.52 at.% N – 13.12 at.%	0.95 V vs RHE	0.84 V vs RHE	3.8	[172]
Co ₄ N/NG	One step synthesis	Co – 5 at.%	0.91 V vs RHE	0.77 V vs RHE	3.6	[144]
Fe-WO ₃ NF/NG)	one-step thermal treatment	W – 1.01 at.% Fe – 0.96 at.% N – 6.8 at.%	0.98 V vs	0.85 V vs	3.97	[173]
MnO/Co–N-G (MnO/Co	carbonization process	N – 1.91 at.% Mn – 0.34 at.% Co – 0.32 at.%	NR	–0.116 V vs Hg/HgO	3.89	[174]
Fe ₃ Co@NG-C	synthesis of a NPME composed of Fe ₃ Co alloy nanoparticles encapsulated	N – 6.1 at.%	1.067 V vs RHE	0.886 V vs RHE	3.9	[175]
FN ₃ SG	pyrolyzing cheap, nontoxic, and eco-friendly	S – 0.95 at.% F – 1.09 at.% N – 6.39 at.%	0.988 V vs RHE	0.803 V vs RHE	3.97	[137]
FePc-33/N-GP950	pyrolysis under NH ₃ atmosphere	N – 1.7 at.%	0.97 V vs RHE	0.89 V vs RHE	NR	[147]
Cu@NG	thermal decomposition proces	Cu – 0.82 wt %	0.94 V vs RHE	0.84 V vs RHE	4	[176]
Co@NG	facile annealing strategy	Co – 1.3 wt%	0.97 V vs RHE	0.87 V vs RHE	4	[143]
Al–N-Gr	thermal annealing treatment	Al – 0.53 at.% N – 8 at.%	0.99 V vs RHE	0.86 V vs RHE	3.9	[177]
P-CD/Gr	biomass-deriving method	P – 2.31 at.%	NR	NR	3.87	[130]
BNr-GO	synthesized using a modified Hummer's method	N – 0.6% B – 1.4%	0.84 V vs RHE	0.77 V vs RHE	3.93	[135]
B–F-rGO and N–F-rGO	high temperature pyrolysis method	NR	B–F-rGO 0.8 V vs RHE N–F-rGO 0.78 V vs RHE	NR	B–F-rGO 3.54 N–F-rGO 3.41	[134]
Fe ₃ C@Fe/N-	polymerization of dopamine on GO and thermal annealing in Ar	Fe – 6.24 wt%	0.003 V vs Pt/C	NR	3.6	[149]

N-Co-Mo-GF/CNT	one-step catalytic chemical vapor deposition method to	Co – 4.96 wt% Mo – 1.65 wt% N – 1 at. %	0.9 V vs RHE	+0.05 V vs RHE	4	[178]
Co/NCNTs/NS	pyrolysis of Co/Zn-MOF nanosheets.	N – 11.67 wt%	–0.04 V vs RHE	0.78 V vs RHE	3.88	[179]
PG	scalable thermal annealing method of PG using GO and TPP	P – 1.81 at%	0.92 V vs G and Pt/C	NR	3	[129]

N-RGO (Nitrogen-reduced-graphene oxide), NG (Nitrogen-Doped Graphene), Fe₃O₄/N-Gas (Nitrogen-Doped Graphene Aerogel-Supported Fe₃O₄ Nanoparticles), S-graphene (Sulfur-Doped Graphene), g-FePc (graphene-iron phthalocyanine), CoO-rGO(N)(cobalt oxide (CoO) on nitrogen-doped reduced graphene oxide, 3D S-GNs (sulfur-doped graphene networks), Fe-N-graphene (N-self-doped graphene-based non-precious Fe catalyst), N-MG (Nitrogen-Doped Mesoporous Graphene), Co/NrGO (Cobalt-incorporated nitrogen-doped reduced graphene oxide), Fe/N/graphene FePc/ERGO (iron phthalocyanine (FePc) functionalized electrochemically reduced graphene oxide (ERGO)), EA-SFeNG (An edge activated S doped Fe-N-graphene), Co/NeC hybrid (N-doped graphene modified with Co nanoparticle), NG (Nitrogen Doped Graphene), Co₃O₄/NSGF (cobalt oxide-Nitrogen and sulfur dual-doped graphene), Co-N-GA Catalyst (Co-N Decorated Hierarchically Porous Graphene), LaNiO₃/N, S-Gr (LaNiO₃ stabilized nitrogen and sulfur co-doped graphene) N/S-G (Nitrogen/sulfur-doping of graphene), NSG (nitrogen and sulfur co-doped graphene nanosheets), N-pGF (pyridinic-N-doped graphene film), PGF-Fe-NBP (Porous B, N, P and Fe-doped Graphene Foams, Co₄N/NG (Co₄N/nitrogen-doped graphene)iron tungsten oxide nanoflower anchored, nitrogen-doped graphene (Fe-WO₃ NF/NG), MnO/Co-N-G (MnO/Co nanoparticles encapsulated in nitrogen-rich graphene nanosheets), Fe₃Co@NG-C (nitrogen-doped graphene layers encapsulating Fe₃Co nanopar-ticles), NrGO (Nitrogen doped reduced graphene oxide), FN₃SG (N, F, and S tri-doped porous graphene), FePc-33/N-GP950 (FePc onto nitrogen-doped graphene), NGS (porous nitrogen-doped graphene layers), Cu@NG (Cu- and N-codoped graphene), Co@NG (Co/N codoped graphene catalyst), ANG (Al and N codoped graphene), P-CD/G (P-doped carbon dot/graphene), BNr-GO (edge-enriched graphene with boron and nitrogen), Phosphorus- Graphite Layers, B-F-rGO and N-F-rGO (fluorine (F) boron (B) or nitrogen (N) doped on rGO), Fe₃C@Fe/N-graphene (iron carbide (Fe₃C) supported on nitrogen-doped carbon), N-Co-Mo-GF/CNT (graphene nanoflakes (GFs) and CNTs doped with N, Co, and Mo heteroatoms), Co/NCNTs/NS (N-doped carbon nanotube arrays on 2D MOFs-derived nanosheet), PG (Phosphorus-Doped Graphene).

Fig. 10(a). Similarly, thermal annealing of CNTs under NH₃ [63] at low temperature (500–700 °C), predominantly resulted in pyrrolic and pyridinic type N species in NCNTs while at temperatures as high as 800 °C, quaternary and pyridinic N-oxide are also incorporated. The maximum ORR activity was, in that case, obtained for NCNTs bearing higher content of quaternary N species.

Besides varying the temperature, there are other parameters such as tube length, diameter and the nature of the precursor making it difficult to selectively introduce N functionalities. A different approach was proposed by Tiva Sharifi et al. [69] who have not focused their work on controlling N species type during the growth of NCNTs but converted a particular type of N-functionality into another type from already synthesized NCNTs by post thermal treatment (Fig. 10f and g).

It was reported that thermal treatment of NCNTs at 1000 °C in the N₂ atmosphere produced the most active ORR catalyst and the activity of NCNTs was correlated to the quaternary N valley sites while quaternary N center and pyridinic N contributed to lower the onset potential and similar results were obtained by Lai et al. for N doped graphene [70]. By rationalizing these literature reports, one needs to understand that the ORR activity of NCNTs is influenced by the several parameters such as the method of doping (*in-situ/ex-situ*), type of N source, pyrolysis temperature and quantity of particular nitrogen functionality present in NCNTs.

Boron-doped CNTs

Boron also has closer atomic size that of carbon and just an electron less than the nitrogen, hence its substitution in carbon network is also feasible without changing the structure of the original carbon material. However, contrary to nitrogen, boron is an electron deficient atom and the electronegativity difference between B and C is much higher than that of N and C. As a result, incorporation of B in the carbon π conjugated system could transform the electron deficient B to an electron donor. Moreover, owing to the fact that O₂ adsorption is likely to occur on the positively charged species [71], the electron deficient B could be a promising guest for O₂ adsorption which is the primary condition in the ORR process [72]. Inspired by the excellent results demonstrated for NCNTs, many efforts have been made to fabricate boron doped CNTs and explore its ORR activity. Similar to NCNTs, boron doped CNTs can also be obtained by CVD method where the carbon and boron precursor were mixed in presence of a catalyst. For example, CVD of benzene and triphenyl borane (TPB) in presence of ferrocene had resulted the boron doped CNTs with maximum of 2.24 at.% of boron [72]. On the other hand, similar doping level of boron (2.37 at.%) was achieved by post synthesis doping through thermal annealing of CNTs with boric acid in inert atmosphere at 1000 °C [71]. It was established from XPS results that boron substituted in carbon lattice exhibits different bonding configurations such as B₃C, B₄C, BCO₂, and BC₂O as shown in Fig. 11a–c). The correlation between B content in BCNTs and the ORR activity in alkaline media was established (Fig. 11). It was found that ORR activity was proportional to B content. However, the electron transfer number obtained for these BCNTs is way below 3 which was likely a dominating 2e⁻

Table 3 – Various heteroatom doped bio-carbon based catalysts reported for ORR in alkaline media.

Catalyst	Doping method	Doped element (s)	ORR onset potential (V)/	Half wave potential	Electron transfer number	Ref.
Co/N/C (Nitrogen, cobalt-codoped carbon electrocatalyst)	hydrothermal and heat treatment	Co – 4.78 at.% N – 1.02 at.%	–0.005 V vs Co/C	NR	3.8	[198]
Fe/N/C (Fe/C–SOYB)	thermal treatment	Fe – 3.97 wt%	0.84 V vs Pt/C	0.68 V vs Pt/C	3.1	[197]
Nitrogen-doped carbon	facile synthesis method with inclusion of FeCl ₃	NRn	0.975 V vs RHE	0.86 V vs RHE	3.5	[190]
CS ₂ –Fe (N-doped highly porous carbon)	carbonizing pig bones in FeCl ₃	NR	+0.025 V vs Pt/C	–0.035 V vs Pt/C	NR	[199]
AB (self-nitrogen-doped porous carbon)	thermochemical treatments (pyrolysis, chemical activation and doping),	N – 7.65 at.%	–0.145 V vs Pt/C	NR	NR	[200]
NGR (nitrogen doped graphitic carbon)	simultaneously graphitization and nitrogen doping of nano crystalline cellulose	N – 0.66 at.%	0.958 V vs RHE –0.042 V vs Pt/C	NR	3.7	[193]
Fe–N/C (iron and nitrogen co-doped carbon)	one-step pyrolysis of the mixture of FeCl ₃ and the low-cost biomass soybeans in	Fe – 0.24 wt%	0.91 V vs RHE	0.821 V vs RHE	3.4	[201]
BY-Fe-A (Biomass-derived porous heteroatom-doped carbon spheres)	hydrothermal treatment process and subsequent carbonization procedures	Fe – 1.7 wt%	0.985 V vs RHE	0.861 V vs. RHE	3.86	[189]
N–P/CC (N–P co-doped coffee carbon)	solvent purification methods and carbon synthesized with melamine and triphenyl phosphine	N – 3.54 at.% P – 1.15 at.%	0.99 V	–0.18 V vs RHE	3.98	[202]
Fe–N–C catalysts (Biomass based iron and nitrogen co-doped 3D porous carbon)	pyrolysis of the mixture containing red date, iron (III) acetate, and g-C ₃ N ₄ to	Fe – 0.66 at.% N – 14.83 at.%	NR	NR	3.71	[182]
D-PC (defective porous carbon from Seaweed Biomass catalyst)	N-doping-removal process using SA	N – < 0.1 at%	1.01 V vs RHE	0.83 V vs RHE	3.72	[203]
HDCA-X (heteroatom (N, S, and Fe) ternary doped porous carbons aerogel)	Pyrolysis using cocoon	N – 2.88 at.% S – 0.06 at.%	0.94 V vs RHE	0.79 V vs RHE	3.88	[204]
T-NFC (nitrogen (N) and fluorine (F) co-doped porous carbon material)	one-step annealing process	N – 2.8 at.% F – 2.2 at.%	0.81 V vs RHE	0.66 V vs RHE	3.8	[205]
CoNASS (nitrogen and cobalt dual-doped porous biocarbon electrocatalysts)	Two step method	N – 1.92 at.% Co – 2.71 at.%	0.87 V vs RHE	0.786 V vs RHE	3.84	[206]
Fe–N–PC (Fe–N co-doped porous carbon materials)	One-step pyrolysis strategy using soybean straw biomass	N – 6.24 wt% Fe – 1.79 wt%	0.989 V vs RHE	0.854 V vs RHE	3.97	[207]
SKHD (N-doped carbon synthesis from Sargassum spp)	Pyrolysis and acid treatment	N – 0.2% S – 2.63%	0.82 V vs RHE	NR	3.94	[208]

AOB700 (non-noble metal electrocatalysts from onion skin wastes)	Pyrolysis and chemical treatment with HNO ₃	N – 3.3 at. %	0.82 V vs RHE	NR	NR	[195]
NBSCP (Co ₂ P nanoparticles supported on N-doped carbon)	Eco-friendly synthesis method using bean sprouts.	NR	NR	0.836 V vs RHE	3.56	[181]
Fe–N–PC (biomass-derived Fe–N co-doped porous carbon)	One-step pyrolysis strategy using soybean straw biomass as	Fe – 1.79 wt% N – 6.24 wt%	0.886 V vs RHE	0.754 V vs RHE	3.89	[209]
NSG (nitrogen (N) and sulfur (S) dual-doped 3D porous graphene catalyst)	single-row pyrolysis using biomass	S – 0.22 at. %	NR	–0.23 V vs Pt/C	3.52	[210]
N-CNT(800)/GCE	Co-pyrolysis of blood biomass from pig	NR	0.91 V vs RHE	0.7 V vs RHE	3.7	[188]

process and was far away from the commercial Pt/C and hence further tuning of BCNTs is indeed important to reach the benchmark ORR activity.

Phosphorous-doped CNTs

Being a nitrogen family member, phosphorus has similar electronic properties than nitrogen but bigger in size which makes it difficult to substitute it within the carbon lattice. This is the reason why P doping was not very well explored [73]. But still it was established that P doping can alter the electron donor properties of carbon materials to host oxygen molecules for the reduction. Similar to nitrogen, phosphorus can also act as electron donor to carbon nanomaterials and induces a shift in Fermi level to conduction band [74]. P is often bonded to O and/or C in the heteroatom doped carbon structures. P doping in sp² carbon matrix was reported to show excellent thermal and electronic conductivity [75]. This is the reason why P doped nanocarbons have been also considered to prepare ORR catalysts. Meng-Qing Guo et al. [76] have developed P-doped CNTs prepared by the hydrothermal treatment of CNTs and H₃PO₃ is one possible way to dope P in CNTs (Fig. 12(a)), It was reported that various bonding configurations such as P–C, P–O and P=O tend to exist in PCNTs (Fig. 12(b)). The phosphonate functional groups containing oxygen could tune the electronic properties of CNTs and made them as a promising catalyst for ORR. The ORR activity of PCNTs obtained in alkaline electrolyte was superior to that of pristine CNTs. However, the catalytic activity remained relatively lower compared with another heteroatom doped CNTs. Further understanding and effective doping strategies are necessary to consider PCNTs as a viable option for cathode catalyst in AEMFC.

Co-doped CNTs

Although, N doping was largely explored to prepare an efficient ORR catalyst, co-doping of N with other elements such as P, B and S was also considered to further boost the catalytic activity by taking advantage from both of the heteroatoms. Many research studies have proved that co-doped CNTs outperformed single doped CNTs due to synergistic effects [77–79]. For example, co-doping of nitrogen and sulfur together in the carbon lattice could change the charge density and spin density and thereby its electronic structure. It was reported that, inclusion of sulfur in NCNTs changed the state of N species and alter the spin and charge distribution over the carbon network which facilitated the electron transfer for ORR [80]. As a result, the ORR on NSCNTs proceeds with 4e[−] transfer while it was a mixed 2e[−] and 4e[−] pathways on NCNTs. On the other hand, co-doping of nitrogen and boron also benefit from the synergistic effects where the electron rich nitrogen favors the activation of the sp² carbon while electron deficient boron (B⁺) acts as active site for oxygen adsorption. Thus, in the BCN nanotubes, B and N were in conjugation with π -carbon and activate its electrons for favorable O₂ reduction [81]. It was reported that a single precursor melamine-diborate can be used to derive N,B co-doped CNTs through CVD method. The resultant vertically aligned co-doped CNTs (VA-BCN) have 85.5% of carbon, 10.3% of

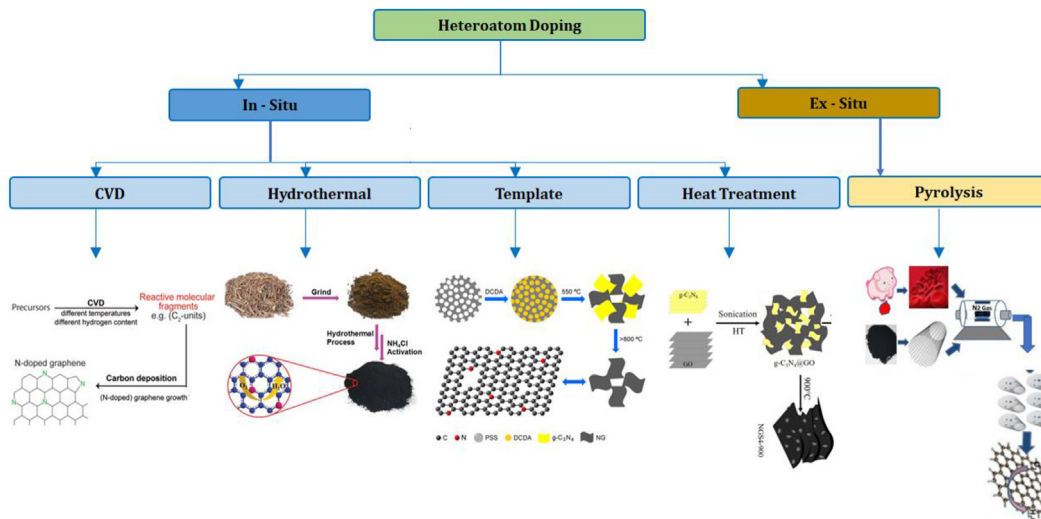


Fig. 8 – Classification of commonly used methods to prepare heteroatom doped carbon catalysts. Reproduced with permission from Refs. [55–58].

nitrogen and 4.2% of boron. The vertical alignment of the CNTs was proved to be beneficial to the diffusion of electrolyte ions and oxygen molecules during ORR. As result of synergistic effect, B, N co-doped CNTs can be considered as better catalysts for ORR than the N doped CNT or B doped CNTs, in terms of ORR overpotential, these BCN showed 20% lower value than NCNT and 100% lower value than BCNT in 0.1 M KOH. However, to get the real insight into the effects of B, N co-doping on the ORR activity, it is also important to understand the bonding configurations of boron and nitrogen in the carbon lattice. For example, if B and N are bonded (B–N) together, owing to their opposite ionic forms (B^+ , N^-), the electroneutrality of the sp^2 carbon will not be broken, in other words the electronic structure of carbon remains unchanged, so in this case BN doped CNTs behave like pristine CNTs. If N and B are only bonded separately to the carbon (C–N and C–B bonds and no bonding between B and N), then the electronic structure of CNTs would be effectively modified for favorable O_2 chemisorption and consequently an excellent ORR catalyst.

This was experimentally proven by Yu Zhao et al. who have prepared two kinds of BNCNTs (with BN bonded and B, N individual) [82]. They have correlated the ORR activity to the bonding configuration of boron and nitrogen and claimed that the ORR peak current density was almost three times higher for BCNTs where B, N are sufficiently spread over the carbon lattice compared to BCNTs where B, N are bonded to each other as shown in Fig. 13.

Similar kind of beneficial effect was also reported in the case of phosphorus and nitrogen co-doped CNTs. Owing to the larger atomic size of phosphorus than carbon, this latter can induce substitutional defects in carbon framework and alter the electronic properties behaving as n-type donor (P^+) [83]. Inversely, the p-type donor N could induce a net positive charge on the adjacent carbon breaking electrical neutrality of sp^2 carbon framework to participate in electron transfer for the reduction of O_2 . P, N co-doped vertically aligned CNTs synthesized by the CVD of pyridine, and triphenylphosphine have very low phosphorus content 0.8 at.% due to the larger

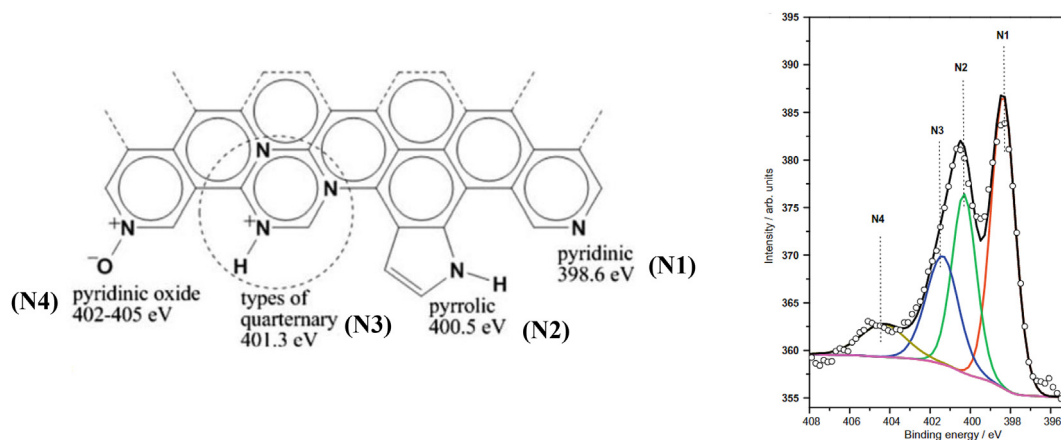


Fig. 9 – Various configurations of nitrogen doping of graphite framework along with their binding energies. N1: pyridinic, N2: pyrrolic, N3: graphitic, N4: N-oxide. Reproduced with permission from Ref. [63].

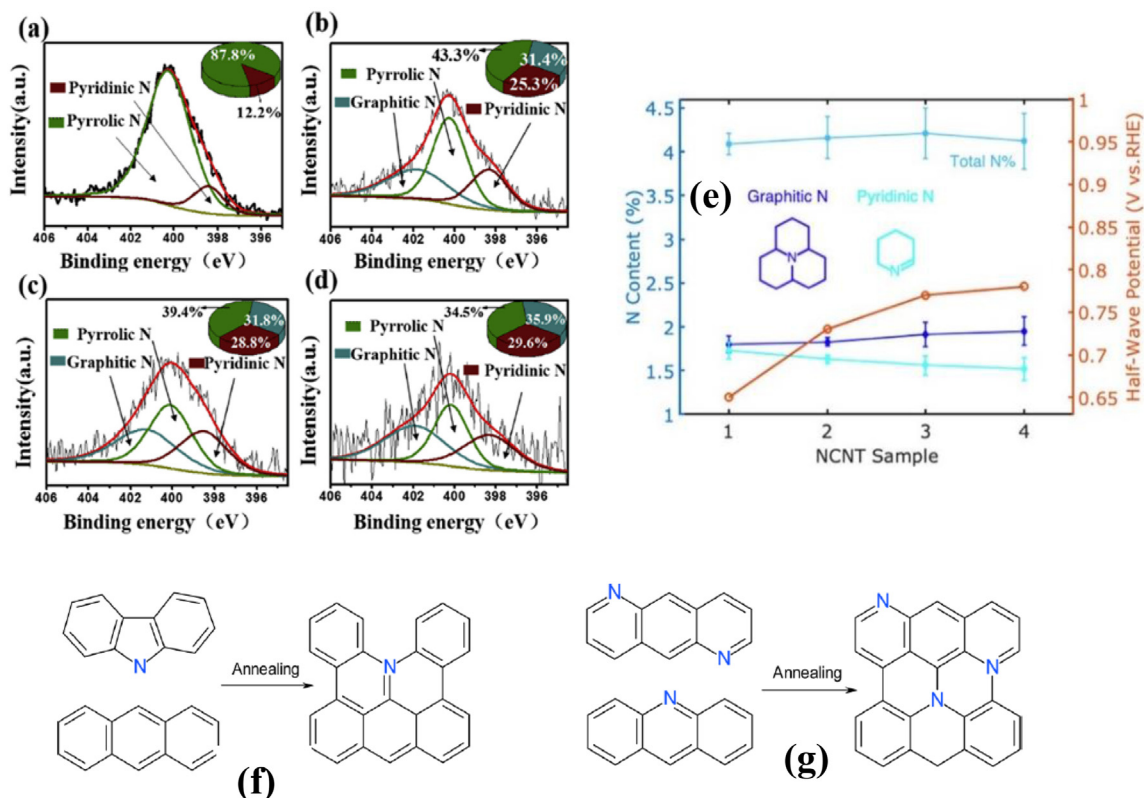


Fig. 10 – (a–d) N1s XPS spectra of NCNTs samples obtained at different pyrolysis temperature (600, 700, 800 and 900 °C, respectively). (e) Dependence of ORR activity on nitrogen content (f) modification of pyrrolic N to quaternary N and (g) pyridinic N to quaternary N by thermal annealing. Reproduced with permission from. [64,66,69].

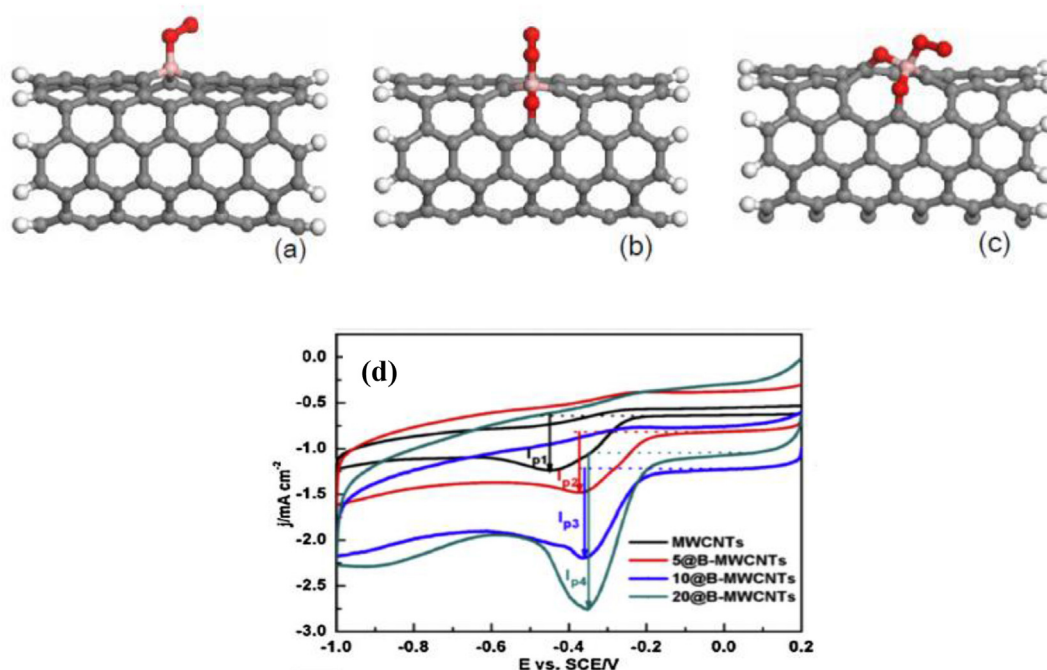


Fig. 11 – (a–c) Different configurations O₂ adsorption on B-CNTs (d) comparison of ORR activity with various boron content in CNT. Reproduced with permission from [71].

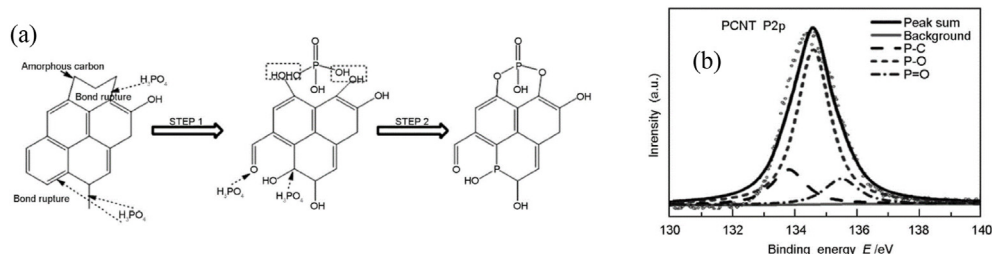


Fig. 12 – (a) Proposed mechanism for hydrothermal functionalization of PCNTs from CNTs. (b) XPS showing various phosphorus configurations in PCNTs. Reproduced with permission from Ref. [76].

atomic size of phosphorus which is why phosphorus doping was seldom reported in carbon materials [77]. Despite such low concentration of phosphorous, when doped together with nitrogen, the synergistic effect plays a critical role to catalyze the oxygen reduction in much better way compared to P doped CNTs or N doped CNTs.

Metal-nitrogen-doped CNTs

Carbon frameworks are extensively considered to provide sufficient electrical conductivity for non-precious metals due to which they have shown poor results for ORR. In addition, carbon framework enables the wide distribution of metal particles preventing their agglomeration, providing chemical and mechanical stability and high surface volume ratio [84]. However instead of pristine carbons, N doped carbon has been recently considered, thanks to the developed M-N_x active centers. Numerous reports have come up with this idea and developed methods to incorporate non-precious metals on heteroatom doped CNTs to promote their ORR activity by taking the advantage of active sites of metallic nanoparticles. The synergistic effect between the metal active centers and heteroatoms together with the high conducting CNTs was identified as the beneficial factors to promote ORR. Some of Fe or/and Co based heteroatom doped CNTs have shown comparable activity than that of Pt based catalysts [85–87]. To support metal nanoparticles, N doped CNTs were largely

considered due to their ease of fabrication and excellent ORR properties. The typical synthesis procedure involves pyrolysis of CNTs with nitrogen, metal precursors. For example, Sander Ratso et al. immobilized Fe nanoparticles on N doped CNTs by the pyrolysis of mixture of MWCNT, FeCl₃, dicyanodiamide [88]. Hongwei Zhao et al. reported the synthesis of Co incorporated N doped CNTs by the pyrolysis of polypyrrole grafted CNTs and cobalt nitrate [89]. Both Fe and Co incorporated into NCNTs have shown greater ORR activity than that of metal free N doped CNTs and N free metal-CNTs. The onset and half wave potential exhibited by Fe-N-CNTs were inferior only of 15 mV and 35 mV, respectively compared with commercial Pt/C. And Co incorporated in CNT framework showed similar ORR activity than that of Pt/C. The found high ORR activity was attributed to the presence of metal-coordinated N centers M-N_x (where x is the coordination number ranging from 2 to 4 which were identified as ORR promoters in addition to pyridinic and graphitic N species. The difference in their activity could be related to the particle size and the surface area of the composite catalyst as reported in other M-N-C type catalysts [90]. Simultaneous Co and Fe incorporation was also explored to increase the number of catalytic active centers. Taotao Gao et al. reported that coupling of Fe and Co on NCNTs could be favorable to create efficient active sites by increasing electrochemical active surface area [91]. Similarly, Zhun Dong et al. derived Fe–Mn alloy decorated NCNTs from the pyrolysis of bimetallic MOF [92]. It was reported that, Mn played a

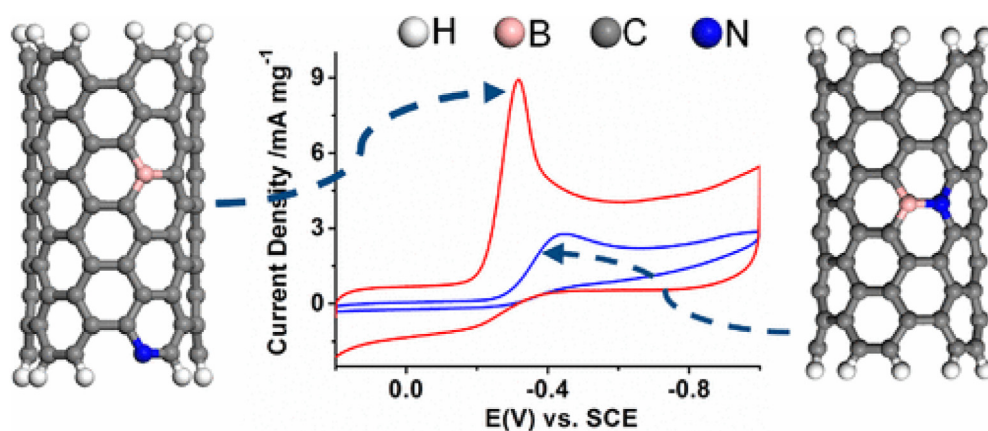


Fig. 13 – ORR activity of BCNTs with boron and nitrogen spatially separated in carbon lattice and NCNTs with boron and nitrogen bonded together. Reproduced with permission from Ref. [82].

little role in enhancing the ORR activity while a greater role in enhancing the durability of the catalyst. Hence an optimum composition is key to design the non-noble metal catalysts. The core-shell structure of the catalyst combined with the synergistic effects between pyridinic N and Fe-N_x resulted in superior catalytic properties comparable to commercial Pt/C. Saadia Hanif et al. have developed porous NiCo-NCNTs from NiCo-ZIF by hydrothermal treatment followed by thermal annealing [93]. The resultant catalyst showed better onset potential and cycling stability for ORR in 0.1 M KOH.

Nitrogen-doped graphene

Like any other heteroatom doped carbon structures, nitrogen doped graphene is the most commonly employed as ORR catalysts in alkaline media. Several methods have been investigated to produce N doping graphene sheets. In the beginning days, CVD method was largely used to prepare N graphene. Liangti Qu et al. derived N graphene with N/C atomic ratio 4 at.% via CVD of methane and ammonia gas [109]. This N-graphene was explored as metal free ORR catalyst which delivered excellent electrochemical activity and good operational stability compared to Pt/C. Later, researchers have explored thermal annealing of graphene oxide with high concentrated N precursor to prepare N-graphene without sophisticated instruments. It is a more commonly used method due to its simplicity and quick reaction time. For example, Kumar et al. synthesized N doped graphene by the thermal annealing of GO by melamine. The optimized ratio between GO and melamine to get the N- doped graphene with maximum catalytic activity was reported to be 1:5 [110].

An electrochemical method was developed by Karim Kakae et al. to synthesize N doped graphene from graphite and urea solution under DC power supply [111]. The prepared N graphene showed 6.8% of N content and was successfully employed as ORR catalyst in alkaline media showing 3.9 electrons per oxygen molecule.

The fascinating electrochemical properties of graphene have been attributed to many factors such as morphology, accessibility of active sites, density of nitrogen-carbon active sites, and the type of nitrogen species (graphitic, pyridinic), as explained in the case of CNTs. It is still ambiguous which nitrogen type is more active towards ORR, there is no single opinion about this question in the research community. Some literature point out that quaternary N species are more active for ORR [112–114], while others reported that it is pyridinic N species which are contributing mostly for ORR [70,115]. Recent reports enlighten that both pyridinic and quaternary N species have a positive effect on ORR activity [116]. Further the structure of N species has a great influence on the properties of ORR catalyst. Lemes et al. fabricated N doped graphene composite-carbon nitride with N contents as high as 35% by the thermal treatment of urea and GO at 500–800 °C. At temperatures below 650 °C, a composite of carbon nitride and N doped graphene was obtained and further heat treatment above 700 °C resulted in N doped graphene with N content as high as 19.8%. The resultant N doped graphene sheets showed a mixed composition of pyrrolic, pyridinic and quaternary N configurations. Despite of higher N content, the ORR activity of the composite was lower than that of N doped graphene

prepared without carbon nitride revealing that ORR activity does not directly depend on N quantity but on several other factors such as the type of N species [117]. On the other hand, this two-step process was also proposed by Qin Xiang et al. They first pyrolyzed melamine at 550 °C to get g-C₃N₄ [118]. Then this latter was combined with GO and pyrolyzed from 700 to 1000 °C to yield N doped graphene (NG) sheets with nitrogen content 2 at.%. The optimum ORR activity was shown by NG which was pyrolyzed at 900 °C attributing to the formation of intrinsic active pyridinic N sites.

Although in many cases, N doping requires high temperature, few researchers have developed low temperature doping methods. For example, Gyeong Sook Bang et al. reported simultaneous reduction doping of N to perforated GO using N₂H₂/NH₃ at 95 °C. Doping reaction time also has critical influence on the doping level of different N functionalities. It was reported that, shorter reaction time between perforated GO and NH₃ resulted in a pyridinic N doped graphene while prolonged reaction time yielded graphitic N doped graphene with high nitrogen content about 6.6% [119]. Interestingly, in spite of higher N content, graphitic N-graphene showed poorer ORR activity than that of pyridinic N-graphene which has N content of only 4.7%. GO perforation (Fig. 14(a)) during the synthesis was a unique strategy to create holes and defects where strong adsorption of NH₃ with oxygen functional groups during N doping resulted in a greater number of pyridinic N species.

Along with nitrogen doping, ORR activity can be further stimulated by the structural engineering of graphene by enlarging the porosity and constructing 3D structures [120]. Conventional NGs often form stacked structures due to van der Waal forces between the graphene sheets which will affect the oxygen absorption capacities of NG and active sites [121]. On the other hand, porous NGs offer a high specific surface area and a large number of oxygen molecules can adsorb on the surface for an enhanced ORR activity. Sheng Tang et al. reported the synthesis of 3D porous NG (3D-PNG) from the mixture of GO and 3-aminopropyltriethoxysilane (AMPTS) [122]. The AMPTS used was not only as the nitrogen source but it was also a silica template to form 3D porous structure as shown in Fig. 14(b).

The obtained 3D-PNG exhibited a super large specific surface area of 920 m²/g with the presence of mesopores and micropores. The smaller micropores acted as hosting sites for the oxygen while the larger mesopores accumulate the reactant molecules and shortened the diffusion path [123]. Together with N doping, this 3D porous graphene showed comparable ORR activity to commercial Pt/C. This exceptionally high ORR activity and performance was attributed to the synergistic effect of N doping the 3D porous structure.

Sulfur-doped graphene

It is also interesting to see the behavior of graphene when doped with an atom having similar electronegativity of carbon. Unlike N doped graphene, in S doped graphene, change of atomic charge distribution is relatively smaller owing to similar electronegativity of S and C. In that case, the resulting modified spin-density is responsible for enhanced ORR activity of S doped graphene and not the atomic charge density

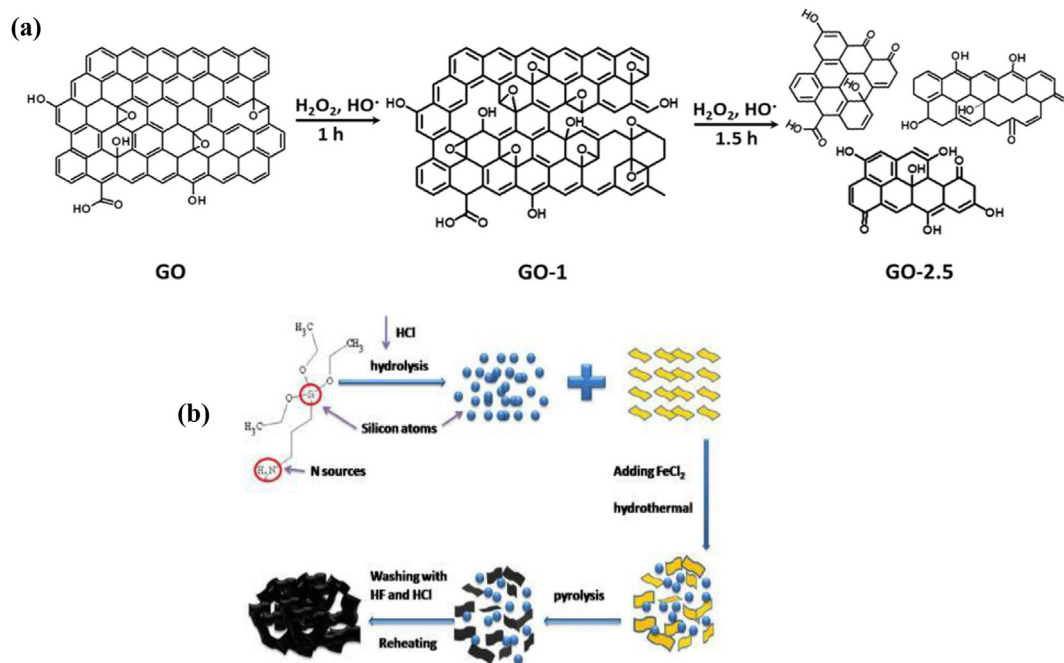


Fig. 14 – (a) Schematic representation of synthesis of perforated holly-graphene by time dependent etching process. (b) Schematic illustration of the synthesis procedures of the 3D-PNGs. Reproduced with permission from Refs. [119,122].

which is a minor contributor as explained by the DFT calculations by Zhang et al. [124] atomic charge and spin density distribution (Fig. 15) was calculated by considering the four different bonding structures surface S-adsorbed, edge S-substituted, edge SO_2 -substituted and sulfur-ring connecting graphene clusters [125]. Carbon atoms at the zig-zag edges or near to SO_2 doping structures possess high positive charge or spin density and are able to catalyze ORR by four electron transfer. On the other hand, $2e^-$ reduction pathway can be observed on the substituted S atom emphasizing S doped graphene which can reduce oxygen in both $2e^-$ and $4e^-$ pathways simultaneously. Further first principle DFT calculations revealed that S doped graphene was a suitable material to catalyze ORR, however its activity was lower than that of N doped graphene [126].

Sulfur was reported to possible dope graphene frameworks in the form of sulfides and sulfonates [127]. Among these two, sulfide C–S bond configurations mostly contribute to ORR and the catalytic activity is comparable to that of commercial Pt/C as shown in Fig. 16(a). On the other hand, a three-dimensional graphene sheet was identified as the most suitable morphology to fabricate S-graphene with high ORR activity. 3D-S graphene synthesized by the thermal annealing of sulfonic acid ion exchange resin [128]. The resultant catalyst exhibited, high specific surface area ($2129 \text{ m}^2/\text{g}$), crystallinity with appropriate sulfur doping (17 wt%) has shown an excellent ORR activity compared to 2D-S-graphene and only a 45 mV negative shift in onset potential compared to Pt/C.

Even though the ORR activity of S doped graphene is lower than that of N doped -raphene and commercial Pt/C, but the synergistic effects occurring between sulfur and carbon in carbon materials could be considered as a key strategy to design novel metal-free catalysts.

Phosphorus-doped graphene

Despite the difficulties to synthesize P doped graphene, few strategies have been proposed, for example, pyrolysis of toluene and triphenylphosphine produced P doped graphene with 0.26 at.% [74], such P doped graphene was reported to reduce the oxygen first to peroxide and then partially to water at lower potentials ($<0.3 \text{ V}$). On the other hand, P doped graphene was prepared with 1.8 at.% of P by thermal annealing of graphene oxide and triphenylphosphine [129]. They have reported that 1.8 at.% of phosphorus was incorporated in the graphene layers. P-doped graphene has shown good ORR activity and better performance in Li ion batteries compared to undoped graphene. It was established that, annealing temperature plays the critical role in controlling the doping level. At 900°C , 5% phosphorus doping was reported on carbon dots-graphene (P-CD/G) synthesized by the hydrothermal treatment of graphene oxide and phytic acid (Fig. 16(b)) [130]. The formation of carbon dots together with P doping enhances the electronic conductivity, catalytic sites of graphene and delivered much positive ORR onset potential (0.92 V) compared to graphene (0.82 V) (Fig. 16(c)).

Co-doped/multi heteroatom doped graphene

Compared to single heteroatom doping dual doping offers more flexibility to modify electronic/charge distribution on the carbon framework. According to dopant density and dopant ratios, dual doping induces synergistic effects. The source of the heteroatom and the reaction time between carbon precursor and heteroatom precursor play a critical role towards ORR activity. It was established that there can be a single source for different heteroatoms or each heteroatom

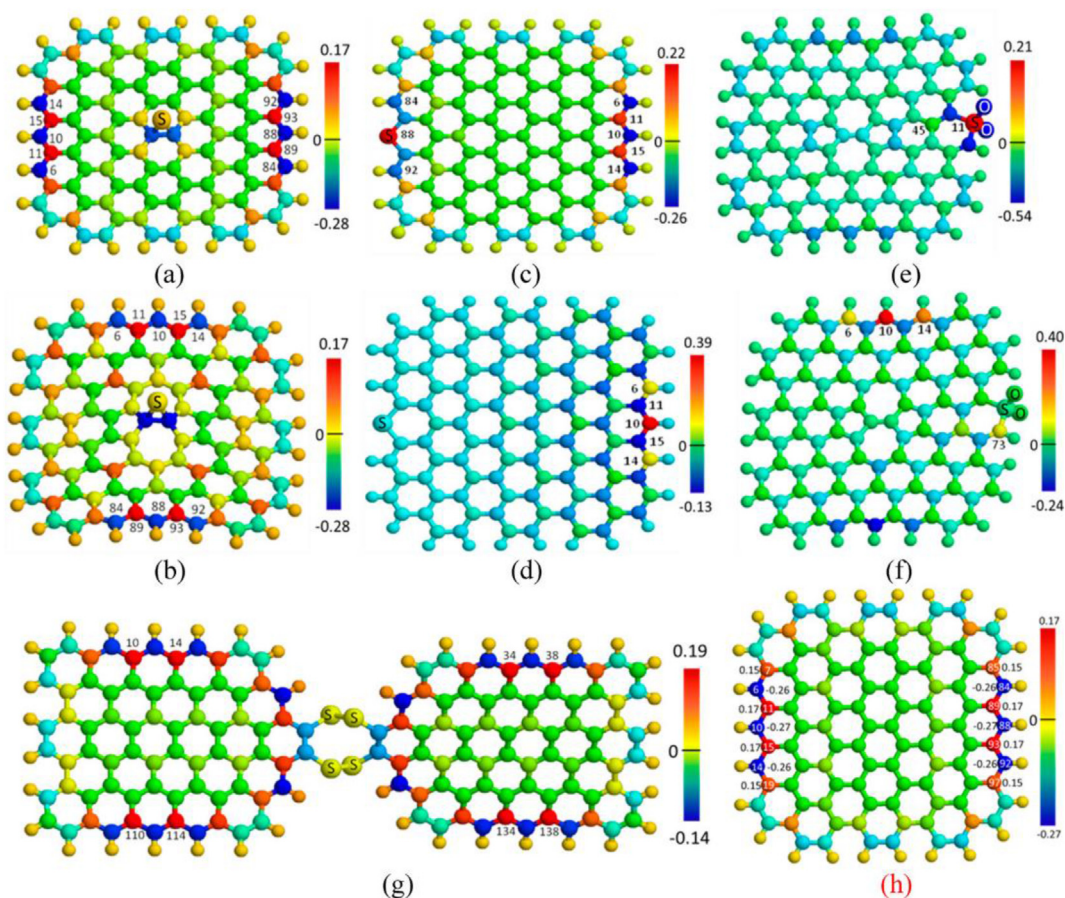


Fig. 15 – Atomic spin and charge density distribution in S-doped graphene. Reproduced with permission from [125].

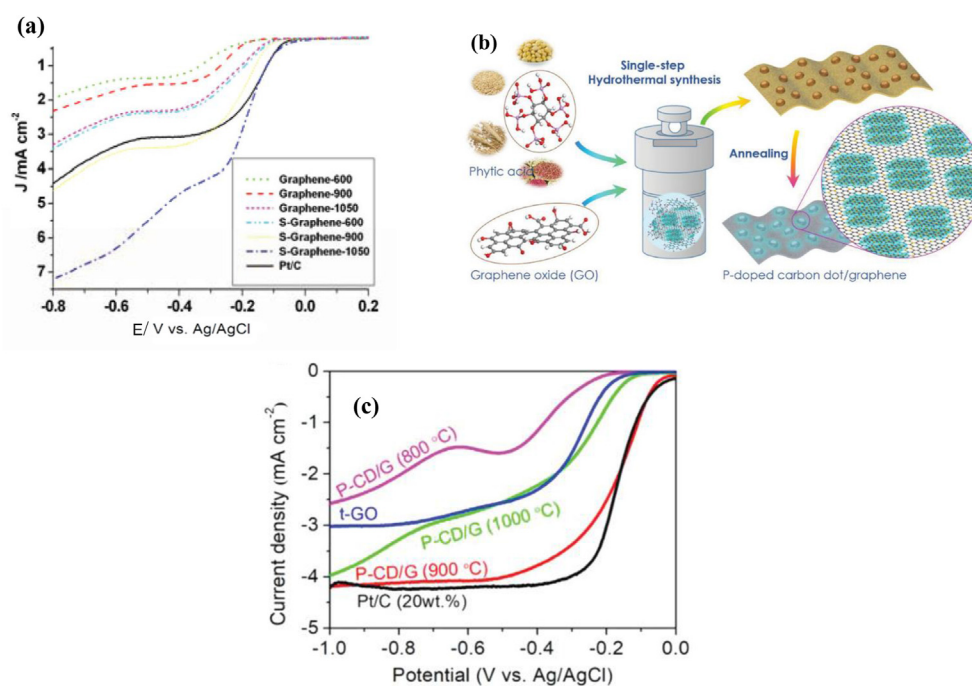


Fig. 16 – (a) ORR activity of graphene and S-graphene obtained at different annealing temperatures (b) Schematic representation of the synthesis of P-CD/G, (c) ORR activity of P doped carbon dot/graphene composites compared with Pt/C and GO. Reproduced with permission from Refs. [127,130].

source can be different. In addition, *in-situ* chemical modifications of these heteroatom sources are suggested to achieve better doping levels. For example, H. Zhang et al. unveiled the effect of N,S doping in graphene to explore its ORR activity. N,S-doped graphene was prepared by the reaction between cysteine and graphene oxide followed by thermal annealing [131]. Cysteine is considered as good reducing agent and can be oxidized by dissolved oxygen under neutral pH to form a dimer. Cysteine and GO are subjected to various reaction times (from 1 day to 14 days) and optimized at 7 days where it showed a maximum S/N ratio of 1.29. This catalyst showed a more positive onset potential of 0.09 V vs. Hg/HgO (0.188 V/RHE) and comparable limiting current density to commercial Pt/C in 0.1 KOH electrolyte. Similarly, Arun chander et al. reported N,S co-doped graphene by the *in-situ* polymerization of 6-N,N-dibutylamine-1,3,5-triazine-2,4-dithiol (single precursor for N,S) followed by the thermal annealing (Fig. 17(a)) [132]. The optimized N,S-graphene showed the ORR onset potential as 0.92 V and 0.79 V as half-wave potential. The superior ORR activity was attributed to the asymmetric spin and charge densities that originated from the synergistic coupling between N, S and adjacent carbon atoms.

In addition to the conventional thermal annealing, a solution-based method was reported to fabricate N,P co-doped graphene from GO, phytic acid and ammonium hydroxide [133]. The larger size and lower electronegativity of P compared to N could promote active sites for the absorption of molecular oxygen which is a key step during ORR. It is quite challenging to load P atoms on the carbon network compared

to other heteroatoms such as N, S etc. due to its larger atomic size. However even small quantity of P (0.6 at.%) could result in an appreciable ORR activity when co-doped with nitrogen. The N-P-rGO shows good selectivity of four electron transfer with an onset potential of 0.89 V while commercial Pt/C shows 1.03 V vs RHE and. Musico et al. compared the ORR activity of NF and BF co-doped graphene prepared by hydrothermal method [134]. The electronegative N and electropositive B behave differently when combined with highly electronegative F atoms. Nitrogen can induce positive charge on adjacent carbon for O₂ absorption while B itself acts as a host for the O₂ chemisorption. On the other hand, in the case of co-doping with F, the ORR activity was further enhanced due to additional active sites created at the adjacent sites of F. N-F-rGO showed an onset potential of 0.8 V and limiting current density of 4.09 mA/cm² while its counterpart B-F-rGO showed 0.79 V as onset potential and limiting current of 3.69 mA/cm². The slight difference in ORR activity of these co-doped graphene was attributed to the difference in their heteroatom ratios [135].

Owing to the fact that the combination of dopants increases the catalytically active sites, tri-doped graphene was explored as a potential ORR catalyst. Chuyen Van Pham et al. reported S,N,F doped graphene via a two-step process (S doping followed by N,F doping) using P4S10 and Nafion as S and N,F sources, respectively (Fig. 17(b)) [136]. N,F doping could facilitate catalytic sites via charge polarization at C–N, C–F bonds while S doping resulted in unpaired electrons localized at C–S bonding forming catalytic active sites. The

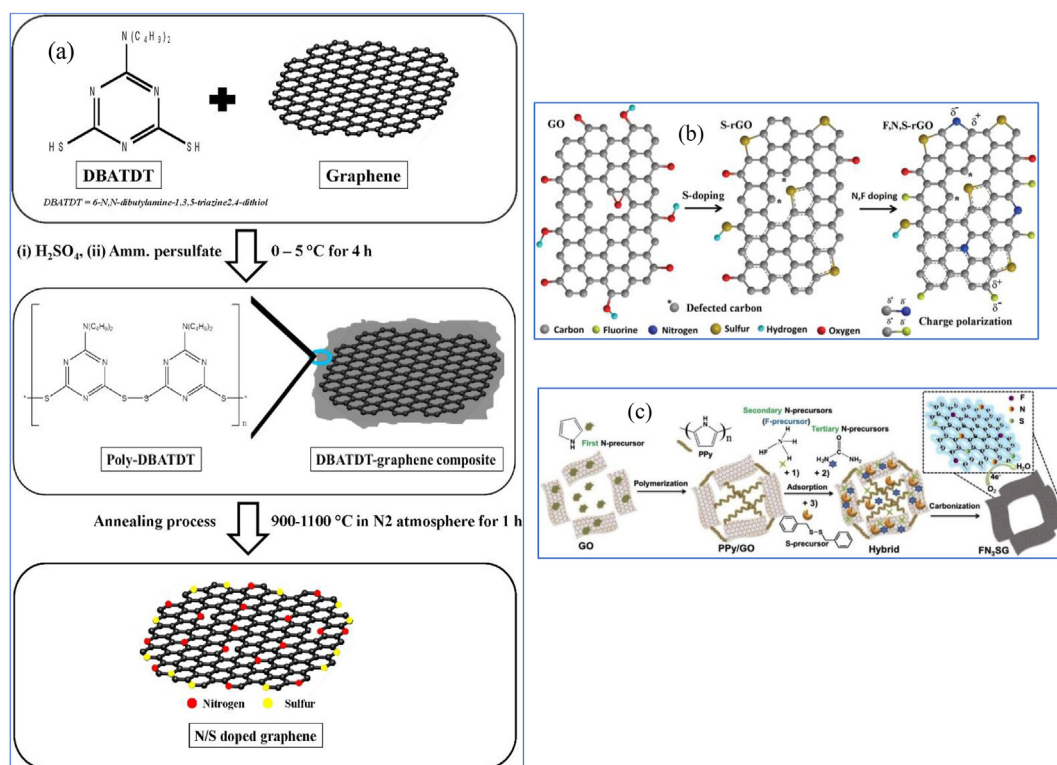


Fig. 17 – (a) Schematic illustration of the synthesis process of N–S co-doped graphene derived from 6-N,N-dibutylamine-1,3,5-triazine-2,4-dithiol (b) Schematic illustration of the hypothetical chemical structures and synthetic route for F,N,S-rGO. (c) Schematic representation for the synthesis process of FN₃SG. Reproduced with permission from [132,136,137].

combination of both types of active sites contributed to enhanced ORR activity. This tri-doped graphene showed an onset potential of 0.85 V vs RHE and a limiting current of 3.5 mA/cm². However, the ORR activity of this catalyst does not reach the benchmark Pt/C as it reduces 75% of oxygen via 4e⁻ transfer path and 25% of O₂ via 2e⁻ path.

On the other hand, Y. Li et al. reported ternary doped graphene with ternary nitrogen (FN₃S-G) obtained from three different N sources, polypyrrole (Ppy), NH₄F and urea as the primary dopant [137] Fig. 17(c). Inspired by the fact that secondary and ternary N-precursors could increase the composition of active sites for ORR. The resultant FN₃SG exhibited porous architecture with multiple active sites including pyridinic N, graphitic N, thiophenic S, ionic and semi-ionic C–F bonds. With this controlled doping strategy this tri-doped graphene showed a more positive onset potential of 0.988 V vs RHE and electron transfer number identified as 3.93 which is comparable to Pt/C 0.1 M KOH electrolyte.

Metal, heteroatom co-doped graphene

Although the metal free heteroatom doped graphene delivered promising results as ORR catalysts in alkaline media, still there is a large performance gap in comparison to commercial Pt. Hence, further efforts are indeed to find a better electrocatalyst that can deliver stable ORR activity. Transition metals have been recognized as ORR active centers, but their

electronic conductivity is too low hindering its potential applications in electrocatalysis. Combining these metals with heteroatom doped graphene could boost the ORR activity due to increased ORR active sites and electronic conductivity. The active metallic center coordinated to several nitrogen atoms and form M-N_x clusters. These clusters regulate the electronic configuration of graphene network and elevate the ORR activity [138]. Transition metals namely cobalt and iron are widely considered to fabricate M-heteroatom doped graphene composites [139,140]. These composites are derived by various synthetic methods namely metal organic framework precursors [141], polymerization of heteroatom containing monomers [142] etc. In addition to the *in-situ* formation of graphene structures, graphene or graphene oxide is directly used as carbon support while mixing with heteroatoms and metal precursors. Xudong Wen et al. have fabricated cobalt, nitrogen doped graphene by mixing CoCl₂ with GO followed by thermal annealing in NH₃ atmosphere [143]. In the developed catalysts, cobalt and nitrogen are homogeneously and closely dispersed on graphene sheets (Fig. 18(a–d)) leading to the favorable formation of Co-N_x active centers (Fig. 18(e)). XPS results further predicted that approximately 8 mol.% of nitrogen and 0.2 mol.% cobalt.

Further, the authors showed that this Co,N-graphene was a multifunctional catalyst showing good ORR properties not only in alkaline media (E_{onset} 0.97 V vs 0.95 V for Pt/C represented in Fig. 18(f)) but also in acidic medium and as hydrogen

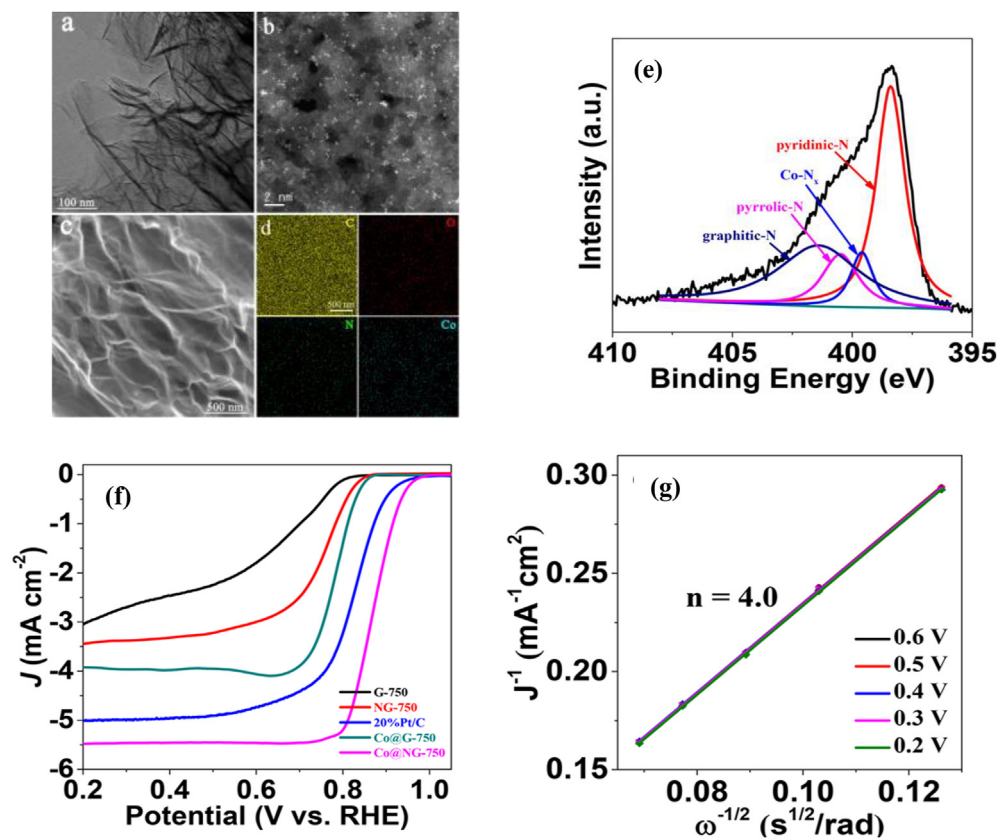


Fig. 18 – (a) TEM image, (b) HAADF-STEM image, (c) SEM image used in the EDS mapping test, and (d) the corresponding EDS mapping of Co@NG-750. (f) deconvoluted XPS of N-1s in Co@NG (f) ORR activity of Co@NG catalyst compared with Pt/C in 0.1 M KOH at 1600 rpm and (g) K-L plots of Co@NG-750. Reproduced with permission from Ref. [143].

evolution catalyst. The electron transfer number was calculated as 4 in the wide potential window 0.2 V–0.6 V vs RHE as shown in Fig. 18(g).

Similarly, formation of Co_4N particles was observed on graphene sheets when cobalt acetate and GO compositions were annealed in NH_3 atmosphere at 600°C [144]. Varying the cobalt precursor concentration yielded the Co_4N -graphene with different cobalt loading starting from 5% to 20% with varied N/C ratios.

When the concentration of cobalt precursor increased during the preparation of the composite, the average particle size of Co_4N also increases (14–200 nm) resulting in ORR onset potentials from 0.87 V to 0.91 V. The beneficial ORR properties of Co_4N -graphene arise from the number of active sites in the composite. Since N is a more electronegative atom it can induce positive charge on the carbon and cobalt atoms making them as suitable hosts for the oxygen adsorption [145]. Thermal annealing of GO, CoCl_2 and 1,10-phenanthroline under argon atmosphere above 800°C resulted Co loaded N doped graphene [146]. Raman spectroscopy reveals that cobalt was present as CoO moieties which may be formed by the thermal decomposition of CoO_x species due to the oxygen functionalities in GO. These CoO active centers together with N doped carbon moieties can catalyze ORR individually or synergistically leading to a better ORR activity with nearly four electron transfer in alkaline media.

Similar to Co–N doped graphene, Fe–N doped graphene was also largely explored as potential non-precious ORR catalyst. In addition to the simple iron salts like FeCl_3 , iron containing macromolecules such as iron phthalocyanines (FePC) and ferrocene are used as iron sources. Nathanael Komba et al. have reported the immobilization of FePC on N doped graphene by simple low temperature (95°C) solution chemistry as represented in Fig. 19(a) [147].

The π - π interactions between the phthalocyanine rings and N doped graphene could promote the homogeneous distribution of FePC over N doped graphene. In addition, this π - π interactions prevent the agglomeration of Fe- N_4 structures. Introduction of electron rich FePC on the graphene framework could effectively alter the charge distribution and

electronic properties of surrounding carbon atoms favoring oxygen adsorption. The composite catalyst FePC-N-graphene with 33% FePC has shown best ORR properties in terms of onset potential 0.97 V and limiting current density of 6.3 mA/cm^2 which are very close to that of the commercial Pt/C tested in alkaline electrolyte. Along with underlying ORR activity of FePC/N graphene, the N/C ratio of precursors used in the preparation plays an important role in terms of texture, elemental composition and nature of surface and bulk phases in the catalyst [148]. In the first step of the synthesis, N/C composites were obtained by the ball milling of two N precursors (1,4,8,11-tetraazacyclotetradecane and urea), one after another to achieve N/C ratios starting from 0.8 to 0.25. In the second step, these N/C composites were annealed at 800°C to get Fe/N/G catalyst. Although several Fe containing species such as FeNx , Fe_3C and metallic Fe are observed in Fe/N/G catalyst, the only stable phases at the surface of the catalyst is FeNx which is predominantly ORR active. The best ORR properties are observed for the catalyst with N/C of 0.3 and 0.25 as shown in Fig. 19(b). It reveals that ORR activity was decreased with increasing the Fe and N which resulted in lowering the active surface area of the catalyst. In addition to the Fe/N/G catalyst Yanli Niu et al. reported Fe_3C nanoparticle encapsulated Fe/N/G catalyst as a promising ORR catalyst in alkaline media [149]. Spontaneous oxidative polymerization of dopamine was carried out with dopamine and GO in presence of FeCl_3 catalyst to yield PDA-Fe-rGO which upon thermal annealing resulted $\text{Fe}_3\text{C}@Fe/N/G$ catalyst. Fe_3C encapsulation has proven to increase the ORR activity of Fe/N doped carbons by activating the Fe-N-C sites for the favorable O_2 adsorption [150]. Strongly bonded Fe-N moieties along with chemically and mechanically stable encapsulation of Fe_3C offer an excellent durability to $\text{Fe}_3\text{C}@Fe/N/G$ catalyst making the way clear to the rational design of non-precious ORR catalyst. In addition, DFT calculations revealed that stable heterostructures are formed when Fe was substituted with metal atoms like Co or Ni near the interface of $\text{Fe}_3\text{C}/\text{NG}$ [151]. The DFT calculations further showed that this type of metal substitution changes the work function of the composite electrocatalyst which is directly related to the

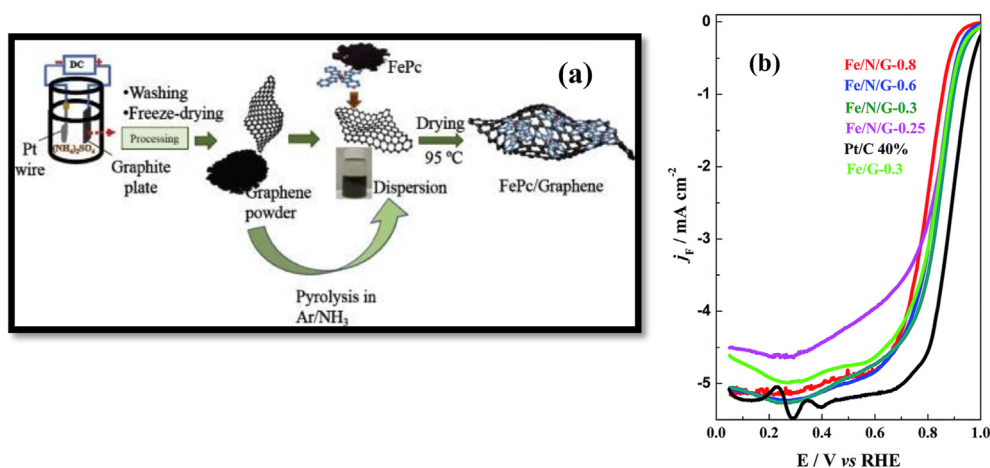


Fig. 19 – (a) Schematic representation of synthesis of FePC–N doped graphene (b) ORR activity of F/N/G catalyst with different N/C ratios tested in alkaline media. Reproduced with permission from Refs. [147,148].

adsorption strength of ORR intermediates. Enhanced ORR activity was found when the concentration of Co or Ni increases at the interface. The relation between formation energy and ORR over potential at different concentrations is shown in Fig. 20(a,b). The substitution of metal in Fe₃C substrate modified the electronic structure of over layer N doped graphene as evident from the change in shift in p band center of graphene substrate which is responsible for the adsorption of intermediates.

ORR activity of Fe–N–C catalysts are greatly influenced by the morphological characteristics of carbon substrate. Fe/N co-doped porous graphene/graphite was synthesized by Qingqing Dong and his coworkers and explored its ORR properties [152]. Firstly, cyclopentadienyliron (CpFe) groups were grafted on to the surface of rGO or graphite by the ligand exchange reaction of ferrocene which upon thermal annealing in NH₃ at 800 °C produced Fe/N-rGO or Fe/N-Graphite (Fig. 20(c)). Obviously, graphene supported Fe–N–C catalysts showed better ORR activity than that prepared with graphite substrate due to relatively large surface attained by the intercalation of Fe particles. The restacking of graphene layers can be avoided when used rGO as support which improves the accessibility of active sites to the adsorption of O₂ contributing positively for ORR [153].

Although Co/Fe-N graphene catalysts are extensively studied for ORR due to their comparable performance with benchmark Pt/C but these Co/Fe dissolve over the time in fuel

cell environment (reaction with H₂O₂). Compared to Fe/Co, the reaction between H₂O₂ and Mn is much weaker offering long-term stability to Mn based catalyst [154]. Lu Bai and his coworkers reported atomically dispersed Mn supported on N-graphene via thermal annealing and acid leaching strategy was an efficient ORR catalyst in alkaline media [155]. The best annealing temperature at 750 °C was chosen where the higher N-doping concentration and Mn–N₄ active sites are formed. DFT calculations (Fig. 20(d–g)) revealed that the theoretical ORR over potential 0.63 V is lower for Mn–N₄-G configuration than other possible configurations such as Mn–N₃ (1.48 V) and Mn–N₃O-G (2.33 V). On the other hand, the theoretical ORR over potential for metal free graphitic N configuration was predicted as 1.18 V lower than its competing configuration pyridinic-N 1.58 V. On the whole M–N₄ moieties with higher graphitic-N is a key factor to design non-precious M–N–C type catalysts for ORR.

Bio-inspired ORR catalysts

Heteroatom doped carbons derived from biomass have been explored for ORR catalysts, hetero atoms such as nitrogen, sulfur, phosphorus etc can be introduced into the carbon structure upon pre-treatment and pyrolysis of biomass. In addition, biomass mixed with metal precursors such as iron and cobalt could potentially result in metal-heteroatom doped carbons which have shown promising results as ORR

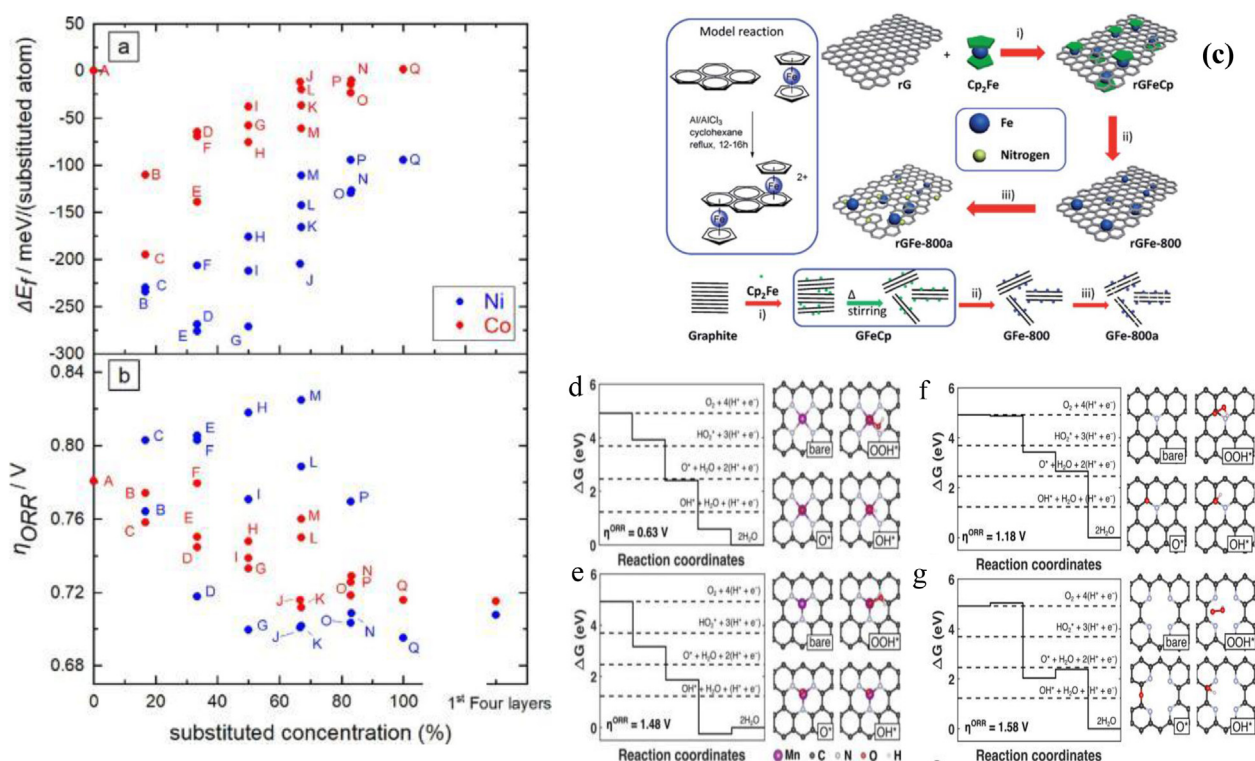


Fig. 20 – (a) Formation energy [meV/(substituted atom)] and b) ORR over potential at the different substituted concentrations of Ni and Co atoms in the Fe₃C substrate. Letters (A)–(Q) refer to the different configurations (c) Synthesis of Fe/N-rGO and Fe/N-G catalysts, free energy diagrams for ORR on (d) Mn–N₄-G, (e) Mn–N₃-G, (f) graphitic-N and (g) pyridinic-N configurations. Reproduced with permission from Refs. [151,152,155].

catalysts. The recently, reported biomass derived electro-catalysts are summarized below.

N doped 2D carbons have been derived from hydrothermal carbonization of carbohydrates (glucose/fructose/cellulose) and guanine at 1000 °C [180]. Among them, the catalysts developed from fructose showed a maximum ORR activity while the cellulose-based catalysts exhibited lowest ORR activity in alkaline media due to heterogeneous morphology and less porous structure. The activity of these biomass derived carbons was correlated to the 2D morphology, defect sites, N doping and hierarchical porous structure.

Owing to the presence of various heteroatoms in biomass, upon carbonization yield heteroatom doped carbons and compared to single doping, binary/ternary doping has been proven to be a better strategy to enhance ORR activity. For

example, controlled pyrolysis of beansprouts (BS) could result in carbon matrix with N, P, S as dopants. Dong Wook Lee et al. converted beansprouts into ORR catalysts by pyrolyzing with CoCl_2 [181]. Fig. 21 (a) and (b) represent the schematic synthesis procedure and Co–N bonding configurations. The derived catalysts (BSCP) contained 4.29% of N, 1.9% of P, 0.77% of S and 0.5% of Co loaded in carbon matrix 72.37%. This catalyst has shown reasonable ORR activity with positive shift in onset potential to 0.767 V, close to commercial Pt/C 0.825 V in 0.1 M KOH electrolyte. The activity of BSCP was further enhanced by increasing the N doping to 7.47 at.% by thermal treatment with NH_3 gas.

Zhaoquan Xu et al. derived Fe and N co-doped 3D porous carbon (Fe–N–C) by the pyrolysis of red dates along with iron acetate and $\text{g-C}_3\text{N}_4$ [182]. The resultant Fe–N–C catalysts

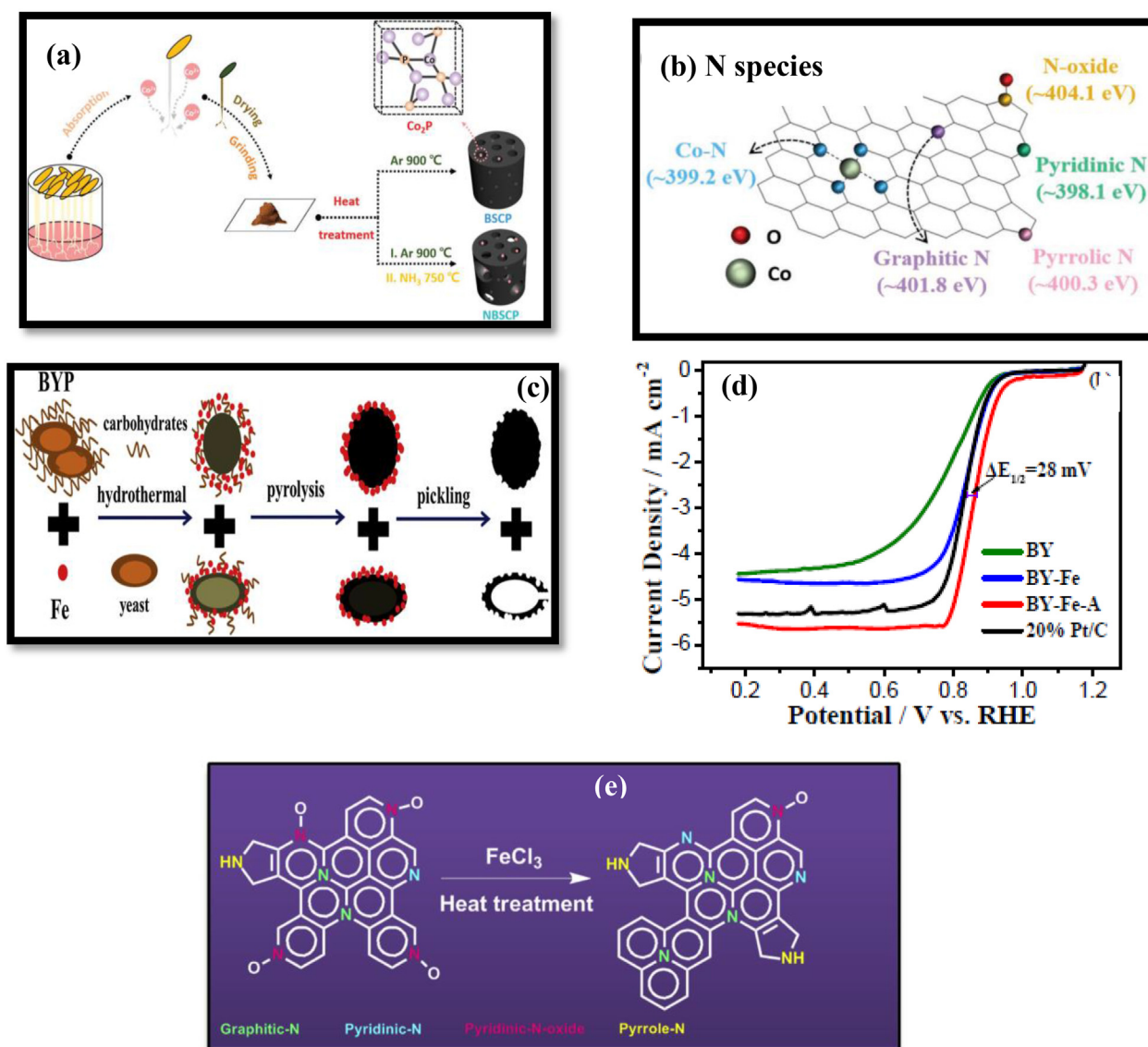


Fig. 21 – (a) Schematic illustration of the synthesis process of BSCP and NBSCP electrocatalyst. (b) types of the N species included in BSCP and NBSCP. (c) Schematic illustration of the proposed mechanism of formation of spherical carbon with adding the iron (d) comparative LSVs at 1600 rpm for three catalysts, along with 20 wt% commercial Pt/C in O_2 saturated 0.1 M KOH solution. (e) Scheme illustrating the transformation of N species from pyridinic-N-oxide to graphitic-N, pyridinic-N, and pyrrolic-N. Reproduced with permission from Refs. [181,189,190].

showed high dispersion of Fe and rich in nitrogen. Introduction of Fe in carbon framework could enhance the graphitization of carbon and thus electronic conductivity. When there is optimization of Fe and N content (i.e. Fe 0.66 at.% and N 14.83 at.%) the iron particles were dispersed as FeN_x which are proven to be ORR active sites. The LSV results showed that the ORR activity of this catalysts is on par with other Fe–N–C based catalysts derived from conventional methods [183,184]. The electron transfer number has been found to be 3.7 which represents a dominant 4 electron ORR path.

Shuyan Gao et al. have derived N doped carbon by the direct pyrolysis of poplar catkins at temperatures between 600 and 900 °C [185]. The resultant catalysts have exhibited rough and porous structure which is beneficial to increase the density of active sites in favor of smooth ion transport. The developed catalysts also showed the combination of meso and micro pores which could lead to exceptionally high specific surface area above 1500 m²/g which is much higher than synthetic carbons (typically below 1000 m²/g). The high surface area of the carbon could maximize the active sites for electron transfer while its porous network enhances the oxygen diffusion through the carbon framework [186]. The N doped carbon derived at 800 °C has been found to be more active towards ORR and exhibited good cycling stability. The ORR activity of this catalyst was simply attributed to high graphitic N.

Animal blood biomass was reported to be a good source for various proteins such as hemoglobin and N precursors. Electrocatalysts derived from hemoglobin have been successfully used as ORR catalysts. However, the lack of methodologies to pyrolyze these blood proteins (BP) is a major concern. Maruyama et al. have reported a two-step pyrolysis method to derive ORR catalysts for acidic fuel cells from bovine blood [187]. In the first step, BP was subjected to thermal treatment below 600 °C to produce catalyst precursor (called pyropolymer) which is usually not fully converted into carbon. Several investigations have been done to explore the characteristics of these blood pyropolymers and proved that they were active precursors to derive alkaline ORR catalysts too. J. Zheng et al. used BP extracted from pig blood to prepare blood pyropolymer by a thermal treatment at 350 °C and this pyropolymer was used as precursor to imprint N in CNTs [188]. The ORR catalysts derived by the pyrolysis of BP and CNTs essentially contained N and Fe. However, it was reported that Fe did not take part in ORR process as it was in metallic state but could act as promoter to incorporate N in carbon framework. Hence the observed ORR activity of these NCNTs was solely attributed to N doping. The catalysts derived at 800 °C have been found to be most active towards ORR in alkaline medium exhibiting an onset potential of 0.9 V slightly lower than that of Pt/C. This catalyst exhibited a dominant $4e^-$ process wherein the electron transfer number was calculated to be 3.7. As deduced from many N doped carbon materials, N configuration has been found to play a significant role in catalyzing the ORR, in this study it was proposed that the observed ORR activity was due to the optimized ratio between planar pyridinic - pyrrolic N groups.

Along with heteroatom doping, morphology of derived carbon is an important factor to influence the ORR activity, Guanghua Wang et al. derived spherical, heteroatom doped

carbon by the hydrothermal treatment of Brewer's yeast powder (ByP) which is a byproduct of Brewer Brewing beer [189]. ByP is rich in carbohydrates along with nitrogen- and phosphorus-containing species which can be converted into P,N doped carbon by the dehydration and thermal annealing process. Hydrothermal treatment of ByP produced N,P doped spherical carbon with high surface area (790 m²/g) and porosity (10–15 nm). These spherical shaped carbon particles showed 27 mV positive shift in half wave potential compared to Pt/C and reduced O₂ through $4e^-$ pathway.

Apart from the doping, carbon itself is considered to show varied ORR activity according to their crystallinity and morphology, for example amorphous carbon and graphitic carbon have shown different ORR activity even with same heteroatom doping [191,192]. Cellulose was reported to be a suitable precursor to derive both amorphous and graphitic carbon depending upon the pyrolysis conditions. Cellulose, another most abundant organic material on the earth, is considered as viable carbon source to derive ORR catalyst. Xiaoxian Wu et al. derived amorphous carbon (AC) and graphitic carbon ribbons (GR) from microcrystalline cellulose and subsequently doped with nitrogen by a thermal treatment with NH₃ gas [193]. Besides NH₃ treatment Fe²⁺ salt was added to catalyze graphitization process. Both N doped amorphous carbon (NAC) and N doped graphitic ribbons (NGR) have shown exceptionally higher ORR activity compared to their undoped versions. Among NAC and NGR, the later one exhibits better activity in alkaline medium approaching commercial Pt/C activity and only short by 42 mV in terms of onset potential (0.958 V vs 1.00 V). On the other hand, NAC showed onset potential of 0.869 V (131 mV lower than Pt/C). However, the electron transfer number for NAC was found to be 3.18 attributing to mixed ORR process while for its analogue NGR the value was determined as 3.98 showing a dominant $4e^-$ ORR process. NAC showed higher surface N-content than NGR (0.9% vs 0.66%) however NGR showed higher graphitic and valley N sites which are highly active towards ORR compared to pyrrolic and pyridinic N species.

Onion is considered as one of the world's largest consumed vegetables, while processing the onion, its skin, i.e. external layers peeled off and disposed. Fibers, proteins and phenolic carbons have been found to be vital constituents of these external layers, owing to its rich carbon building blocks. Porous carbon structures have been derived from onion skin and explored for their applications in supercapacitors [194]. Ivonne L. Alonso-Lemus et al. prepared bio carbon based cathode catalyst for alkaline fuel cells from the waste onion skin [195]. Pyrolysis of onion skin at the temperatures of 600–800 °C was performed to produce N doped carbons with different N species such as N-pyridinic, N-amine, N-quaternary and N-pyrrolic nitrogen. Among all, pyrolysis at 700 °C produced carbon with high surface area of 242 m²/g and was found to be more active than those derived at 600 and 800 °C. However, the activity was much less than the Pt/C in 0.5 M KOH. The onset potential and limiting current density were reported as 0.82 V and 2.3 mA/cm² respectively. Further optimizations and characterizations are required to understand the involved ORR properties to the fullest extent.

Apart from varying the pyrolysis temperature to produce different N doping, it was also reported that variation of

synthetic conditions also produce N doped carbons with different N contents and varied physicochemical properties. Rongfang Wang et al. produced three different types of N doped carbon from biomass of Okra (produced from soya bean) with the inclusion of FeCl_3 at different synthetic steps [190]. They have adopted a two-step pyrolysis, initially Okra was pyrolyzed at $800\text{ }^\circ\text{C}$ followed by ball milling and then pyrolyzed again to ensure the removal of impurities and efficient N doping into carbon framework. FeCl_3 added during 2nd pyrolysis resulted in highest sp^2 carbon, pyridinic and graphitic N than that added in 1st pyrolysis. This study highlighted that it is important to pay attention not only to add iron salt to enhance the N doping but also one should pay attention towards the synthetic procedure and have clear idea in deciding the efficient way of adding Fe salt to maximize the catalytic site density. Further, N doped carbons prepared by the addition of FeCl_3 showed higher ORR activity than that prepared without FeCl_3 . This could be attributed to the transformation of N oxide to pyridinic and graphitic N which are more active towards ORR.

In addition to direct carbonization of bio species, hard and soft template methods have been also greatly explored to synthesize carbon based electrocatalysts. Sucrose was reported to be an active biomaterial to derive ordered mesoporous carbon (OMC) using a hard template. The obtained OMCs have extensively been used as supports for noble and non-noble metal catalysts. Later substantial improvements have been made regarding their synthesis to fabricate metal free ORR catalysts. Nitrogen doped graphene (NG) was derived by high temperature carbonization of sucrose and dicyanamide as using silica templated method [196]. The resultant NG showed comparable ORR activity to that of 20% Pt/C in 0.1 M KOH electrolyte and the electron transfer number was found to be 3.9 depicting a dominant 4e^- ORR process which was attributed to high graphitic N content.

Soybean is another important source that was explored to prepare ORR catalysts, they are available for low cost and abundantly, more than 250 million tons of soybean is produced throughout the world every year. Soybeans contain around 40% of soya protein which is rich in nitrogenous species and have been extensively used as source to prepare N doped carbons. Chao-Zhong Guo et al. prepared Fe–N–C catalyst by the pyrolysis of soybean with Fe supported on vulcan carbon black [197]. This Fe–N–C catalyst exhibited an ORR onset potential of 0.84 V half wave potential of 0.68 V which were inferior by 110 and 170 mV respectively than that of 20% Pt/C in 0.1 KOH electrolyte. The ORR activity of this catalyst was attributed to presence of Fe which could facilitate the transformation of quaternary N species to planar N species result in a higher amount of planar N species. In addition, metallic Fe could be beneficial to form new active sites during the decomposition of soybean. Soy milk was used to derive Co–N–C catalysts by following a different approach than that used to prepare Fe–N–C catalyst [198]. Initially carbon dots have been prepared from soy milk and pyrolyzed with Ppy and CoNO_3 precursor which acted as nitrogen and cobalt sources respectively. The ORR activity of Co–N–C catalyst was studied in both RRDE and RDE experiments. From the RRDE measurements the total peroxide yield was calculated around 10% which showed a dominant 4e^- reduction process for O_2 .

Similarly, the electron transfer number deduced from RDE measurements was close to 4. On the other hand, Co–C indicated much negative onset potential for ORR and pristine carbon dots and Ppy showed a two-step reduction process following 2e^- ORR path.

AEMFC performance and stability

AEMFC performance is a very important and critical parameter to accept the superior performance of catalyst and membrane materials. According to the latest DOE targets, the AEMFC performance $\geq 600\text{ mW/cm}^2$ under H_2/air (maximum pressure of 1.5 atm) in platinum group metal (PGM)-free MEA should be achieved by 2025 to realize viability of AEMFC system [211]. In recent times, a record high AEMFC performance as high as 3.3 W/cm^2 was reported using PtRu anode and Pt/C cathode where the total PGM loading was 1.7 mg/cm^2 [212]. And a few research groups have managed to achieve peak power density between 50 and 100 mW/cm^2 with zero PGM catalyst [213,214]. In addition, PGM free cathodes such as CoFe_2O_4 delivered peak power density of 1.35 W/cm^2 when tested in AEMFC (PtRu anode radiation grafted ETFE based AEM) [215].

Coming to the hetero atom doped-carbon based catalysts, although various hetero atom doped carbons have been developed as alternate catalysts and claimed that the ORR performance was comparable to Pt/C, but their use as AEMFC cathode was not very well explored. Table 4 summarizes various hetero atom doped carbons that are explored as AEMFC cathode and their corresponding AEMFC performance. It was reported that AEMFC employing N doped CNTs cathode had delivered a peak power density of 38 mW/cm^2 while Pt/C shows 61 mW/cm^2 under similar conditions (Fig. 22 (a)). Similarly, N doped graphene, dual doped (N,S) graphene and tri doped (N,S,F) graphene were also explored as AEMFC cathodes and delivered the peak power density of 2.5 mW/cm^2 , 20 mW/cm^2 and 46 mW/cm^2 respectively (Fig. 22(b–d)) [110,132,136]. Interestingly, metal-heteroatom doped carbons have delivered better AEMFC performances than the pure heteroatom doped carbons owing to presence of more active sites. For example, NiCo-NCNT shows a peak power density of 65 mW/cm^2 outperforming the commercial Pt/C (Fig. 22(e)) [93] and bio-derived Co_2P Nanoparticles Supported on Nitrogen-Doped Carbon delivered a peak power density of 172 mW/cm^2 (Fig. 22(f)) [181]. These reports highlight that the combination of transition metal with heteroatom doped carbon could be a potential strategy to fabricate alternative cathode catalysts for AEMFC. However, the reported tests are not sufficient to prove their capability to replace Pt in the catalyst, more robust testing protocols should be adopted to claim the superior catalytic activity of heteroatom doped carbons.

Stability of the electrocatalysts is a very important factor to deliver sustainable device performance. The stability of the heteroatom doped carbons have been studied in half cell (ex situ) mode and compared with commercial Pt/C. For example, potential cycling of NCNTs in 3 M KOH for ORR up to 3500 cycles does not show any noticeable change in the voltammogram (Fig. 23(a)) [62]. Similarly, chronoamperometric response for NCNTs shows that the catalyst could retain 89% of the

Table 4 – AEMFC performance of various heteroatom doped carbons which are employed as cathode in AEMFC.

Hetero atom doped carbon as cathode in AEMFC	Anode	Membrane	Operating temperature (°C)	AEMFC performance (mW/cm ²)	Ref.
NiCo/NCNTs	Pt/C	FAA-3-50	60	65	[93]
N-(CDC/CNT)	Pt–Ru/C	Poly[2,2'-(2,2'',4,4'',6,6''-hexamethyl- <i>p</i> -terphenyl-3,3''-diyl)-5,5'-bibenzimidazole]	60	260 mW cm ⁻²	[216]
CoFe–N-CDC/CNT	Pt–Ru/C	crosslinked polystyrene functionalized with trimethylamine (Fumatech)	60	1120	[217]
N-CNTs	Pt/C	FAA, Fuma-Tech	50	37.3	[65]
NG	Pt/C	AHA (Neosepta)	60	2.5	[110]
N,S-Graphene	Pt/C	Fumapem	RT	20	[132]
F,N,S-rGO	Pt/C	poly(benzimidazolium)	85	46	[136]
MnO-NG	Pt/C	AHA (Neosepta)	30	13	[218]
CoO/rGO(N)	Pt/C	A201 Tokuyama	248	60	[219]
NG-CoO _x	Pt–Ru	low-density polyethylene (LDPE)-benzyltrimethylammonium (BTMA)	60	1005	[220]
N-doped bagasse-derived carbon	Pt/C	Fumapem	RT	6	[221]
Bio-Derived Co2P-Ndoped carbon	Pt/C	FAA-3-50, Fumatech	60	172.2	[181]

initial current after 2 h in 0.1 M KOH while Pt/C only shows 80% of initial current (Fig. 23(b)) [65]. On the other hand, P doped CNTs also did not show any degradation in current until 12,000 cycles (Fig. 23(c)) [74]. Similarly, graphene based catalysts were also tested for *ex situ* durability for few hours in half-cell mode, for example, N doped graphene shows only 32 mV negative shift in half-wave potential after 10,000 potential cycles in 0.1 M KOH (Fig. 23(d)) [110]. On the other hand, biowaste derived carbons are not much explored for their stability.

However, the actual stability of catalysts can only be understood from the full cell durability studies (in situ), according to the DOE targets, durability of catalyst in H₂/air (CO₂-free) after AST ≤40% loss after 10,000 square-wave cycles 0.6–0.95 V should be achieved by 2024 [207], so far in the literature, durability aspects heteroatom doped carbons concerning full cell are hardly reported. Adequate focus on the AEMFC performance and durability in AEMFC operation mode is indeed to fully understand the potentiality of these catalysts.

Conclusions and future prospective

Three available and commonly studied carbon materials (MWCNTs, graphene and biowaste derived carbon) have been reviewed for their application as ORR catalysts in alkaline media. Irrespective of the carbon source, heteroatom doping substantially enhances the ORR activity of carbon-based materials. It is widely admitted that the exact effect depends on the nature of the dopant (N,S,P,B etc.) and their chemical states; for example, in the case of N-doped carbons graphitic and pyridinic-N are more beneficial to enhance ORR activity while pyrrolic-N is less pronounced. Co-doping/multi heteroatom doping is an effective strategy compared to single atom

doping where the synergistic effects between the different heteroatoms are believed to play a crucial role in modifying the electronic structure of the carbon material. There are three categories of dopants: dopants with higher electronegativity than carbon (electron rich ex: N, F), dopants with lower electronegativity than carbon (electron deficient, ex: B), dopants having similar electronegativity than that of carbon (ex: S). Depending on the electronic characteristics of the dopants, the electrical neutrality of carbon will be affected. In the case of highly electronegative dopants, the carbon atom next to the doping site will experience a positive charge and can act as a host for oxygen adsorption which is primary step in the ORR. On the other hand, electro positive dopants themselves act as host for oxygen adsorption. If the electronegativity difference between the dopant and the carbon atom is not significant, the change in charge density is insignificant while the ORR could be promoted by altering the spin density of the carbon network. Compared to the metal free heteroatom doped carbons, making composites with the transition metal nanoparticles of M-X-C type (where M-transition metal, X-heteroatom-C carbon substrate) is identified as a good strategy to improve the ORR efficiencies in alkaline media. Metal nanoparticles are rich in ORR active sites but suffer from low surface area and poor stability, while heteroatom doped carbons have high surface area and good stability. Hence the hybridization of these two materials is an ideal scenario to design a potential ORR catalysts for their use in alkaline medium.

Although the use of heteroatom doped carbon materials has made significant advances in the electrocatalysis research, they are still far behind the commercial Pt/C catalysts in terms of activity and stability. This gap should be narrowed to realize the commercial applications of non-precious metal ORR catalysts by the design of robust

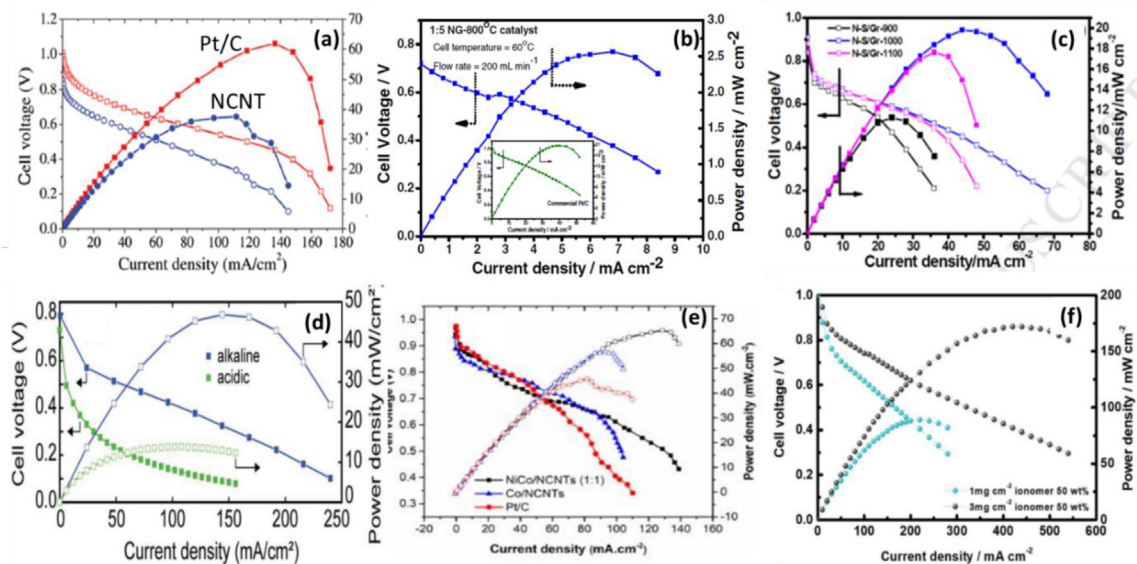


Fig. 22 – AEMFC performance with heteroatom doped carbons employed as cathode for (a) NCNT, (b) N-Graphene (c) N,S-codoped graphene (d) N,S,F doped graphene (e) NiCo/NCNTs (f) Co_2PN carbon derived from bean sprouts. Reproduced with permission from Refs. [65,93,110,132,136,181].

synthesis methodologies. As evident from many literature reports, the better ORR activity of heteroatom doped carbons are attributed to the change in charge and spin density of the carbon network upon doping. However, the mechanism of

charge and spin distribution is still unclear. Hence the future research needs to be focused on the understanding of these mechanisms through simulation and numerical approaches. The very important concern about this type of materials is

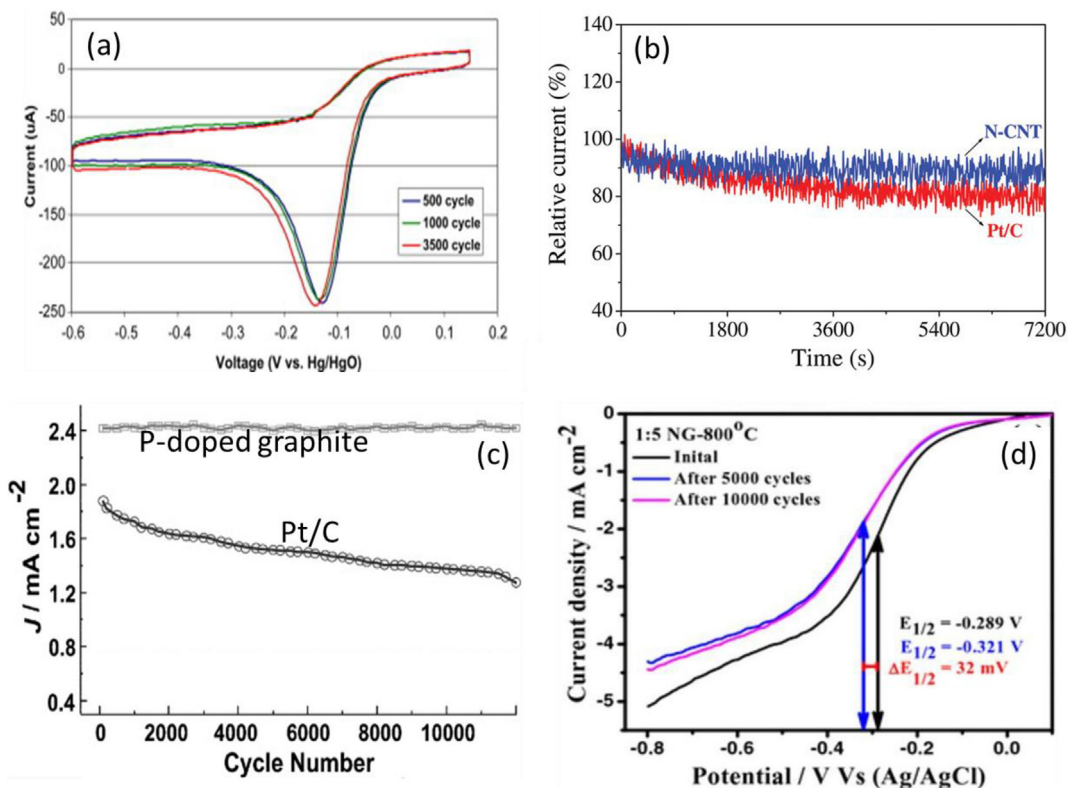


Fig. 23 – (a) Ex situ stability NCNTs up to 3500 cycles (b) chronoamperometric stability of NCNTs and Pt/C (c) stability of P-doped graphite and Pt/C and (d) Linear sweep voltammograms of N-graphene initial and after 10,000 cycles. Reproduced with permission from Refs. [62,65,74,110].

that, most of the literature focus on the half-cell (three electrode electrochemical cell) results and very limited results are available on the actual system. Since the actual system (fuel cell) environment is significantly different than that of a conventional three electrode electrochemical cell. Hence, future studies should focus in this direction to fully understand the electrocatalytic activity of the prepared electrocatalysts in the real system environment. In addition, stability of these catalysts under ORR conditions is an important factor to consider while designing this type of materials. The stability of these materials can be improved by gaining the more knowledge on the reaction mechanism and the intermediated formed during the ORR. It is important to establish more effective descriptors to assign the electro catalytic activity by considering the sufficient kinetic conditions and computer codes. On the other hand, experimental should be focused on adjusting the location and concentration of dopants, advanced characterization of dopants and defects, detecting the reaction intermediates during the ORR. In this direction, new synthesis methods should be developed. In our opinion, in situ doping is more suitable to prepare stable heteroatom doped carbons as there is direct bonding between carbon and heteroatom. Also it is important to improve the graphitic/crystalline nature of the doped carbons as they seem to be less prone to corrosion and oxidation. And finally, it is important to establish a correlation between the experimental results and theoretical calculations for the better understanding in designing the new generation of electrocatalysts.

In summary, by the design of appropriate synthesis methodologies and robust testing methodologies, a true alternative to Pt for ORR in alkaline media can be realized in near future.

Declaration of competing interest

The authors declare that they have no known competing financial interests or personal relationships that could have appeared to influence the work reported in this paper.

Acknowledgements

The authors acknowledge support for LEMTA and IJL by the “IMPACT ULHyS, Universite de Lorraine Hydrogene Science et Technologie” project of the “Lorraine Universite d’Excellence” (Investissements d’avenir e ANR). This work was supported partly by the French PIA project « Lorraine Universite d’Excellence », reference ANR-15-IDEX-04-LUE.

REFERENCES

- [1] Xiao L, Wang Z, Guan J. 2D MOFs and their derivatives for electrocatalytic applications: recent advances and new challenges. *Coord Chem Rev Dec.* 2022;472:214777. <https://doi.org/10.1016/j.ccr.2022.214777>.
- [2] Nie Y, Li L, Wei Z. Recent advancements in Pt and Pt-free catalysts for oxygen reduction reaction. *Chem Soc Rev Apr.* 2015;44(8):2168–201. <https://doi.org/10.1039/C4CS00484A>.
- [3] Lee Y, Suntivich J, May KJ, Perry EE, Shao-Horn Y. Synthesis and activities of rutile IrO₂ and RuO₂ nanoparticles for oxygen evolution in acid and alkaline solutions. *J Phys Chem Lett Feb.* 2012;3(3):399–404. https://doi.org/10.1021/JZ2016507/SUPPL_FILE/JZ2016507_SI_001.PDF.
- [4] Bai X, Wang L, Nan B, Tang T, Niu X, Guan J. Atomic manganese coordinated to nitrogen and sulfur for oxygen evolution. *Nano Res Apr.* 2022;15(7):6019–25. <https://doi.org/10.1007/S12274-022-4293-7>.
- [5] Yang H, Han X, Ibro Douka A, Huang L, Gong L, et al. Advanced oxygen electrocatalysis in energy conversion and storage. *Adv Funct Mater Mar.* 2021;31(12):2007602. <https://doi.org/10.1002/ADFM.202007602>.
- [6] Kiani M, Tian XQ, Zhang W. Non-precious metal electrocatalysts design for oxygen reduction reaction in polymer electrolyte membrane fuel cells: recent advances, challenges and future perspectives. *Coord Chem Rev Aug.* 2021;441:213954. <https://doi.org/10.1016/j.ccr.2021.213954>.
- [7] Han J, Zhang M, Bai X, Duan Z, Tang T, Guan J. Mesoporous Mn–Fe oxyhydroxides for oxygen evolution. *Inorg Chem Front Jul.* 2022;9(14):3559–65. <https://doi.org/10.1039/D2QJ00722C>.
- [8] Bai X, Duan Z, Nan B, Wang L, Tang T, Guan J. Unveiling the active sites of ultrathin Co-Fe layered double hydroxides for the oxygen evolution reaction. *Chin J Catal Aug.* 2022;43(8):2240–8. [https://doi.org/10.1016/S1872-2067\(21\)64033-0](https://doi.org/10.1016/S1872-2067(21)64033-0).
- [9] Bai X, Guan J. MXenes for electrocatalysis applications: modification and hybridization. *Chin J Catal Aug.* 2022;43(8):2057–90. [https://doi.org/10.1016/S1872-2067\(21\)64030-5](https://doi.org/10.1016/S1872-2067(21)64030-5).
- [10] Huang J, Yu Z, Tang J, Wang P, Tan Q, Wang J, Lei X. A review on anion exchange membranes for fuel cells: anion-exchange polyelectrolytes and synthesis strategies. *Int J Hydrogen Energy Jul.* 2022;47(65):27800–20. <https://doi.org/10.1016/j.ijhydene.2022.06.140>.
- [11] Ferriday TB, Middleton PH. Alkaline fuel cell technology - a review. *Int J Hydrogen Energy May* 2021;46(35):18489–510. <https://doi.org/10.1016/j.ijhydene.2021.02.203>.
- [12] Kang SY, Park JE, Jang GY, Kim OH, Kwon OJ, Cho YH, Sung YE. High-performance and durable water electrolysis using a highly conductive and stable anion-exchange membrane. *Int J Hydrogen Energy Feb.* 2022;47(15):9115–26. <https://doi.org/10.1016/j.ijhydene.2022.01.002>.
- [13] Mustain WE, Chatenet M, Page M, Kim YS. Durability challenges of anion exchange membrane fuel cells. *Energy Environ Sci Sep.* 2020;13(9):2805–38. <https://doi.org/10.1039/D0EE01133A>.
- [14] Ziv N, Mustain WE, Dekel DR. The effect of ambient carbon dioxide on anion-exchange membrane fuel cells. *ChemSusChem Apr.* 2018;11(7):1136–50. <https://doi.org/10.1002/CSSC.201702330>.
- [15] Cheng J, He G, Zhang F. A mini-review on anion exchange membranes for fuel cell applications: stability issue and addressing strategies. *Int J Hydrogen Energy Jun.* 2015;40(23):7348–60. <https://doi.org/10.1016/j.ijhydene.2015.04.040>.
- [16] Miller HA, Vizza F, Marelli M, Zadick A, Dubau L, Chatenet M, Geiger S, Cherevko S, Doan H, Pavlicek RK, Mukerjee S, Dekel DR. Highly active nanostructured palladium-ceria electrocatalysts for the hydrogen oxidation reaction in alkaline medium. *Nano Energy Mar.* 2017;33:293–305. <https://doi.org/10.1016/j.nanoen.2017.01.051>.
- [17] Dekel DR. Alkaline membrane fuel cell (AMFC) materials and system improvement - state-of-the-art. *ECS Trans Mar.* 2013;50(2):2051–2. <https://doi.org/10.1149/05002.2051ECST/XML>.

- [18] Hren M, Božič M, Fakin D, Kleinschek KS, Gorgieva S. Alkaline membrane fuel cells: anion exchange membranes and fuels. *Sustain Energy Fuels* Feb. 2021;5(3):604–37. <https://doi.org/10.1039/DOSE01373K>.
- [19] Gottesfeld S, Dekel DR, Page M, Bae C, Yan Y, Zelenay P, Kim YS. Anion exchange membrane fuel cells: current status and remaining challenges. *J Power Sources* Jan. 2018;375:170–84. <https://doi.org/10.1016/J.JPOWSOUR.2017.08.010>.
- [20] Gutru R, Turtayeva Z, Xu F, Maranzana G, Vigolo B, Desforges A. A comprehensive review on water management strategies and developments in anion exchange membrane fuel cells. *Int J Hydrogen Energy* Jul. 2020;45(38):19642–63. <https://doi.org/10.1016/J.IJHYDENE.2020.05.026>.
- [21] Eriksson B, Grimler H, Carlson A, Ekström H, Wreland Lindström R, Lindbergh G, Lagergren C. Quantifying water transport in anion exchange membrane fuel cells. *Int J Hydrogen Energy* Feb. 2019;44(10):4930–9. <https://doi.org/10.1016/J.IJHYDENE.2018.12.185>.
- [22] Ahmad S, Nawaz T, Ali A, Orhan MF, Samreen A, Kannan AM. An overview of proton exchange membranes for fuel cells: materials and manufacturing. *Int J Hydrogen Energy* May 2022;47(44):19086–131. <https://doi.org/10.1016/J.IJHYDENE.2022.04.099>.
- [23] Mooste M, Tkesheliadze T, Kozlova J, Kikas A, Kisand V, Treshchalov A, Tamm A, Aruväli J, Zagal JH, Kannan AM, Tammeveski K. Transition metal phthalocyanine-modified shungite-based cathode catalysts for alkaline membrane fuel cell. *Int J Hydrogen Energy* 2021;46(5):4365–77. <https://doi.org/10.1016/j.ijhydene.2020.10.231>.
- [24] Li Y, Dai H. Recent advances in zinc–air batteries. *Chem Soc Rev* Jul. 2014;43(15):5257–75. <https://doi.org/10.1039/C4CS00015C>.
- [25] Wang HF, Chen L, Pang H, Kaskel S, Xu Q. MOF-derived electrocatalysts for oxygen reduction, oxygen evolution and hydrogen evolution reactions. *Chem Soc Rev* Mar. 2020;49(5):1414–48. <https://doi.org/10.1039/C9CS00906J>.
- [26] Hussain S, Erikson H, Kongi N, Sarapuu A, Solla-Gullón J, Maia G, Kannan AM, Alonso-Vante N, Tammeveski K. Oxygen reduction reaction on nanostructured Pt-based electrocatalysts: a review. *Int J Hydrogen Energy* 2020;45(56):31775–97. <https://doi.org/10.1016/j.ijhydene.2020.08.215>.
- [27] Raj CR, Samanta A, Noh SH, Mondal S, Okajima T, Ohsaka T. Emerging new generation electrocatalysts for the oxygen reduction reaction. *J Mater Chem Jul.* 2016;4(29):11156–78. <https://doi.org/10.1039/C6TA03300H>.
- [28] Cheng F, Chen J. Metal–air batteries: from oxygen reduction electrochemistry to cathode catalysts. *Chem Soc Rev* Feb. 2012;41(6):2172–92. <https://doi.org/10.1039/C1CS15228A>.
- [29] Wang Z-L, Xu D, Xu J-J, Zhang X-B. Oxygen electrocatalysts in metal–air batteries: from aqueous to nonaqueous electrolytes. *Chem Soc Rev* 2014;43(22):7746–86. <https://doi.org/10.1039/C3CS60248F>.
- [30] Bard AJ, Faulkner LR. Basic potential step methods. *Electrochem. Methods Fundam. Appl. Dec.* 2001:156–225.
- [31] Ge X, Sumboja A, Wu D, An T, Li B, Goh FWT, Hor TSA, Zong Y, Liu Z. Oxygen reduction in alkaline media: from mechanisms to recent advances of catalysts. *ACS Catal* Aug. 2015;5(8):4643–67. https://doi.org/10.1021/ACSCATAL.5B00524/ASSET/IMAGES/LARGE/CS-2015-005246_0016.JPEG.
- [32] Guo S, Yuan P, Zhang J, Jin P, Sun H, Lei K, Pang X, Xu Q, Cheng F. Atomic-scaled cobalt encapsulated in P,N-doped carbon sheaths over carbon nanotubes for enhanced oxygen reduction electrocatalysis under acidic and alkaline media. *Chem Commun* Aug. 2017;53(71):9862–5. <https://doi.org/10.1039/C7CC05476A>.
- [33] Vielstich W, Gasteiger HA, Yokokawa H, editors. *Handbook of fuel cells: advances in electrocatalysis, material, diagnostics and durability*; 2009. p. 1090.
- [34] J. O. Bockris, A. K. N. Reddy, and M. E. Gamboa-Aldeco, *Modern electrochemistry. Volume 2A : fundamentals of electrocatalysis*.
- [35] Chu Y, Gu L, Ju X, Du H, Zhao J, Qu K. Carbon supported multi-branch nitrogen-containing polymers as oxygen reduction catalysts. *Catalyst* Jun. 2018;8(6):245. <https://doi.org/10.3390/CATAL8060245>. Page 245.
- [36] Wu J, Yang Z, Li X, Sun Q, Jin C, Strasser P, Yang R. Phosphorus-doped porous carbons as efficient electrocatalysts for oxygen reduction. *J Mater Chem Aug.* 2013;1(34):9889–96. <https://doi.org/10.1039/C3TA11849E>.
- [37] Hu P, Song Y, Chen L, Chen S. Electrocatalytic activity of alkyne-functionalized AgAu alloy nanoparticles for oxygen reduction in alkaline media. *Nanoscale* May 2015;7(21):9627–36. <https://doi.org/10.1039/C5NR01376C>.
- [38] Goswami C, Hazarika KK, Bharali P. Transition metal oxide nanocatalysts for oxygen reduction reaction. *Mater. Sci. Energy Technol.* Dec. 2018;1(2):117–28. <https://doi.org/10.1016/J.MSET.2018.06.005>.
- [39] Gupta S, Kellogg W, Xu H, Liu X, Cho J, Wu G. Bifunctional perovskite oxide catalysts for oxygen reduction and evolution in alkaline media. *Chem Asian J* Jan. 2016;11(1):10–21. <https://doi.org/10.1002/ASIA.201500640>.
- [40] Fu G, Lee JM. Ternary metal sulfides for electrocatalytic energy conversion. *J Mater Chem Apr.* 2019;7(16):9386–405. <https://doi.org/10.1039/C9TA01438A>.
- [41] Rambabu G, Bhat SD, Figueiredo FML. Carbon nanocomposite membrane electrolytes for direct methanol fuel cells-A concise review. *Nanomaterials* 2019. <https://doi.org/10.3390/nano9091292>.
- [42] Rambabu G, Bhat SD. Amino acid functionalized graphene oxide based nanocomposite membrane electrolytes for direct methanol fuel cells. *J Membr Sci* 2018;551(June 2017):1–11. <https://doi.org/10.1016/j.memsci.2018.01.026>.
- [43] Rambabu G, Bhat SD. Simultaneous tuning of methanol crossover and ionic conductivity of sPEEK membrane electrolyte by incorporation of PSSA functionalized MWCNTs: a comparative study in DMFCs. *Chem Eng J* 2014;243:517–25. <https://doi.org/10.1016/j.cej.2014.01.030>.
- [44] Saifuddin N, Raziah AZ, Junizah AR. Carbon nanotubes: a review on structure and their interaction with proteins. *J Chem* 2013. <https://doi.org/10.1155/2013/676815>.
- [45] Zeeshan A, Shehzad N, Atif M, Ellahi R, Sait SM. Electromagnetic flow of SWCNT/MWCNT suspensions in two immiscible water- and engine-oil-based Newtonian fluids through porous media. *Symmetry* Feb. 2022;14(2):406. <https://doi.org/10.3390/SYM14020406>.
- [46] Higgins D, Zamani P, Yu A, Chen Z. The application of graphene and its composites in oxygen reduction electrocatalysis: a perspective and review of recent progress. *Energy Environ Sci* 2016;9(2):357–90. <https://doi.org/10.1039/c5ee02474a>.
- [47] Kumar R, Sahoo S, Joanni E, Singh RK, Maegawa K, Tan WK, Kawamura G, Kar KK, Matsuda A. Heteroatom doped graphene engineering for energy storage and conversion. *Mater Today* Oct. 2020;39:47–65. <https://doi.org/10.1016/j.mattod.2020.04.010>.
- [48] Li J-C, Hou P-X, Liu C. Heteroatom-doped carbon nanotube and graphene-based electrocatalysts for oxygen reduction reaction. *Small* Dec. 2017;13(45):1702002. <https://doi.org/10.1002/smll.201702002>.
- [49] Mbayachi VB, Ndayiragije E, Sammani T, Taj S, Mbuta ER, ullah Khan A. Graphene synthesis, characterization and its

- applications: a review. *Results Chem Jan.* 2021;3:100163. <https://doi.org/10.1016/j.rechem.2021.100163>.
- [50] Escobar B, Martínez-Casillas DC, Pérez-Salcedo KY, Rosas D, Morales L, Liao SJ, Huang LL, Shi X. Research progress on biomass-derived carbon electrode materials for electrochemical energy storage and conversion technologies. *Int J Hydrogen Energy Jul.* 2021;46(51):26053–73. <https://doi.org/10.1016/j.ijhydene.2021.02.017>.
- [51] Pérez-Salcedo KY, Shi X, Kannan AM, Barbosa R, Quintana P, Escobar B. N-doped porous carbon from sargassum spp. as efficient metal-free electrocatalysts for O₂ reduction in alkaline fuel cells. *2019 Energies Jan.* 2019;12(3):346. <https://doi.org/10.3390/EN12030346>.
- [52] Dhyani V, Bhaskar T. A comprehensive review on the pyrolysis of lignocellulosic biomass. *Renew Energy Dec.* 2018;129:695–716. <https://doi.org/10.1016/j.renene.2017.04.035>.
- [53] Wang C, Waje M, Wang X, Tang JM, Haddon RC, Yan Y. Proton exchange membrane fuel cells with carbon nanotube based electrodes. *Nano Lett Feb.* 2004;4(2):345–8. <https://doi.org/10.1021/NL034952P/ASSET/IMAGES/LARGE/NL034952PF00004.JPEG>.
- [54] Shao Y, Liu J, Wang Y, Lin Y. Novel catalyst support materials for PEM fuel cells: current status and future prospects. *J Mater Chem Dec.* 2008;19(1):46–59. <https://doi.org/10.1039/B808370C>.
- [55] Ito Y, Christodoulou C, Nardi MV, Koch N, Sachdev H, Müllen K. Chemical vapor deposition of N-doped graphene and carbon films: the role of precursors and gas phase. *ACS Nano Apr.* 2014;8(4):3337–46. https://doi.org/10.1021/NN405661B/SUPPL_FILE/NN405661B_SI_001.PDF.
- [56] Wang C, Wu WD, Wang Y, Xu D, Yan F. Nitrogen doped carbon materials derived from *Gentiana scabra* Bunge as high-performance catalysts for the oxygen reduction reaction. *New J Chem Jul.* 2017;41(15):7392–9. <https://doi.org/10.1039/C7NJ01178D>.
- [57] Pan F, Guo S, Zhang J. Swelling-induced synthesis of nitrogen-doped graphene for oxygen reduction reaction. *Electrochim Acta Oct.* 2015;180:29–36. <https://doi.org/10.1016/j.electacta.2015.08.079>.
- [58] Zheng J, Guo C, Chen C, Fan M, Gong J, Zhang Y, Zhao T, Sun Y, Xu X, Li M, Wang R, Luo Z, Chen C. High content of pyridinic- and pyrrolic-nitrogen-modified carbon nanotubes derived from blood biomass for the electrocatalysis of oxygen reduction reaction in alkaline medium. *Electrochim Acta Jun.* 2015;168:386–93. <https://doi.org/10.1016/j.electacta.2015.03.173>.
- [59] Kruusenberg I, Ratto S, Vikkisk M, Kanninen P, Kallio T, Kannan AM, Tammeveski K. Highly active nitrogen-doped nanocarbon electrocatalysts for alkaline direct methanol fuel cell. *J Power Sources May* 2015;281:94–102. <https://doi.org/10.1016/j.jpowsour.2015.01.167>.
- [60] Gong K, Du F, Xia X, Durstock M, Dai L. Nitrogen-doped carbon nanotube arrays with high electrocatalytic activity for oxygen reduction. *Science Feb.* 2009;323(5915):760–4. https://doi.org/10.1126/SCIENCE.1168049/SUPPL_FILE/GONG.SOM.PDF.
- [61] Chen Z, Higgins D, Tao H, Hsu RS, Chen Z. Highly active nitrogen-doped carbon nanotubes for oxygen reduction reaction in fuel cell applications. *J Phys Chem C Dec.* 2009;113(49):21008–13. <https://doi.org/10.1021/jp908067v>.
- [62] Li H, Liu H, Jong Z, Qu W, Geng D, Sun X, Wang H. Nitrogen-doped carbon nanotubes with high activity for oxygen reduction in alkaline media. *Int J Hydrogen Energy Feb.* 2011;36(3):2258–65. <https://doi.org/10.1016/j.ijhydene.2010.11.025>.
- [63] Nagaiah TC, Kundu S, Bron M, Muhler M, Schuhmann W. Nitrogen-doped carbon nanotubes as a cathode catalyst for the oxygen reduction reaction in alkaline medium. *Electrochim Commun Mar.* 2010;12(3):338–41. <https://doi.org/10.1016/j.elecom.2009.12.021>.
- [64] Deng H, Li Q, Liu J, Wang F. Active sites for oxygen reduction reaction on nitrogen-doped carbon nanotubes derived from polyaniline. *Carbon N. Y. Feb.* 2017;112:219–29. <https://doi.org/10.1016/j.carbon.2016.11.014>.
- [65] Venkateswara Rao C, Ishikawa Y. Activity, selectivity, and anion-exchange membrane fuel cell performance of virtually metal-free nitrogen-doped carbon nanotube electrodes for oxygen reduction reaction. *J Phys Chem C Feb.* 2012;116(6):4340–6. <https://doi.org/10.1021/jp210840a>.
- [66] Xu Z, Zhou Z, Li B, Wang G, Leu PW. Identification of efficient active sites in nitrogen-doped carbon nanotubes for oxygen reduction reaction. *J Phys Chem C* 2020;124:8689–96. https://doi.org/10.1021/ACS.JPC.9B11090/ASSET/IMAGES/LARGE/JP9B11090_0004.JPEG.
- [67] Rocha IM, Soares OSGP, Fernandes DM, Freire C, Figueiredo JL, Pereira MFR. N-Doped carbon nanotubes for the oxygen reduction reaction in alkaline medium: synergistic relationship between pyridinic and quaternary nitrogen. *ChemistrySelect* 2016;1(10):2522–30. <https://doi.org/10.1002/slct.201600615>.
- [68] Vikkisk M, Kruusenberg I, Ratto S, Joost U, Shulga E, Kink I, Rauwel P, Tammeveski K. Enhanced electrocatalytic activity of nitrogen-doped multi-walled carbon nanotubes towards the oxygen reduction reaction in alkaline media. *RSC Adv* 2015;5(73):59495–505. <https://doi.org/10.1039/C5RA08818F>.
- [69] Sharifi T, Hu G, Jia X, Wågberg T. Formation of active sites for oxygen reduction reactions by transformation of nitrogen functionalities in nitrogen-doped carbon nanotubes. *ACS Nano Oct.* 2012;6(10):8904–12. https://doi.org/10.1021/NN302906R/SUPPL_FILE/NN302906R_SI_001.PDF.
- [70] Lai L, Potts JR, Zhan D, Wang L, Poh CK, Tang C, Gong H, Shen Z, Lin J, Ruoff RS. Exploration of the active center structure of nitrogen-doped graphene-based catalysts for oxygen reduction reaction. *Energy Environ Sci Jun.* 2012;5(7):7936–42. <https://doi.org/10.1039/C2EE21802J>.
- [71] Cheng Y, Tian Y, Fan X, Liu J, Yan C. Boron doped multi-walled carbon nanotubes as catalysts for oxygen reduction reaction and oxygen evolution reaction in alkaline media. *Electrochim Acta* 2014;143:291–6. <https://doi.org/10.1016/j.electacta.2014.08.001>.
- [72] Yang L, Jiang S, Zhao Y, Zhu L, Chen S, et al. Boron-doped carbon nanotubes as metal-free electrocatalysts for the oxygen reduction reaction. *Angew Chem Int Ed Jul.* 2011;50(31):7132–5. <https://doi.org/10.1002/anie.201101287>.
- [73] Paraknowitsch JP, Thomas A. Doping carbons beyond nitrogen: an overview of advanced heteroatom doped carbons with boron, sulphur and phosphorus for energy applications. *Energy Environ Sci Sep.* 2013;6(10):2839–55. <https://doi.org/10.1039/c3ee41444b>. The Royal Society of Chemistry.
- [74] Liu Z-W, Peng F, Wang H-J, Yu H, Zheng W-X, Yang J. Phosphorus-doped graphite layers with high electrocatalytic activity for the O₂ reduction in an alkaline medium. *Angew Chem Mar.* 2011;123(14):3315–9. <https://doi.org/10.1002/ange.201006768>.
- [75] Some S, Kim J, Lee K, Kulkarni A, Yoon Y, Lee S, Kim T, Lee H. Highly air-stable phosphorus-doped n-type graphene field-effect transistors. *Adv Mater Oct.* 2012;24(40):5481–6. <https://doi.org/10.1002/adma.201202255>.
- [76] Guo MQ, Huang JQ, Kong XY, Peng HJ, Shui H, Qian FY, Zhu L, Zhu WC, Zhang Q. Hydrothermal synthesis of porous phosphorus-doped carbon nanotubes and their use in the oxygen reduction reaction and lithium-sulfur batteries.

- Xinxing Tan Cailiao/New Carbon Mater. 2016;31(3):352–62. [https://doi.org/10.1016/S1872-5805\(16\)60019-7](https://doi.org/10.1016/S1872-5805(16)60019-7).
- [77] Yu D, Xue Y, Dai L. Vertically aligned carbon nanotube Arrays Co-doped with phosphorus and nitrogen as efficient metal-free electrocatalysts for oxygen reduction. *J Phys Chem Lett Oct.* 2012;3(19):2863–70. <https://doi.org/10.1021/jz3011833>.
- [78] Wang S, Iyyamperumal E, Roy A, Xue Y, Yu D, Dai L. Vertically aligned BCN nanotubes as efficient metal-free electrocatalysts for the oxygen reduction reaction: a synergetic effect by Co-doping with boron and nitrogen. *Angew Chem Int Ed Dec.* 2011;50(49):11756–60. <https://doi.org/10.1002/anie.201105204>.
- [79] Rambabu G, Turtayeva Z, Xu F, Maranzana G, Emo M, Hupont S, Mamlouk M, Desforges A, Vigolo B. Insights into the electrocatalytic behavior of nitrogen and sulfur co-doped carbon nanotubes toward oxygen reduction reaction in alkaline media. *J Mater Sci Sep.* 2022;57(35):16739–54. <https://doi.org/10.1007/S10853-022-07653-3/TABLES/4>.
- [80] Shi Q, Peng F, Liao S, Wang H, Yu H, Liu Z, Zhang B, Su D. Sulfur and nitrogen co-doped carbon nanotubes for enhancing electrochemical oxygen reduction activity in acidic and alkaline media. *J Mater Chem* 2013;1(47):14853. <https://doi.org/10.1039/c3ta12647a>.
- [81] Khalfoun H, Hermet P, Henrard L, Latil S. B and N codoping effect on electronic transport in carbon nanotubes. *Phys Rev B May* 2010;81(19):193411. <https://doi.org/10.1103/PhysRevB.81.193411>.
- [82] Zhao Y, Yang L, Chen S, Wang X, Ma Y, Wu Q, Jiang Y, Qian W, Hu Z. Can boron and nitrogen Co-doping improve oxygen reduction reaction activity of carbon nanotubes? *J Am Chem Soc Jan.* 2013;135(4):1201–4. <https://doi.org/10.1021/ja310566z>.
- [83] Cruz-Silva E, Cullen DA, Gu L, Romo-Herrera JM, Muñoz-Sandoval E, López-Urías F, Sumpter BG, Meunier V, Charlier J-C, Smith DJ, Terrones H, Terrones M. Heterodoped nanotubes: theory, synthesis, and characterization of Phosphorus–Nitrogen doped multiwalled carbon nanotubes. *ACS Nano Mar.* 2008;2(3):441–8. <https://doi.org/10.1021/nn700330w>.
- [84] Ganguly D, Sundara R, Ramanujam K. Chemical vapor deposition-grown nickel-encapsulated N-doped carbon nanotubes as a highly active oxygen reduction reaction catalyst without direct metal–nitrogen coordination. *ACS Omega Oct.* 2018;3(10):13609–20. <https://doi.org/10.1021/acsomega.8b01565>.
- [85] Liang J, Zhou RF, Chen XM, Tang YH, Qiao SZ. Fe-N decorated hybrids of CNTs grown on hierarchically porous carbon for high-performance oxygen reduction. *Adv Mater Sep.* 2014;26(35):6074–9. <https://doi.org/10.1002/adma.201401848>.
- [86] Yang G, Choi W, Pu X, Yu C. Scalable synthesis of bi-functional high-performance carbon nanotube sponge catalysts and electrodes with optimum C–N–Fe coordination for oxygen reduction reaction. *Energy Environ Sci* 2015;8(6):1799–807. <https://doi.org/10.1039/C5EE00682A>.
- [87] Kruusenberg I, Ramani D, Ratso S, Joost U, Saar R, Rauwel P, Kannan AM, Tammeveski K. Cobalt-nitrogen Co-doped carbon nanotube cathode catalyst for alkaline membrane fuel cells. *Chemelectrochem Sep.* 2016;3(9):1455–65. <https://doi.org/10.1002/celec.201600241>.
- [88] Ratso S, Kruusenberg I, Sarapuu A, Rauwel P, Saar R, Joost U, Aruväli J, Kanninen P, Kallio T, Tammeveski K. Enhanced oxygen reduction reaction activity of iron-containing nitrogen-doped carbon nanotubes for alkaline direct methanol fuel cell application. *J Power Sources* 2016;332:129–38. <https://doi.org/10.1016/j.jpowsour.2016.09.069>.
- [89] Zhao H, Xing T, Li L, Geng X, Guo K, Sun C, Zhou W, Yang H, Song R, An B. Synthesis of cobalt and nitrogen co-doped carbon nanotubes and its ORR activity as the catalyst used in hydrogen fuel cells. *Int J Hydrogen Energy Sep.* 2019;44(46):25180–7. <https://doi.org/10.1016/j.ijhydene.2019.03.271>.
- [90] Kong A, Kong Y, Zhu X, Han Z, Shan Y. Ordered mesoporous Fe (or Co)–N–graphitic carbons as excellent non-precious-metal electrocatalysts for oxygen reduction. *Carbon N. Y.* Nov. 2014;78:49–59. <https://doi.org/10.1016/j.carbon.2014.06.047>.
- [91] Gao T, Jin Z, Zhang Y, Tan G, Yuan H, Xiao D. Coupling cobalt-iron bimetallic nitrides and N-doped multi-walled carbon nanotubes as high-performance bifunctional catalysts for oxygen evolution and reduction reaction. *Electrochim Acta Dec.* 2017;258:51–60. <https://doi.org/10.1016/j.electacta.2017.07.172>.
- [92] Dong Z, Liu G, Zhou S, Zhang Y, Zhang W, Fan A, Zhang X, Dai X. Restructured Fe–Mn alloys encapsulated by N–doped carbon nanotube catalysts derived from bimetallic MOF for enhanced oxygen reduction reaction. *ChemCatChem Dec.* 2018;10(23):5475–86. <https://doi.org/10.1002/cctc.201801412>.
- [93] Hanif S, Iqbal N, Shi X, Noor T, Ali G, Kannan AM. NiCo–N-doped carbon nanotubes based cathode catalyst for alkaline membrane fuel cell. *Renew Energy Jul.* 2020;154:508–16. <https://doi.org/10.1016/j.renene.2020.03.060>.
- [94] Sharifi T, Hu G, Jia X, Wågberg T. formation of active sites for oxygen reduction reactions by transformation of nitrogen functionalities in nitrogen-doped carbon nanotubes. *ACS Nano Oct.* 2012;6(10):8904–12. <https://doi.org/10.1021/nn302906r>.
- [95] Chen L, Zhou H, Wei S, Chen Z, Huang Z, Huang Z, Zhang C, Kuang Y. Facile synthesis of nitrogen-doped unzipped carbon nanotubes and their electrochemical properties. *RSC Adv* 2015;5(11):8175–81. <https://doi.org/10.1039/c4ra15008b>.
- [96] Yang L, Jiang S, Zhao Y, Zhu L, Chen S, Wang X, Wu Q, Ma J, Ma Y, Hu Z. Boron-doped carbon nanotubes as metal-free electrocatalysts for the oxygen reduction reaction. *Angew Chem Int Ed Jul.* 2011;50(31):7132–5. <https://doi.org/10.1002/anie.201101287>.
- [97] Zhang Y, Zhang J, Su DS. Substitutional doping of carbon nanotubes with heteroatoms and their chemical applications. *ChemSusChem May* 2014;7(5):1240–50. <https://doi.org/10.1002/cssc.201301166>.
- [98] Osmieri L, Monteverde Videla AHA, Specchia S. Activity of Co–N multi walled carbon nanotubes electrocatalysts for oxygen reduction reaction in acid conditions. *J Power Sources Mar.* 2015;278:296–307. <https://doi.org/10.1016/j.jpowsour.2014.12.080>.
- [99] Liu Y, Jiang H, Zhu Y, Yang X, Li C. Transition metals (Fe, Co, and Ni) encapsulated in nitrogen-doped carbon nanotubes as bi-functional catalysts for oxygen electrode reactions. *J Mater Chem* 2016;4(5):1694–701. <https://doi.org/10.1039/c5ta10551j>.
- [100] Zhang X, Lu P, Cui X, Chen L, Zhang C, Li M, Xu Y, Shi J. Probing the electro-catalytic ORR activity of cobalt-incorporated nitrogen-doped CNTs. *J Catal* 2016;344:455–64. <https://doi.org/10.1016/j.jcat.2016.10.019>.
- [101] Li JC, Yang ZQ, Tang DM, Zhang L, Hou PX, Zhao SY, Liu C, Cheng M, Li GX, Zhang F, Cheng HM. N-doped carbon nanotubes containing a high concentration of single iron atoms for efficient oxygen reduction. *NPG Asia Mater* 2018;10(1):e461. <https://doi.org/10.1038/am.2017.212>.
- [102] Türk KK, Kruusenberg I, Kibena-Pöldsepp E, Bhowmick GD, Kook M, Tammeveski K, Matisen L, Merisalu M, Sammelselg V, Ghangrekar MM, Mitra A, Banerjee R. Novel multi walled carbon nanotube based nitrogen impregnated

- Co and Fe cathode catalysts for improved microbial fuel cell performance. *Int J Hydrogen Energy* 2018;43(51):23027–35. <https://doi.org/10.1016/j.ijhydene.2018.10.143>.
- [103] Du P, Bao Y, Guo C, Wu L, Pan J, Zhao C, Ma F-X, Lu J, Li YY. Design of Fe,N co-doped multi-walled carbon nanotubes for efficient oxygen reduction. *Chem Commun* 2020. <https://doi.org/10.1039/d0cc05520d>.
- [104] Zehtab Yazdi A, Fei H, Ye R, Wang G, Tour J, Sundararaj U. Boron/nitrogen co-doped helically unzipped multiwalled carbon nanotubes as efficient electrocatalyst for oxygen reduction. *ACS Appl Mater Interfaces* 2015;7(14):7786–94. <https://doi.org/10.1021/acsami.5b01067>.
- [105] Peera SG, Sahu AK, Arunchander A, Bhat SD, Karthikeyan J, Murugan P. Nitrogen and fluorine co-doped graphite nanofibers as high durable oxygen reduction catalyst in acidic media for polymer electrolyte fuel cells. *Carbon N. Y.* 2015;93:130–42. <https://doi.org/10.1016/j.carbon.2015.05.002>.
- [106] Xu Z, Zhou Z, Li B, Wang G, Leu PW. Identification of efficient active sites in nitrogen-doped carbon nanotubes for oxygen reduction reaction. *J Phys Chem C Apr.* 2020;124(16):8689–96. <https://doi.org/10.1021/acs.jpcc.9b11090>.
- [107] Yang L, Ding H, Xu G, Zhang L, Wei B. Efficient ORR activity of N-doped porous carbon encapsulated cobalt electrocatalyst derived from a novel bimetal-organic framework. *Mater Res Bull Jun.* 2021;138:111237. <https://doi.org/10.1016/j.materresbull.2021.111237>.
- [108] Rauf M, Wang J, Handschuh-Wang S, Zhou Z, Iqbal Waheed, Khan SA, Zhuang L, Ren X, Li Y, Sun S. Highly stable N-containing polymer-based Fe/Nx/C electrocatalyst for alkaline anion exchange membrane fuel cell applications. *Prog. Nat. Sci. Mater. Int., Nov.* 2021. <https://doi.org/10.1016/j.pnsc.2021.10.016>.
- [109] Qu L, Liu Y, Baek J-B, Dai L. Nitrogen-doped graphene as efficient metal-free electrocatalyst for oxygen reduction in fuel cells. *ACS Nano Mar.* 2010;4(3):1321–6. <https://doi.org/10.1021/nn901850u>.
- [110] Kumar MP, Raju MM, Arunchander A, Selvaraj S, Kalita G, Narayanan TN, Sahu AK, Pattanayak DK. Nitrogen doped graphene as metal free electrocatalyst for efficient oxygen reduction reaction in alkaline media and its application in anion exchange membrane fuel cells. *J Electrochem Soc* 2016;163(8):F848–55. <https://doi.org/10.1149/2.0541608jes>.
- [111] Kakaei K, Ghadimi G. A green method for Nitrogen-doped graphene and its application for oxygen reduction reaction in alkaline media. *Mater Technol* 2020;1–8. <https://doi.org/10.1080/10667857.2020.1724692>.
- [112] Bin Yang H, Miao J, Hung S-F, Chen J, Tao HB, Wang X, Zhang L, Chen R, Gao J, Chen HM, Dai L, Liu B. Identification of catalytic sites for oxygen reduction and oxygen evolution in N-doped graphene materials: development of highly efficient metal-free bifunctional electrocatalyst. *Sci Adv Apr.* 2016;2(4). <https://doi.org/10.1126/sciadv.1501122>.
- [113] Lin Z, Song M, Ding Y, Liu Y, Liu M, Wong C. Facile preparation of nitrogen-doped graphene as a metal-free catalyst for oxygen reduction reaction. *Phys Chem Chem Phys* 2012;14(10):3381. <https://doi.org/10.1039/c2cp00032f>.
- [114] Guo D, Shibuya R, Akiba C, Saji S, Kondo T, Nakamura J. Active sites of nitrogen-doped carbon materials for oxygen reduction reaction clarified using model catalysts. *Science Jan.* 2016;351(6271):361–5. <https://doi.org/10.1126/science.aad0832>.
- [115] Gopalakrishnan K, Govindaraj A, Rao CNR. Extraordinary supercapacitor performance of heavily nitrogenated graphene oxide obtained by microwave synthesis. *J Mater Chem* 2013;1(26):7563. <https://doi.org/10.1039/c3ta11385j>.
- [116] Vikkisk M, Kruusenberg I, Joost U, Shulga E, Kink I, Tammeveski K. Electrocatalytic oxygen reduction on nitrogen-doped graphene in alkaline media. *Appl Catal B Environ Apr.* 2014;147:369–76. <https://doi.org/10.1016/j.apcatb.2013.09.011>.
- [117] Lemes G, Sebastián D, Pastor E, Lázaro MJ. N-doped graphene catalysts with high nitrogen concentration for the oxygen reduction reaction. *J Power Sources* 2019;438(September). <https://doi.org/10.1016/j.jpowsour.2019.227036>.
- [118] Xiang Q, Liu Y, Zou X, Hu B, Qiang Y, Yu D, Yin W, Chen C. Hydrothermal synthesis of a new kind of N-doped graphene gel-like hybrid as an enhanced ORR electrocatalyst. *ACS Appl Mater Interfaces Apr.* 2018;10(13):10842–50. <https://doi.org/10.1021/acsami.7b19122>.
- [119] Bang GS, Shim GW, Shin GH, Jung DY, Park H, Hong WG, Choi J, Lee J, Choi SY. Pyridinic-N-Doped graphene paper from perforated graphene oxide for efficient oxygen reduction. *ACS Omega* 2018;3(5):5522–30. <https://doi.org/10.1021/acsomega.8b00400>.
- [120] Farzaneh A, Saghatoleslami N, Goharshadi EK, Gharibi H, Ahmadzadeh H. 3-D mesoporous nitrogen-doped reduced graphene oxide as an efficient metal-free electrocatalyst for oxygen reduction reaction in alkaline fuel cells: role of π and lone pair electrons. *Electrochim Acta Dec.* 2016;222:608–18. <https://doi.org/10.1016/j.electacta.2016.11.015>.
- [121] Huang X, Qian K, Yang J, Zhang J, Li L, Yu C, Zhao D. Functional nanoporous graphene foams with controlled pore sizes. *Adv Mater Aug.* 2012;24(32):4419–23. <https://doi.org/10.1002/adma.201201680>.
- [122] Tang S, Zhou X, Xu N, Bai Z, Qiao J, Zhang J. Template-free synthesis of three-dimensional nanoporous N-doped graphene for high performance fuel cell oxygen reduction reaction in alkaline media. *Appl Energy* 2016;175:405–13. <https://doi.org/10.1016/j.apenergy.2016.04.074>.
- [123] Pristavita R, Mendoza-Gonzalez N-Y, Meunier J-L, Berk D. Carbon blacks produced by thermal plasma: the influence of the reactor geometry on the product morphology. *Plasma Chem Plasma Process Apr.* 2010;30(2):267–79. <https://doi.org/10.1007/s11090-010-9218-7>.
- [124] Zhang L, Xia Z. Mechanisms of oxygen reduction reaction on nitrogen-doped graphene for fuel cells. *J Phys Chem C Jun.* 2011;115(22):11170–6. <https://doi.org/10.1021/jp201991j>.
- [125] Zhang L, Niu J, Li M, Xia Z. Catalytic mechanisms of sulfur-doped graphene as efficient oxygen reduction reaction catalysts for fuel cells. *J Phys Chem C Feb.* 2014;118(7):3545–53. <https://doi.org/10.1021/jp410501u>.
- [126] Jin J, Pan F, Jiang L, Fu X, Liang A, Wei Z, Zhang J, Sun G. Catalyst-free synthesis of crumpled boron and nitrogen Co-doped graphite layers with tunable bond structure for oxygen reduction reaction. *ACS Nano Apr.* 2014;8(4):3313–21. <https://doi.org/10.1021/nn404927n>.
- [127] Yang Z, Yao Z, Li G, Fang G, Nie H, Liu Z, Zhou X, Chen X, Huang S. Sulfur-doped graphene as an efficient metal-free cathode catalyst for oxygen reduction. *ACS Nano Jan.* 2012;6(1):205–11. <https://doi.org/10.1021/nn203393d>.
- [128] Zhang Y, Chu M, Yang L, Deng W, Tan Y, Ma M, Xie Q. Synthesis and oxygen reduction properties of three-dimensional sulfur-doped graphene networks. *Chem Commun* 2014;50(48):6382. <https://doi.org/10.1039/c4cc01939c>.
- [129] Zhang C, Mahmood N, Yin H, Liu F, Hou Y. Synthesis of phosphorus-doped graphene and its multifunctional applications for oxygen reduction reaction and lithium ion batteries. *Adv Mater Sep.* 2013;25(35):4932–7. <https://doi.org/10.1002/adma.201301870>.

- [130] Wang M, Li Y, Fang J, Villa CJ, Xu Y, Hao S, Li J, Liu Y, Wolverton C, Chen X, Dravid VP, Lai Y. Superior oxygen reduction reaction on Phosphorus-Doped carbon dot/graphene aerogel for All-Solid-State flexible Al-air batteries. *Adv Energy Mater Jan.* 2020;10(3):1902736. <https://doi.org/10.1002/aenm.201902736>.
- [131] Zhang H, Niu Y, Hu W. Nitrogen/sulfur-doping of graphene with cysteine as a heteroatom source for oxygen reduction electrocatalysis. *J Colloid Interface Sci* 2017;505:32–7. <https://doi.org/10.1016/j.jcis.2017.05.069>.
- [132] Arunchander A, Peera SG, Panda SK, Chellammal S, Sahu AK. Simultaneous co-doping of N and S by a facile in-situ polymerization of 6-N,N-dibutylamine-1,3,5-triazine-2,4-dithiol on graphene framework: an efficient and durable oxygen reduction catalyst in alkaline medium. *Carbon N. Y.* 2017;118:531–44. <https://doi.org/10.1016/j.carbon.2017.03.093>.
- [133] Jang D, Lee S, Kim S, Choi K, Park S, Oh J, Park S. Production of P, N Co-doped graphene-based materials by a solution process and their electrocatalytic performance for oxygen reduction reaction. *ChemNanoMat Jan.* 2018;4(1):118–23. <https://doi.org/10.1002/cnma.201700241>.
- [134] Musico YLF, Kakati N, Labata MFM, Ocon JD, Chuang PYA. One-pot hydrothermal synthesis of heteroatom co-doped with fluorine on reduced graphene oxide for enhanced ORR activity and stability in alkaline media. *Mater Chem Phys* 2019;236(May):121804. <https://doi.org/10.1016/j.matchemphys.2019.121804>.
- [135] Kang GS, Lee S, Lee DC, Yoon CW, Joh HI. Edge-enriched graphene with boron and nitrogen co-doping for enhanced oxygen reduction reaction. *Curr Appl Phys* 2020;20(3):456–61. <https://doi.org/10.1016/j.cap.2020.01.008>.
- [136] Van Pham C, Klingele M, Britton B, Vuyyuru KR, Unmuessig T, Holdcroft S, Fischer A, Thiele S. Tridoped reduced graphene oxide as a metal-free catalyst for oxygen reduction reaction demonstrated in acidic and alkaline polymer electrolyte fuel cells. *Adv. Sustain. Syst.* 2017;1(5):1–10. <https://doi.org/10.1002/adus.201600038>.
- [137] Li Y, Wen H, Yang J, Zhou Y, Cheng X. Boosting oxygen reduction catalysis with N, F, and S tri-doped porous graphene: tertiary N-precursors regulates the constitutions of catalytic active sites. *Carbon N. Y.* 2019;142:1–12. <https://doi.org/10.1016/j.carbon.2018.09.079>.
- [138] Shao M, Chang Q, Dodelet J-P, Chenitz R. Recent advances in electrocatalysts for oxygen reduction reaction. *Chem Rev Mar.* 2016;116(6):3594–657. <https://doi.org/10.1021/acs.chemrev.5b00462>.
- [139] Zhang G, Lu W, Cao F, Xiao Z, Zheng X. N-doped graphene coupled with Co nanoparticles as an efficient electrocatalyst for oxygen reduction in alkaline media. *J Power Sources* 2016;302:114–25. <https://doi.org/10.1016/j.jpowsour.2015.10.055>.
- [140] Parvez K, Yang S, Hernandez Y, Winter A, Turchanin A, Feng X, Müllen K. Nitrogen-doped graphene and its iron-based composite as efficient electrocatalysts for oxygen reduction reaction. *ACS Nano Nov.* 2012;6(11):9541–50. <https://doi.org/10.1021/nn302674k>.
- [141] Zhao D, Shui J-L, Grabstanowicz LR, Chen C, Commet SM, Xu T, Lu J, Liu D-J. Highly efficient non-precious metal electrocatalysts prepared from one-pot synthesized zeolitic imidazolate frameworks. *Adv Mater Feb.* 2014;26(7):1093–7. <https://doi.org/10.1002/adma.201304238>.
- [142] Wu G, Johnston CM, Mack NH, Artyushkova K, Ferrandon M, Nelson M, Lezama-Pacheco JS, Conradson SD, More KL, Myers DJ, Zelenay P. Synthesis–structure–performance correlation for polyaniline–Me–C non-precious metal cathode catalysts for oxygen reduction in fuel cells. *J Mater Chem* 2011;21(30):11392. <https://doi.org/10.1039/c0jm03613g>.
- [143] Wen X, Bai L, Li M, Guan J. Atomically dispersed cobalt- and nitrogen-codoped graphene toward bifunctional catalysis of oxygen reduction and hydrogen evolution reactions. *ACS Sustainable Chem Eng* 2019;7(10):9249–56. <https://doi.org/10.1021/acssuschemeng.9b00105>.
- [144] Varga T, Ballai G, Vászrhelyi L, Haspel H, Kukovecz Á, Kónya Z. Co4N/nitrogen-doped graphene: a non-noble metal oxygen reduction electrocatalyst for alkaline fuel cells. *Appl Catal B Environ* 2018;237(March):826–34. <https://doi.org/10.1016/j.apcatb.2018.06.054>.
- [145] Wang W, Lin L, Yu D, Liu B. Study on the photocatalytic performance of BiVO₄/Bi₂WO₆/multi-walled carbon nanotube nanocomposites in one-pot hydrothermal process. *J Nanosci Nanotechnol Nov.* 2018;18(11):7691–702. <https://doi.org/10.1166/jnn.2018.15559>.
- [146] Kottakkat T, Bron M. One-Pot synthesis of cobalt-incorporated nitrogen-doped reduced graphene oxide as an oxygen reduction reaction catalyst in alkaline medium. *Chemelectrochem Dec.* 2014;1(12):2163–71. <https://doi.org/10.1002/celec.201402231>.
- [147] Komba N, Zhang G, Wei Q, Yang X, Prakash J, Chenitz R, Rosei F, Sun S. Iron (II) phthalocyanine/N-doped graphene: a highly efficient non-precious metal catalyst for oxygen reduction. *Int J Hydrogen Energy* 2019;44(33):18103–14. <https://doi.org/10.1016/j.ijhydene.2019.05.032>.
- [148] Domínguez C, Pérez-Alonso FJ, Salam MA, Al-Thabaiti SA, Peña MA, Barrio L, Rojas S. Effect of the N content of Fe/N/graphene catalysts for the oxygen reduction reaction in alkaline media. *J Mater Chem* 2015;3(48):24487–94. <https://doi.org/10.1039/c5ta04355g>.
- [149] Niu Y, Huang X, Hu W. Fe₃C nanoparticle decorated Fe/N doped graphene for efficient oxygen reduction reaction electrocatalysis. *J Power Sources* 2016;332:305–11. <https://doi.org/10.1016/j.jpowsour.2016.09.130>.
- [150] Ouyang L, Guo L, Cai W, Ye J, Hu R, Liu J, Yang L, Zhu M. Facile synthesis of Ge@FLG composites by plasma assisted ball milling for lithium ion battery anodes. *J Mater Chem* 2014;2(29):11280–5. <https://doi.org/10.1039/C4TA01267D>.
- [151] Patniboon T, Hansen HA. N-Doped graphene supported on Metal-Iron carbide as a catalyst for the oxygen reduction reaction: density functional theory study. *ChemSusChem Mar.* 2020;13(5):996–1005. <https://doi.org/10.1002/cssc.201903035>.
- [152] Dong Q, Zhuang X, Li Z, Li B, Fang B, Yang C, Xie H, Zhang F, Feng X. Efficient approach to iron/nitrogen co-doped graphene materials as efficient electrochemical catalysts for the oxygen reduction reaction. *J Mater Chem* 2015;3(15):7767–72. <https://doi.org/10.1039/C5TA00556F>.
- [153] Wu Z-S, Chen L, Liu J, Parvez K, Liang H, Shu J, Sachdev H, Graf R, Feng X, Müllen K. High-performance electrocatalysts for oxygen reduction derived from cobalt porphyrin-based conjugated mesoporous polymers. *Adv Mater Mar.* 2014;26(9):1450–5. <https://doi.org/10.1002/adma.201304147>.
- [154] Li J, Chen M, Cullen DA, Hwang S, Wang M, et al. Atomically dispersed manganese catalysts for oxygen reduction in proton-exchange membrane fuel cells. *Nat. Catal. Dec.* 2018;1(12):935–45. <https://doi.org/10.1038/s41929-018-0164-8>.
- [155] Bai L, Duan Z, Wen X, Si R, Guan J. Atomically dispersed manganese-based catalysts for efficient catalysis of oxygen reduction reaction. *Appl Catal B Environ Nov.* 2019;257:117930. <https://doi.org/10.1016/j.apcatb.2019.117930>.
- [156] Lu Z-J, Bao S-J, Gou Y-T, Cai C-J, Ji C-C, Xu M-W, Song J, Wang R. Nitrogen-doped reduced-graphene oxide as an efficient metal-free electrocatalyst for oxygen reduction in

- fuel cells. *RSC Adv* 2013;3(12):3990. <https://doi.org/10.1039/c3ra22161j>.
- [157] Bayram E, Yilmaz G, Mukerjee S. A solution-based procedure for synthesis of nitrogen doped graphene as an efficient electrocatalyst for oxygen reduction reactions in acidic and alkaline electrolytes. *Appl Catal B Environ* 2016;192:26–34. <https://doi.org/10.1016/j.apcatb.2016.03.043>.
- [158] Farzaneh A, Saghatoleslami N, Goharshadi EK, Gharibi H, Ahmadzadeh H. Substitutional doping of carbon nanotubes with heteroatoms and their chemical applications. *Electrochim Acta* 2016;222:608–18. <https://doi.org/10.1016/j.electacta.2016.11.015>.
- [159] Alonso-Lemus IL, Figueroa-Torres MZ, García-Hernández AB, Escobar-Morales B, Rodríguez-Varela FJ, Fuentes AF, Lardizabal-Gutierrez D, Quintana-Owen P. Low-cost sonochemical synthesis of nitrogen-doped graphene metal-free electrocatalyst for the oxygen reduction reaction in alkaline media. *Int J Hydrogen Energy* 2017;42(51):30330–8. <https://doi.org/10.1016/j.ijhydene.2017.09.057>.
- [160] Chen X, Liang Y, Wan L, Xie Z, Easton CD, Bourgeois L, Wang Z, Bao Q, Zhu Y, Tao S, Wang H. Construction of porous N-doped graphene layer for efficient oxygen reduction reaction. *Chem Eng Sci* 2019;194:36–44. <https://doi.org/10.1016/j.ces.2018.04.004>.
- [161] Xiao J, Bian X, Liao L, Zhang S, Ji C, Liu B. Nitrogen-doped mesoporous graphene as a synergistic electrocatalyst matrix for high-performance oxygen reduction reaction. *ACS Appl Mater Interfaces* Oct. 2014;6(20):17654–60. <https://doi.org/10.1021/am503895w>.
- [162] Wu Z-S, Yang S, Sun Y, Parvez K, Feng X, Müllen K. 3D nitrogen-doped graphene aerogel-supported Fe₃O₄ nanoparticles as efficient electrocatalysts for the oxygen reduction reaction. *J Am Chem Soc* Jun. 2012;134(22):9082–5. <https://doi.org/10.1021/ja3030565>.
- [163] Huang Z, Zhou H, Yang W, Fu C, Chen L, Kuang Y. Three-dimensional hierarchical porous nitrogen and sulfur-codoped graphene nanosheets for oxygen reduction in both alkaline and acidic media. *ChemCatChem* 2017;9(6):987–96. <https://doi.org/10.1002/cctc.201601387>.
- [164] He C, Zhang JJ, Shen PK. Nitrogen-self-doped graphene-based non-precious metal catalyst with superior performance to Pt/C catalyst toward oxygen reduction reaction. *J Mater Chem* 2014;2(9):3231. <https://doi.org/10.1039/c3ta14070a>.
- [165] Liu D, Long YT. Superior catalytic activity of electrochemically reduced graphene oxide supported iron phthalocyanines toward oxygen reduction reaction. *ACS Appl Mater Interfaces* 2015;7(43):24063–8. <https://doi.org/10.1021/acsami.5b07068>.
- [166] Oh S, Kim J, Kim M, Nam D, Park J, Cho E, Kwon H. Synergetic effects of edge formation and sulfur doping on the catalytic activity of a graphene-based catalyst for the oxygen reduction reaction. *J Mater Chem* 2016;4(37):14400–7. <https://doi.org/10.1039/C6TA05020D>.
- [167] Ma XX, He XQ. Cobalt oxide anchored on nitrogen and sulfur dual-doped graphene foam as an effective oxygen electrode catalyst in alkaline media. *Appl Mater Today* 2016;4:1–8. <https://doi.org/10.1016/j.apmt.2016.04.002>.
- [168] Fu X, Choi JY, Zamani P, Jiang G, Hoque MA, Hassan FM, Chen Z. Co-N decorated hierarchically porous graphene aerogel for efficient oxygen reduction reaction in acid. *ACS Appl Mater Interfaces* 2016;8(10):6488–95. <https://doi.org/10.1021/acsami.5b12746>.
- [169] Thanh TD, Chuong ND, Balamurugan J, Van Hien H, Kim NH, Lee JH. Porous hollow-structured LaNiO₃ stabilized N,S-codoped graphene as an active electrocatalyst for oxygen reduction reaction. *Small* Oct. 2017;13(39):1701884. <https://doi.org/10.1002/smll.201701884>.
- [170] Jiang Y, Lu Y, Lv X, Han D, Zhang Q, Niu L, Chen W. Enhanced catalytic performance of Pt-free iron phthalocyanine by graphene support for efficient oxygen reduction reaction. *ACS Catal Jun.* 2013;3(6):1263–71. <https://doi.org/10.1021/cs4001927>.
- [171] He Q, Li Q, Khene S, Ren X, López-Suárez FE, Lozano-Castelló D, Bueno-López A, Wu G. High-loading cobalt oxide coupled with nitrogen-doped graphene for oxygen reduction in anion-exchange-membrane alkaline fuel cells. *J Phys Chem C May* 2013;117(17):8697–707. <https://doi.org/10.1021/jp401814f>.
- [172] Dong F, Cai Y, Liu C, Liu J, Qiao J. Heteroatom (B, N and P) doped porous graphene foams for efficient oxygen reduction reaction electrocatalysis. *Int J Hydrogen Energy* 2018;43(28):12661–70. <https://doi.org/10.1016/j.ijhydene.2018.04.118>.
- [173] Maiti K, Balamurugan J, Gautam J, Kim NH, Lee JH. Hierarchical flowerlike highly synergistic three-dimensional iron tungsten oxide nanostructure-anchored nitrogen-doped graphene as an efficient and durable electrocatalyst for oxygen reduction reaction. *ACS Appl Mater Interfaces Sep.* 2018;10(38):32220–32. <https://doi.org/10.1021/acsami.8b11406>.
- [174] Wu F, Niu Y, Huang X, Mei Y, Wu X, Zhong C, Hu W. Manganese/cobalt bimetal nanoparticles encapsulated in nitrogen-rich graphene sheets for efficient oxygen reduction reaction electrocatalysis. *ACS Sustainable Chem Eng Aug.* 2018;6(8):10545–51. <https://doi.org/10.1021/acssuschemeng.8b01890>.
- [175] Li J, Liu JX, Gao X, Goldsmith BR, Cong Y, et al. Nitrogen-doped graphene layers for electrochemical oxygen reduction reaction boosted by lattice strain. *J Catal* 2019;378:113–20. <https://doi.org/10.1016/j.jcat.2019.08.018>.
- [176] Bai L, Hou C, Wen X, Guan J. Catalysis of oxygen reduction reaction on atomically dispersed copper- and nitrogen-codoped graphene. *ACS Appl Energy Mater* 2019;2(7):4755–62. <https://doi.org/10.1021/acsaem.9b00386>.
- [177] Qin Y, Wu H-H, Zhang LA, Zhou X, Bu Y, et al. Aluminum and nitrogen codoped graphene: highly active and durable electrocatalyst for oxygen reduction reaction. *ACS Catal Jan.* 2019;9(1):610–9. <https://doi.org/10.1021/acscatal.8b04117>.
- [178] Tavakkoli M, Flahaut E, Peljo P, Sainio J, Davodi F, Lobiak EV, Mustonen K, Kauppinen EI. Mesoporous single-atom-doped graphene-carbon nanotube hybrid: synthesis and tunable electrocatalytic activity for oxygen evolution and reduction reactions. *ACS Catal* 2020;10(8):4647–58. <https://doi.org/10.1021/acscatal.0c00352>.
- [179] Wan S, Wu J, Wang D, Liu H, Zhang Z, Ma J, Wang C. Co/N-doped carbon nanotube arrays grown on 2D MOFs-derived matrix for boosting the oxygen reduction reaction in alkaline and acidic media. *Chin Chem Lett* 2020;(2019):2–7. <https://doi.org/10.1016/j.ccllet.2020.04.040>.
- [180] Huang B, Liu Y, Xie Z. Biomass derived 2D carbons via a hydrothermal carbonization method as efficient bifunctional ORR/HER electrocatalysts. *J Mater Chem* 2017;5(45):23481–8. <https://doi.org/10.1039/C7TA08052B>.
- [181] Lee DW, Jang J, Jang I, Kang YS, Jang S, Lee KY, Jang JH, Kim H, Yoo SJ. Bio-Derived Co₂P nanoparticles supported on Nitrogen-Doped carbon as promising oxygen reduction reaction electrocatalyst for anion exchange membrane fuel cells. *Small Sep.* 2019;15(36):1902090. <https://doi.org/10.1002/smll.201902090>.
- [182] Xu Z, Ma J, Shi M, Xie Y, Feng C. Biomass based iron and nitrogen co-doped 3D porous carbon as an efficient oxygen reduction catalyst. *J Colloid Interface Sci* 2018;523:144–50. <https://doi.org/10.1016/j.jcis.2018.03.092>.

- [183] Qiu Y, Yu J, Wu W, Yin J, Bai X. Fe–N/C nanofiber electrocatalysts with improved activity and stability for oxygen reduction in alkaline and acid solutions. *J Solid State Electrochem Mar.* 2013;17(3):565–73. <https://doi.org/10.1007/s10008-012-1888-z>.
- [184] Osmieri L, Monteverde Videla AHA, Specchia S. The use of different types of reduced graphene oxide in the preparation of Fe–N–C electrocatalysts: capacitive behavior and oxygen reduction reaction activity in alkaline medium. *J Solid State Electrochem Dec.* 2016;20(12):3507–23. <https://doi.org/10.1007/s10008-016-3332-2>.
- [185] Gao S, Li X, Li L, Wei X. A versatile biomass derived carbon material for oxygen reduction reaction, supercapacitors and oil/water separation. *Nano Energy* 2017;33:334–42. <https://doi.org/10.1016/j.nanoen.2017.01.045>.
- [186] Yuan H, Hou Y, Wen Z, Guo X, Chen J, He Z. Porous carbon nanosheets codoped with nitrogen and sulfur for oxygen reduction reaction in microbial fuel cells. *ACS Appl Mater Interfaces Aug.* 2015;7(33):18672–8. <https://doi.org/10.1021/acsami.5b05144>.
- [187] Maruyama J, Okamura J, Miyazaki K, Uchimoto Y, Abe I. Hemoglobin pyropolymer used as a precursor of a noble-metal-free fuel cell cathode catalyst. *J Phys Chem C Feb.* 2008;112(7):2784–90. <https://doi.org/10.1021/jp709912d>.
- [188] Zheng J, Guo C, Chen C, Fan M, Gong J, Zhang Y, Zhao T, Sun Y, Xu X, Li M, Wang R, Luo Z, Chen C. High content of pyridinic- and pyrrolic-nitrogen-modified carbon nanotubes derived from blood biomass for the electrocatalysis of oxygen reduction reaction in alkaline medium. *Electrochim Acta* 2015;168:386–93. <https://doi.org/10.1016/j.electacta.2015.03.173>.
- [189] Wang G, Peng H, Qiao X, Du L, Li X, Shu T, Liao S. Biomass-derived porous heteroatom-doped carbon spheres as a high-performance catalyst for the oxygen reduction reaction. *Int J Hydrogen Energy* 2016;41(32):14101–10. <https://doi.org/10.1016/j.ijhydene.2016.06.023>.
- [190] Wang R, Wang H, Zhou T, Key J, Ma Y, Zhang Z, Wang Q, Ji S. The enhanced electrocatalytic activity of okara-derived N-doped mesoporous carbon for oxygen reduction reaction. *J Power Sources* 2015;274:741–7. <https://doi.org/10.1016/j.jpowsour.2014.10.049>.
- [191] Zhao A, Masa J, Muhler M, Schuhmann W, Xia W. N-doped carbon synthesized from N-containing polymers as metal-free catalysts for the oxygen reduction under alkaline conditions. *Electrochim Acta May* 2013;98:139–45. <https://doi.org/10.1016/j.electacta.2013.03.043>.
- [192] Shamsunnahar SM, Nagai M. Nitrogen doping of ash-free coal and effect of ash components on properties and oxygen reduction reaction in fuel cell. *Fuel Jun.* 2014;126:134–42. <https://doi.org/10.1016/j.fuel.2014.02.049>.
- [193] Wu X, Yu X, Lin Z, Huang J, Cao L, Zhang B, Zhan Y, Meng H, Zhu Y, Zhang Y. Nitrogen doped graphitic carbon ribbons from cellulose as non noble metal catalyst for oxygen reduction reaction. *Int J Hydrogen Energy* 2016;41(32):14111–22. <https://doi.org/10.1016/j.ijhydene.2016.05.275>.
- [194] Wang D, Liu S, Fang G, Geng G, Ma J. From trash to treasure: direct transformation of onion husks into three-dimensional interconnected porous carbon frameworks for high-performance supercapacitors in organic electrolyte. *Electrochim Acta Oct.* 2016;216:405–11. <https://doi.org/10.1016/j.electacta.2016.09.053>.
- [195] Alonso-Lemus IL, Escobar-Morales B, Lardizabal-Gutierrez D, de la Torre-Saenz L, Quintana-Owen P, Rodriguez-Varela FJ. Short communication: onion skin waste-derived biocarbon as alternative non-noble metal electrocatalyst towards ORR in alkaline media. *Int J Hydrogen Energy* 2019;44(24):12409–14. <https://doi.org/10.1016/j.ijhydene.2018.10.050>.
- [196] Pan F, Guo S, Zhang J. Swelling-induced synthesis of nitrogen-doped graphene for oxygen reduction reaction. *Electrochim Acta Oct.* 2015;180:29–36. <https://doi.org/10.1016/j.electacta.2015.08.079>.
- [197] Guo CZ, Liao WL, Chen CG. Design of a non-precious metal electrocatalyst for alkaline electrolyte oxygen reduction by using soybean biomass as the nitrogen source of electrocatalytically active center structures. *J Power Sources* 2014;269:841–7. <https://doi.org/10.1016/j.jpowsour.2014.07.024>.
- [198] Wang L, Zhang L, Bai L, Han L, Dong S. Nitrogen, cobalt-codoped carbon electrocatalyst for oxygen reduction reaction using soy milk and cobalt salts as precursors. *Electrochim Commun* 2013;34:68–72. <https://doi.org/10.1016/j.elecom.2013.05.019>.
- [199] Wang R, Wang K, Wang Z, Song H, Wang H, Ji S. Pig bones derived N-doped carbon with multi-level pores as electrocatalyst for oxygen reduction. *J Power Sources* 2015;297:295–301. <https://doi.org/10.1016/j.jpowsour.2015.07.107>.
- [200] Alonso-Lemus IL, Rodriguez-Varela FJ, Figueroa-Torres MZ, Sanchez-Castro ME, Hernandez-Ramírez A, Lardizabal-Gutierrez D, Quintana-Owen P. Novel self-nitrogen-doped porous carbon from waste leather as highly active metal-free electrocatalyst for the ORR. *Int J Hydrogen Energy* 2016;41(48):23409–16. <https://doi.org/10.1016/j.ijhydene.2016.09.033>.
- [201] Liu Y, Ruan J, Sang S, Zhou Z, Wu Q. Iron and nitrogen-codoped carbon derived from soybeans as efficient electrocatalysts for the oxygen reduction reaction. *Electrochim Acta* 2016;215:388–97. <https://doi.org/10.1016/j.electacta.2016.08.090>.
- [202] Srinu A, Peera SG, Parthiban V, Bhuvaneshwari B, Sahu AK. Heteroatom engineering and Co-doping of N and P to porous carbon derived from spent coffee grounds as an efficient electrocatalyst for oxygen reduction reactions in alkaline medium. *ChemistrySelect* 2018;3(2):690–702. <https://doi.org/10.1002/slct.201702042>.
- [203] Hao Y, Zhang X, Yang Q, Chen K, Guo J, Zhou D, Feng L, Slanina Z. Highly porous defective carbons derived from seaweed biomass as efficient electrocatalysts for oxygen reduction in both alkaline and acidic media. *Carbon N. Y.* 2018;137:93–103. <https://doi.org/10.1016/j.carbon.2018.05.007>.
- [204] Li C, Sun F, Lin Y. Refining cocoon to prepare (N, S, and Fe) ternary-doped porous carbon aerogel as efficient catalyst for the oxygen reduction reaction in alkaline medium. *J Power Sources* 2018;384(March):48–57. <https://doi.org/10.1016/j.jpowsour.2018.01.020>.
- [205] Wu D, Shi Y, Jing H, Wang X, Song X, Si D, Liang S, Hao C. Tea-leaf-residual derived electrocatalyst: hierarchical pore structure and self nitrogen and fluorine co-doping for efficient oxygen reduction reaction. *Int J Hydrogen Energy* 2018;43(42):19492–9. <https://doi.org/10.1016/j.ijhydene.2018.08.201>.
- [206] Lu G, Li Z, Fan W, Wang M, Yang S, Li J, Chang Z, Sun H, Liang S, Liu Z. Sponge-like N-doped carbon materials with Co-based nanoparticles derived from biomass as highly efficient electrocatalysts for the oxygen reduction reaction in alkaline media. *RSC Adv* 2019;9(9):4843–8. <https://doi.org/10.1039/c8ra10462j>.
- [207] Sun Y, Zhong R, Zhang H, Huang T, Yu J, Fang H, Liang D, Guo Z. Soybean milk derived carbon intercalated with reduced graphene oxide as high efficient electrocatalysts for oxygen reduction reaction. *Int J Hydrogen Energy*

- 2019;44(39):21790–802. <https://doi.org/10.1016/j.ijhydene.2019.06.174>.
- [208] Pérez-Salcedo KY, Alonso-Lemus IL, Quintana P, Mena-Durán CJ, Barbosa R, Escobar B. Self-doped Sargassum spp. derived biocarbon as electrocatalysts for ORR in alkaline media. *Int J Hydrogen Energy* 2019;44(24):12399–408. <https://doi.org/10.1016/j.ijhydene.2018.10.073>.
- [209] Liu Y, Su M, Li D, Li S, Li X, Zhao J, Liu F. Soybean straw biomass-derived Fe-N co-doped porous carbon as an efficient electrocatalyst for oxygen reduction in both alkaline and acidic media. *RSC Adv* 2020;10(12):6763–71. <https://doi.org/10.1039/c9ra07539a>.
- [210] Amiin IS, Zhang J, Kou Z, Liu X, Asare OK, Zhou H, Cheng K, Zhang H, Mai L, Pan M, Mu S. Self-organized 3D porous graphene dual-doped with biomass-sponsored nitrogen and sulfur for oxygen reduction and evolution. *ACS Appl Mater Interfaces* 2016;8(43):29408–18. <https://doi.org/10.1021/acsami.6b08719>.
- [211] Thompson ST, Peterson D, Ho D, Papageorgopoulos D. Perspective—the next decade of AEMFCs: near-term targets to accelerate applied R&D. *J Electrochem Soc* 2020;167(8):084514. <https://doi.org/10.1149/1945-7111/ab8c88>.
- [212] Huang G, Mandal M, Peng X, Yang-Neyerlin AC, Pivovar BS, Mustain WE, Kohl PA. Composite poly(norbornene) anion conducting membranes for achieving durability, water management and high power (3.4 W/cm²) in hydrogen/oxygen alkaline fuel cells. *J. Electrochem. Soc.* 2019. <https://doi.org/10.1149/2.1301910jes>.
- [213] Lu S, Pan J, Huang A, Zhuang L, Lu J. Alkaline polymer electrolyte fuel cells completely free from noble metal catalysts. *Proc. Natl. Acad. Sci. U.S.A* 2008;105(52):20611–4. <https://doi.org/10.1073/pnas.0810041106>.
- [214] Gu S, Sheng W, Cai R, Alia SM, Song S, Jensen KO, Yan Y. An efficient ag-ionomer interface for hydroxide exchange membrane fuel cells. *Chem Commun* 2013;49(2):131–3. <https://doi.org/10.1039/c2cc34862d>.
- [215] Peng X, Kashyap V, Ng B, Kurungot S, Wang L, Varcoe JR, Mustain WE. High-performing pgm-free aemfc cathodes from carbon-supported cobalt ferrite nanoparticles. *Catalysts* 2019;9(3):1–12. <https://doi.org/10.3390/catal9030264>.
- [216] Lilloja J, Kibena-Pöldsepp E, Sarapuu A, Kikas A, Kisand V, Käärik M, Merisalu M, Treshchalov A, Leis J, Sammelselg V, Wei Q, Holdcroft S, Tammeveski K. Nitrogen-doped carbide-derived carbon/carbon nanotube composites as cathode catalysts for anion exchange membrane fuel cell application. *Appl Catal B Environ Sep.* 2020;272:119012. <https://doi.org/10.1016/j.APCATB.2020.119012>.
- [217] Lilloja J, Kibena-Pöldsepp E, Sarapuu A, Douglin JC, Käärik M, Kozlova J, Paiste P, Kikas A, Aruväli J, Leis J, Sammelselg V, Dekel DR, Tammeveski K. Transition-metal- and nitrogen-doped carbide-derived carbon/carbon nanotube composites as cathode catalysts for anion-exchange membrane fuel cells. *ACS Catal Feb.* 2021;11(4):1920–31. https://doi.org/10.1021/ACSCATAL.0C03511/ASSET/IMAGES/LARGE/CS0C03511_0008.JPEG.
- [218] Arunchander A, Vivekanantha M, Peera SG, Sahu AK. MnO–nitrogen doped graphene as a durable non-precious hybrid catalyst for the oxygen reduction reaction in anion exchange membrane fuel cells. *RSC Adv Oct.* 2016;6(98):95590–600. <https://doi.org/10.1039/C6RA20627A>.
- [219] He Q, Li Q, Khene S, Ren X, Lo FE, Lozano-Castello D, Bueno-Lo A, Wu G. High-loading cobalt oxide coupled with nitrogen-doped graphene for oxygen reduction in anion-exchange-membrane. *Alkaline Fuel Cells* 2013. <https://doi.org/10.1021/jp401814f>.
- [220] Peng X, Omasta TJ, Magliocca E, Wang L, Varcoe JR, Mustain WE. Nitrogen-doped carbon–CoOx nanohybrids: a precious metal free cathode that exceeds 1.0 W cm^{−2} peak power and 100 h life in anion-exchange membrane fuel cells. *Angew Chem Int Ed Jan.* 2019;58(4):1046–51. <https://doi.org/10.1002/ANIE.201811099>.
- [221] Bosubabu D, Parthiban V, Sahu AK, Ramesha K. Nitrogen-doped graphene-like carbon from bio-waste as efficient low-cost electrocatalyst for fuel cell application. *Bull Mater Sci* 2021. <https://doi.org/10.1007/s12034-021-02367-9>.